

NAIST-IS-DD1361020

Doctoral Dissertation

**Proportional Myoelectric Control of High-DOF Finger
Kinematics Using Synergistic Models**

Jimson Gelbolingo Ngeo

March 14, 2016

Department of Information Science
Graduate School of Information Science
Nara Institute of Science and Technology

A Doctoral Dissertation
submitted to Graduate School of Information Science,
Nara Institute of Science and Technology
in partial fulfillment of the requirements for the degree of
Doctor of ENGINEERING

Jimson Gelbolingo Ngeo

Thesis Committee:

Professor Kazushi Ikeda	(Supervisor)
Professor Tsukasa Ogasawara	(Co-supervisor)
Professor Tomohiro Shibata	(Co-supervisor)
Professor Jun Morimoto	(Co-supervisor)
Assistant Professor Tomoya Tamei	(Co-supervisor)

Proportional Myoelectric Control of High-DOF Finger Kinematics Using Synergistic Models*

Jimson Gelbolingo Ngeo

Abstract

Proportional myoelectric control of multiple degrees-of-freedom (DOF) in active finger joints is important in replicating dexterous hand motion in robotic prostheses and orthoses. However, this is still difficult to achieve as current myoelectric control strategies often require the separate control of each joint and do not consider the strong correlations that exist between these joints. To address this problem, we propose using a shared low-dimensional encoding based on synergistic models to represent both the high-DOF finger joint kinematics and the coordination of muscle activities taken from electromyographic (EMG) signals in the forearm. A Bayesian Gaussian Process Latent Variable Model (GPLVM) is used to learn a shared latent structure model that not only allows the automatic selection of the dimensionality but also captures the information variance, both shared and specific to the observed EMG and hand kinematic data.

In the first part of this study, we show how using features obtained from an EMG-to-Muscle Activation is not only suitable for continuous and simultaneous estimation of finger kinematics, but is also shown to perform better than time-domain based features. In the next part, we demonstrate that the proposed shared model is able to reconstruct the full-joint continuous finger kinematics from muscle activation inputs, whose results are inferred from a shared latent manifold. We show that the proposed method outperforms commonly used simultaneous regression and linear dimensionality reduction methods. The proposed approach not only presents a viable solution for a myoelectric strategy for handling high-DOF finger control, but also aims to open new avenues in developing novel myoelectric interfaces for synergy development and long-term control and adaptation.

*Doctoral Dissertation, Department of Information Science, Graduate School of Information Science, Nara Institute of Science and Technology, NAIST-IS-DD1361020, March 14, 2016.

Keywords:

Electromyography (EMG), muscle activation model, multi-fingered hand, finger joint kinematics, regression, synergies, dimensionality reduction

Contents

1	Introduction	1
1.1.	Research motivation	2
1.2.	Overview of the problem	4
1.3.	Research contribution	5
1.4.	Thesis overview	6
2	Related work	7
2.1.	Myoelectric control of robotic hands	8
2.1.1	The EMG as a control signal	10
2.1.2	Myoelectric control strategies	13
2.1.3	Characteristics of an ideal myoelectric control system	17
2.2.	Synergies	19
2.2.1	Synergies in robot grasping	20
2.2.2	Synergies in myoelectric control	22
2.3.	Mapping finger kinematics from EMG	25
3	Continuous and simultaneous estimation of finger kinematics	27
3.1.	Inherent problems of electromechanical delay	28
3.2.	EMG-to-muscle activation model	29
3.3.	Regression models	32
3.3.1	Artificial neural network	32
3.3.2	Gaussian process for regression	35
3.4.	Methods	38
3.4.1	Experimental setup	38
3.4.2	Data collection	41

3.4.3	Data processing	45
3.4.4	Statistical analysis	47
3.5.	Results	48
3.6.	Discussion	55
3.6.1	On using the EMG-to-Muscle activation model features	55
3.6.2	Neural network versus gaussian process regression	56
3.6.3	Application: control of a finger exoskeleton	58
3.6.4	Implementation and limitations	60
4	Using nonlinear synergistic model for proportional myoelectric control of high-DOF finger postures	61
4.1.	Bayesian GPLVM for multi-observation	63
4.2.	Methods	67
4.2.1	Data collection	67
4.2.2	Data processing	67
4.2.3	Inference and estimation	68
4.2.4	Cross-validation	68
4.3.	Results	69
4.3.1	Synergistic representation	69
4.3.2	Estimation and reconstruction	73
4.3.3	Synergistic representations	75
4.4.	Discussion	77
4.4.1	Shared synergistic features	77
4.4.2	Reconstruction and estimation for control	79
4.4.3	Implementation and limitations	80
5	Conclusion	83
6	Directions for future research	85
	Acknowledgements	87
	References	88
	Publication List	101

List of Figures

2.1	Examples of robotic devices that uses myoelectric control	9
2.2	The EMG signals are generated as neural information	10
2.3	A sample raw EMG recording	11
2.4	Illustrations of myoelectric control paradigms	15
2.5	Criteria of an ideal myoelectric controller	18
2.6	Low-dimensional representation of human posture	21
2.7	Myoelectric control schemes based on synergy representations.	22
2.8	Time-invariant synergies capture spatial regularities	24
3.1	Examples of the electromechanical delays are shown	28
3.2	The parameter A introduces nonlinearity	31
3.3	A sample raw EMG recording	32
3.4	The architecture of a multilayer feedforward neural network.	33
3.5	Experimental setup	39
3.6	Marker placement and sample skeletal model	40
3.7	Finger movements divided according to task	41
3.8	Experimental procedure	42
3.9	Experimental conditions' effect on the recorded data	44
3.10	Schematic overview of the data processing and model training	46
3.11	Single joint angle estimation results	48
3.12	One representative estimation result	50
3.13	The mean correlation coefficient in estimated finger joint angle	51
3.14	The normalized root-mean-square in estimated finger joint angle	51
3.15	The EMD parameters obtained across subjects	52
3.16	Comparing between the use of NN and GP regressors	53
3.17	Learning curves of the ANN and GP Regressor	54

3.18	An application showing an EMG-based control of an exoskeleton . . .	58
4.1	Schematic overview of the proposed shared latent representation . . .	62
4.2	Graphical model of the Bayesian GPLVM	64
4.3	PCA projection and dimensional analysis on the observation data . . .	69
4.4	The GPLVM 2D projections on different data	71
4.5	Discovered latent spaces with the Bayesian GPLVM with ARD	72
4.6	Sample finger kinematics inference of a multi-finger movement	74
4.7	Overall estimation performance across subjects	75
4.8	Discovered shared and private latent space dimensions across subjects	76

List of Tables

- 3.1 Selected EMG channels and the target muscles 40
- 3.2 Finger joints normal range of motion. 43
- 3.3 Performance of the estimator and exoskeleton 59

- 4.1 The mean RMSE of the joint marker and joint angle space 77
- 4.2 Computational time needed training and testing 82

Chapter 1

Introduction

Robotic hand assistive and tele-manipulation devices are developing technologies that hold great promise in revolutionizing modern hand rehabilitation and prosthetic application. It is expected that such technologies will play a significant role in improving the lives and functionality of people with hand injuries and impairments. There are many dexterous robotic hands and powered prostheses that exist today. The number of active controllable joints in these devices are substantially increasing to give them capabilities to perform complex movements involving simultaneous control of large degree-of-freedom (DOFs), very much similar to the human hand. Roughly about 30% to 50% of these devices are operated via myoelectric control. However, the myoelectric capabilities of these devices have not yet reached its full potential due to the limited control strategies offered by using surface electromyographic (EMG) signals. The deployment of simultaneous and proportional control for multiple degrees-of-freedom (DOF) remains a major challenge in improving next-generation prosthetic systems. Thus, increasing current myoelectric control capabilities and providing a good framework for generating human-like dexterous finger kinematic movement from EMG signals can significantly improve current myoelectric robotic hand devices and interfaces.

1.1. Research motivation

Given the dominant role of the human hand, where many everyday functional tasks (e.g. touch, grasp, manipulation and gesture communication) are achieved by our hands. The loss of hand function can greatly impede daily human activities and mobility. Upper-limb myoelectric prostheses, hand/finger exoskeletons, and other neuro-rehabilitation devices are some common solution to rehabilitate and restore some functionality to the lost or impaired hands. As such, the use of neural signals has been very popular in controlling tele-operated devices as these can give unconstrained and precise movement control in a highly dynamic environments. Among the many potential options, however, muscle interfacing using surface electromyographic (EMG) signals is still currently the only viable noninvasive biological signal that can be used for control [1] as these signals have been shown to represent movement kinematic and dynamic information very well.

There are many dexterous robotic hand and upper-limb powered prostheses that exist [2–7], but the difficulty in controlling all the available degree-of-freedom (DOF) via myoelectric control has motivated many researchers to focus on more limited control mechanisms. To this date, the functionality achieved by both commercial and clinical systems that uses surface electromyographic (EMG) signals has been somewhat limited. Clinically available EMG-based controllers are only able to control a few DOFs at a time [8]. Multiple dimensions have to be controlled sequentially, requiring slow mode-switching mechanisms initiated by different muscle co-contractions. To this end, realizing a more intuitive, seamless and natural myoelectric control scheme based on proportional and simultaneous control of multiple DOF is one of the goals of this study.

While many have mapped surface EMG signals to upper and lower limb kinematics and dynamics, very few have focused on mapping to continuous multi-finger movements. This is because dexterous hand manipulation remains to be one of the most complex biological movement to model, and has been proven to be very difficult to replicate even in robots [9]. The human hand not only has a highly articulated mechanical system, with possibly more than 20 kinematic DOFs, but also has a complex muscular system involved in the motor control. Indeed a large part of the human brain is shown to be devoted to controlling the hand and its complex musculotendon network [10].

In neurophysiology, it is argued that synergies control the coordination of muscle recruitment and the modulation of muscle forces for the control of human posture [11–14]. The muscle synergy hypothesis claims that the human motor system directly initiates movement through flexible combinations of control modules recruited by the central nervous system to simplify control. Similarly, the concept of synergies have also been widely used in the field of robotics, where robot control laws are expressed in low-dimensional space to drive forces applied on the higher dimensional robot space. In motion planning for example, synergies can often reduce complexity, where searching for an adequate kinematic configuration can increase exponentially with the dimensionality of the structure [14]. For hand grasping, it has also been consistently shown that functional human hand postures operate in a configuration space of much smaller dimensions, often referred to as postural synergies, than what the kinematic structure would suggest [15].

Estimating finger kinematics from EMG input signals usually involves highly correlated patterns and high dimensionality in both the input and output domains. This study is inspired by studies in the motor control community that claims that synergistic patterns can be observed in both the muscle coordination and kinematic posture space. Thus, the use of synergies can provide a natural modeling paradigm to model correlations that exists in either the muscle coordination system, or in the finger kinematic configuration, or in both spaces simultaneously. This study aims to incorporate a shared latent space model, where both muscle activation and high-dimensional finger kinematics information are embedded on a low-dimensional space where synergistic features are shared.

Although, few studies have given attention in considering such correlations in doing simultaneous and proportional control of the high dimensional finger kinematics from EMG signals. It is important that such correlations must be considered in the realization of an estimation model that can map from EMG or muscle activation signals to the corresponding complete full joint finger kinematic configuration. To the best of the author’s knowledge, no method or framework in the EMG-applications literature has yet to give a straightforward way of fully recreating the continuous movement of a high-dimensional full 23-joint hand model from EMG inputs, considering that many of the dimensions are redundant and highly correlated.

1.2. Overview of the problem

In the past 30 years, discrete classification of hand gestures from EMG signals has been successful, consistently reaching decoding accuracies of above 95% and classifying up to more than six different hand gestures [16–20]. However, classification approaches have been limited to use in controlled laboratory conditions and have not been used by any current commercial myoelectric prosthesis [21]. Despite the success of pattern classification approach to using EMG signals, this type of control strategy is inadequate for actuating all the functions offered by the robotic devices as it uses a sequential-based strategy where usually only one class of movement is active at a time. Natural hand movements are not limited to a number of discrete finger configurations but are continuous, coordinated and have simultaneous control of multiple DOFs.

The first problem presented in this research work is how to improve the current limited control offered by pattern recognition-based myoelectric control. To realize a more intuitive and natural myoelectric control scheme, control strategies based on proportional and simultaneous control are preferred over pattern recognition-based control. The previous studies have also focused training and testing only on simple finger movements and no combinations or variations of multi-finger and random freely movements were considered. Also, in considering continuous or proportional myoelectric control, time delays between the onset of the EMG signal and the exerted movement were present and observed in the previous studies [22–24]. This time delay is called hysteresis or electromechanical delay (EMD) and is a natural phenomenon that occurs in the relationship between muscles force and the output kinematics or dynamics. The EMD can vary depending on many different anatomical factors such as the type of muscle fiber, muscle shortening velocities and fatigue [25]. The previous studies did not consider any dynamical relation, such as the EMD, between EMG and the exerted force in the finger movement.

Even with proportional myoelectric control, this still falls short in only being able to control a few number of DOFs [26,27], with among many other existing limitations listed in [1]. Another problem that we consider in this study is how to consider the correlations that exists in both the hand kinematic configuration and muscle organization for control. Deployment of simultaneous and proportional control that can consider all DOFs available in the hand, although highly redundant and correlated, remains a very challenging task. In all the previous studies, the number of estimated DOFs were

not only limited, but selection of dimensionality were heuristic. Where many previous studies have studied individual synergy representations for muscle and hand configuration separately [14, 26–28], we consider using a nonlinear synergistic model where information and correlation from both muscle activation and finger kinematics are embedded in a shared low-dimensional latent space. Human hand movement is not only high-dimensional but also nonlinear. Previous studies have showed that using linear synergy models failed to represent motion correlation in simple hand movements, such as in a simple hand reach-grasp-retreat task [14]. To fully maximize the functionality of current myoelectric-based hand controllers and interfaces, recovering and mapping information to as many DOFs available as possible are essential.

1.3. Research contribution

This study aims at overcoming the limitations of pattern recognition-based control and proportional myoelectric control of only a few DOFs available in the hand. The main contributions of this study are as follows: (1) we describe a method for improving the estimation of simultaneous finger kinematics from inputs obtained from an EMG-to-Muscle Activation model that parameterizes electromechanical delay (EMD), which has been observed by numerous investigators. In this part, we compare between the use of different EMG time-domain based features and different regression methods, to show which method gives the better performance. In the second part of this study: (2) we describe a new strategy, using a generative model coupled with a nonlinear dimension reduction method, to reconstruct the kinematics of a full 23-joint skeletal hand model. Where studies have shown individual synergy models for muscle activation and kinematics, (3) we present the use of a shared model between these two different but highly correlated data. We employ the use of a Bayesian Gaussian Process Latent Variable Model (GPLVM) with automatic relevance determination (ARD) to learn this shared latent space. We also analyze how a synergistic model can be useful and interpreted in the context of myoelectric control of high-DOF finger kinematics. Finally, (4) we present the combined use of an EMG-to-Muscle Activation model coupled with a Bayesian inference method for estimating high-DOF finger kinematics from EMG. We provide the experimental evaluation that shows how the proposed method outperforms standard techniques, in terms of reconstructing finger kinematics using EMG inputs.

1.4. Thesis overview

This thesis is organized and divided into six chapters. Chapter 2 gives the related literature and works. The chapter introduces the terminologies used in the myoelectric control literature, conventional techniques used, and a thorough introduction of concepts such as synergies in the context of our work. Chapter 3 presents the first part of our work, where we propose an improved method for continuous and simultaneous estimation of finger kinematics from surface EMG signals. We show in this chapter how features obtained from an EMG-to-Muscle Activation model is not only suitable for proportional myoelectric control but is also shown to give better estimation performance than using conventional EMG time-domain based features. Chapter 4 presents the second part of our work, where we present a new framework for proportional myoelectric control of high-DOF finger kinematics using a nonlinear synergistic model. In this chapter, we present how different synergistic models can be used and interpreted in the context of myoelectric estimation of high-DOF finger kinematics. Chapter 5 draws some conclusions to our work on in the overall context of myoelectric control and applications. Lastly, Chapter 6 gives our recommendation and perspective for the future direction of this study.

Chapter 2

Related work

Myoelectric control has the potential to significantly change human-robot interaction due to its ability to non-invasively measure human motion intent. However, current control schemes have struggled to achieve the robust performance needed to seamlessly operate myoelectrically controlled devices in commercial and daily life applications. The trend in myoelectric control recently has gone towards simultaneous multifunctional control from discrete pattern recognition as this gives more functionality and mobility for users. This chapter reviews the related work in the past 5 years that has progressed in the field of myoelectric control for robotic hand applications. We also briefly introduce the concepts of synergies, as used both in the field of robotics and motor control, which has recently gained a following and popularity due to the potential role it may play in improving the current state-of-the-art myoelectric control schemes.

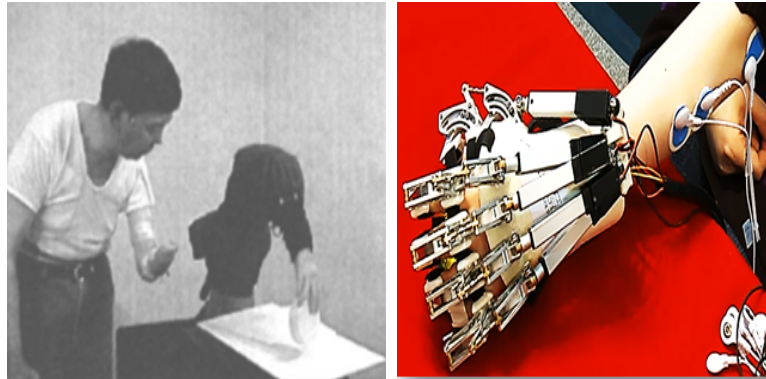
2.1. Myoelectric control of robotic hands

According to the World Health Organization (WHO), about 15 million people worldwide suffer stroke every year. About 5 million of them experience major upper-limb loss or long term hand impairments and are no longer able to participate in Activities of Daily Living without some form of assistance. Providing rehabilitation for impairments and prostheses for amputees are often the solution to help restore functions and some degree of normalcy but are costly, time-consuming and usually need sufficient access to therapists and equipments available only in special places. Robotic hand devices, for example, are developing technologies that hold great promise in revolutionizing modern hand rehabilitation and prosthetic application. Today, many such robotic hand supports, powered prostheses and orthoses with high degrees-of-freedom (DOF) are continuously being developed. Roughly about 30% to 50% of the available prostheses today are based on myoelectric control [29].

The control of such assistive devices is often achieved by man-machine interfacing [1]. When the neuromuscular information system is probed for information extraction, the interfacing can be realized at the level of the brain, peripheral nerves or muscles. Among many potential options, muscle interfacing is still currently the only noninvasive viable biological signal that can be used to control assistive devices in commercial and clinical systems [1, 29–31]. Although other signals such as brain and nerve signals are promising for direct neural interfacing, these usually require invasive procedure which makes their practical applicability quite limited in the clinical setting [1].

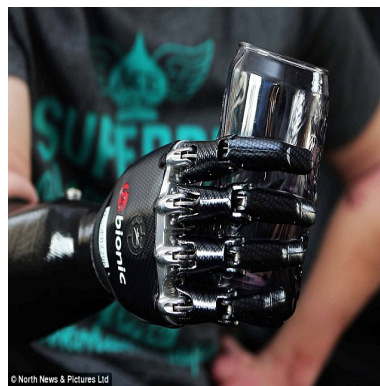
The use of the electromyographic (EMG) signal as a control source for robot interfacing has received considerable attention, because the idea of restoring function by bridging natural neural pathways is a compelling pursuit [31]. Despite not recording directly from neural cells, the surface electromyogram (EMG) signal contains information on the neural drive to muscles, i.e., the spike trains of motor neurons. Using this property, myoelectric control consists of the recording of EMG signals for extracting control signals to command external devices, such as hand prostheses.

Presently, some existing robotic devices that can support hand and finger assistance and rehabilitation are shown in Figure 2.1. Figure 2.1a shows a robot manipulator being controlled by a transradial amputee. Such a manipulator system has been shown to be capable of assisting subjects perform some basic desktop work such as pointing,



(a) Robot Manipulator [32]

(b) HK Polytech's University Hand Exoskeleton [34]



(c) Bebionic's Robot Hand [33,35]

Figure 2.1: Examples of robotic devices that uses myoelectric control.

touching and grasping objects [32]. In Figure 2.1b is a patented hand rehabilitation exoskeleton created by Hong Kong's Polytech University. This device is made for patients with hand impairments or those recovering from stroke to wear, to assist them in doing simple hand opening and closing functional tasks. Lastly, figure 2.1c shows a more modern commercial robot hand prosthesis created by Bebionic [33] which has good dexterity comparable to the human hand. All the devices shown in the figure are controlled using myoelectric signals.

2.1.1 The EMG as a control signal

Basmijian and De Luca described *electromyography* or more commonly known as *EMG* as an experimental technique concerned with the development, recording, and analysis of myoelectric signals. Myoelectric signals are formed by physiological variations in the state of muscle fiber membranes [36].

Movement planning is done by the brain after integration of all sensory information. Motor commands are then generated and transmitted to the muscles by means of motor neurons (also called alpha-motor neurons) located in the spinal cord or brain-stem. These motor neurons travel to the muscle fibers, where it then branches out. Due to this branching, each axon in a nerve innervates several muscle fibers which causes the muscles to contract (see Figure 2.2a to visualize this information flow). The contraction then generates the muscle forces needed to execute the movement task. It is the role of the primary motor cortex, through the motor neurons, that determines how much force each muscle group must exert and sends this information down to the muscles for them to actuate different joints in the body to generate the planned movement.

The EMG signal is the sum of the electrical activity of the muscle fibers, as trig-

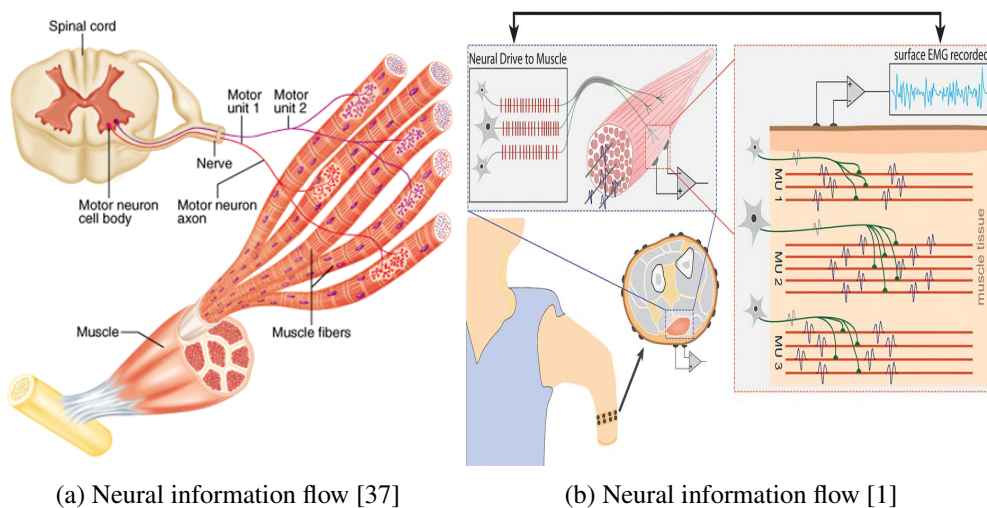


Figure 2.2: The EMG signals are generated as neural information passed down from the brain to the muscles. (a) Neural control information pathway. (b) EMG from motor neuron activities that trigger the generation of muscle fiber action potentials.

gered by the impulses of activation of the innervating motor neurons. As shown in Figure 2.2b, compound action potential of the fibers innervated by each motor neuron (motor unit action potential) is recorded at the skin surface and the interference activity of all active motor units determines the surface EMG recording. As indicated by the arrow, the interference surface EMG contains the original neural information. Features extracted from the EMG are thus associated to the neural code of motion, although this association has variability due to the influence of the shapes of the motor unit action potentials on the signal characteristics [1].

An unfiltered and unprocessed signal detecting the superposed MUAPs is called a raw surface EMG signal. Figure 2.3 shows a sample raw EMG recording done with three static contractions of a muscle. When the muscle is relaxed, a more or less noise-free EMG Baseline can be seen. Typically, we want the baseline to be approximately or as much as possible near zero.

Another interesting feature of the raw EMG signal is that these signals are stochastic in nature or that raw sEMG spikes follow random shape. This means that a raw EMG recording cannot be reproduced in the exact shape. By applying a smoothing algorithm or selecting a proper amplitude parameter (e.g. area under the rectified curve), the non-reproducible contents of the signal is eliminated or at least minimized.

Raw EMG signals can range between +/- 5000 microvolts and typically the frequency contents ranges between 6 and 500 Hz, showing most frequency power between 20 and 150 Hz. However, in practical applications, EMG signals are amplified and typically read in the millivolts range.

Most myoelectric control schemes use macro-features of the surface EMG, that depend on the neural and peripheral information contained in the signal, their perfor-

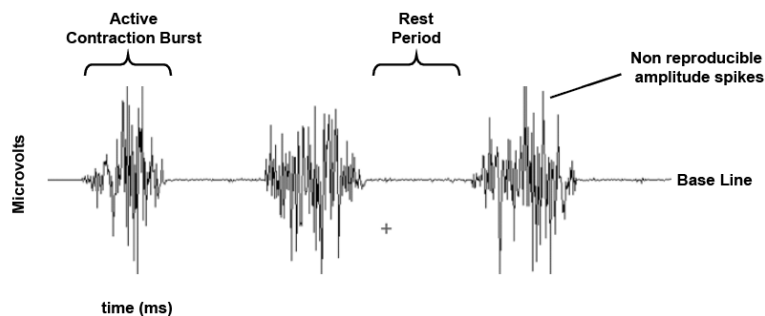


Figure 2.3: A sample raw EMG recording of 3 contraction bursts [38].

mance is influenced by factors that can affect the motor unit action potential shapes [1]. Some of these factors that can influence surface EMG are the following:

1. Tissue Characteristics - the human body is a good electrical conductor, but unfortunately the electrical conductivity varies with tissue type, thickness, physiological changes and temperature. These conditions greatly vary from subject to subject which can prohibit a direct quantitative comparison of EMG amplitude parameters calculated on the unprocessed EMG signal [38].
2. Crosstalk - neighboring muscles (not directly in contact with the electrode) may also produce significant amount of EMG. This can contaminate the target muscle under investigation with signals from other sources.
3. Electrode and Muscle Displacement - in any movement related studies, movement of electrodes, cables and connectors are unavoidable. Any change in distance between the target muscle (signal origin) and the electrode (detection site) will alter the EMG reading. Motion artifacts can also contribute to unwanted noise in the low frequencies (less than 10 Hz).
4. External Noise - special care must be taken in noisy electrical environments. One such noise is the 50 or 60 Hz noise coming from AC power outlets which power many of the hardware and appliances. Incorrect or poor grounding of the EMG devices or other external devices may also contribute as external noise.
5. Electrode and Amplifiers - the selection of the types of electrode and amplifiers is very crucial. Internal amplifier noise should not exceed 5 Vrms. Many hardware factors can be minimized or avoided by accurately preparing and checking the given laboratory or room condition.

It is important to note, however, that factors influencing the EMG signal features are not necessarily always detrimental for myoelectric control. For example, the effects of external known noises sources can be removed with proper filtering settings. For crosstalk, as long as this is consistent across conditions, then its presence may not necessarily be detrimental. In pattern recognition, for example, a specific gesture to be classified may be characterized by a set of EMG recordings from different muscles, all influenced by a certain amount of crosstalk. Nonetheless, if the activity containing

crosstalk is consistent across trials of the same task, task classification can be performed correctly and actually crosstalk may even become a source of information to better differentiate the tasks [1].

2.1.2 Myoelectric control strategies

Myoelectric control uses the EMG signal as the input control signal to command external devices, such as robot assistive devices and prostheses. The ideal condition for myoelectric control is the availability of EMG signals that can be controlled independently and concurrently in a sufficient number to match the number of DOFs to be controlled (*direct control*). In this situation, each EMG channel is used as the only control signal for one DOF each. For example, two EMG channels would be needed for the bidirectional control of each DOF. This can be controlled proportionally, such as using the amplitude or power of the EMG, given the association between power or intensity of muscle activity and the neural activation.

However, *direct control* is often not possible in vast majority of amputees or when a large number of DOF needs to be controlled. Correspondence problem, where the physical structure of the human hand (healthy or amputee) is vastly different from the robot, is also an issue with *direct control*. Pattern recognition or other control strategies are often the solution to dealing with this problem. These use the full information of the multi-channel EMG recordings and mapping it into predefined tasks.

We list some of the commonly available myoelectric control strategies:

1. **On/Off Control** - is achieved by mapping muscle activity to the required output function (e.g. open and closing function of a prosthetic hand). In this method, one function is assigned to one channel of surface EMG. For each processing interval, the EMG amplitude is compared with a predefined threshold and, when the threshold is exceeded, the corresponding function is actuated at a fixed speed, or proportionally to a filtered-EMG amplitude. With the use of multiple signal sites, different functions are assigned to different channels, with the aim of obtaining a direct control. This approach can provide intuitive control, as the control sites can be selected so that the intended function corresponds to the physiologically appropriate muscles. It is, however, impractical for high level limb deficiencies and slow and counterintuitive in controlling multiple joints.

2. **Pattern Recognition-based Control** - uses the full information of the multi-channel EMG recordings and mapping it into predefined tasks. By using multiple EMG sites, effective feature extraction, and multidimensional classifiers, control of several classes of motions can be achieved. The robustness of the resulting control scheme is dependent on robust input features, type of classifiers and a training set representative of the full set of inputs used during interaction. However, despite the success of pattern recognition-based myoelectric control, this type of strategy is inadequate for actuating all the functions offered by the robotic devices as it uses a sequential strategy where only one class of movement is active at a time [39]. Also, natural hand movements are not limited to a set of discrete gestures but are continuous, coordinated and have simultaneous control of multiple DOFs.
3. **Simultaneous and Proportional Control** - when a user can control at least one mechanical output quantity of an active joint (e.g., force, velocity, position) within a finite, useful, and essentially continuous interval by varying the EMG control input within a corresponding continuous interval [29]. This type of control is often times also called as *regression-based* myoelectric control, where regression methods are often used to identify system parameters from a given training set of continuous outputs. Multiple DOFs can be controlled at the same time using EMG inputs in a continuous fashion.
4. **Muscle Synergy-based Control** - requires identification of complex interactions between multiple muscles, commonly referred to as muscle synergies, in the control of multiple DOFs using EMG inputs. Linear combinations of synergies, for example, are capable of describing complex force and motion patterns in reduced dimensions. Thus, robust representations of synergies within a multifunctional control scheme contribute to reliable processing and robust outputs consistent with a users intent [27].

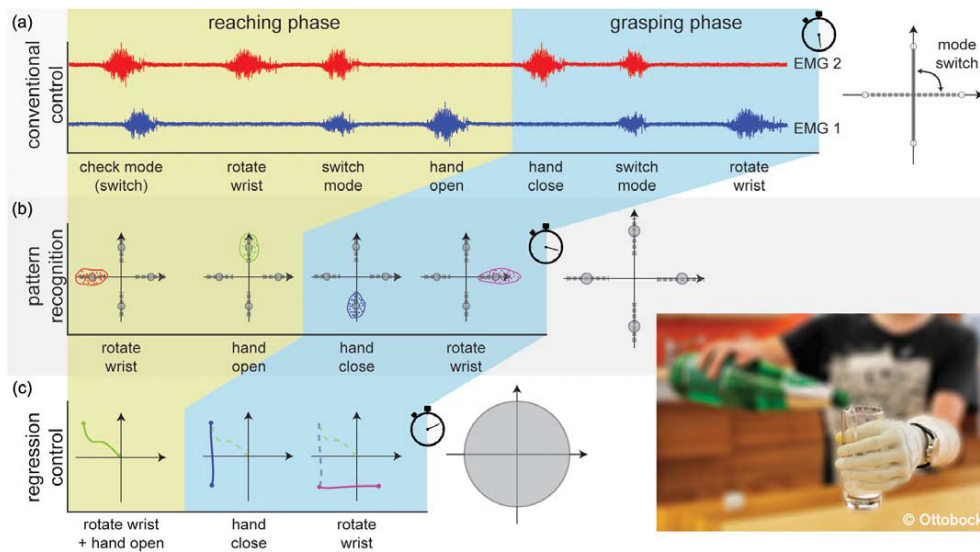


Figure 2.4: Illustrations of myoelectric control paradigms in a simple prosthetic task [1]. (a) On/Off control. (b) Pattern recognition-based control. (c) Simultaneous and proportional control.

A schematic illustration of three myoelectric control strategies when performing a simple functional task with a powered prosthesis is shown in Figure 2.4. This figure was taken from [1]. The task consists of grasping a glass and drinking from it. In Figure 2.4a, two DOFs are controlled by only two EMG signals. The same two signals are used for both DOFs and the system switches from one DOF to another by coactivation of the two muscles. The task is performed in a sequential manner between two DOFs and switching between them. The same task is shown in Figure 2.4b, but now performed using pattern recognition-based control approach. A 2-dimensional feature space is shown for easy visualization, with four classes corresponding to activating in two directions the two DOFs. Figure 2.4c shows a simultaneous and proportional-based control that allows combining DOFs (represented by the two axes) in any combination and thus performing the task in a more natural and faster way.

The main problem with the pattern recognition-based control is that it is inherently a control scheme that is quite different from natural control. In natural control, movements are continuous and there is coordination among multiple DOFs across several joints simultaneously. Most often times, the parameter space that models natural movements in EMG, kinematics or kinetics studies is continuous. On the other hand,

for pattern recognition-based control, the number of patterns are limited and are activated sequentially, only one at a time. This limitation underlines the need for methods that can realize simultaneous and proportional control of multiple DOFs. In particular, deployment of simultaneous and proportional control strategies for multiple DOFs remains one of the major challenges for next-generation prosthetic systems [30, 40].

There are studies that have tried to build continuous models to decode arm motion from EMG signals. The Hill-based muscle model, for example, is often used to estimate muscle force from EMG and other muscle anatomical properties [25, 41, 42]. However, only a few DOFs (≤ 2) were analyzed, since the nonlinearity of the model and the large numbers of unknown parameters for each muscle make the analysis quite complex. Many of these muscle parameters also rely on anatomical and physiological properties which may vary distinctively across subjects. As an alternative to this, a data-fitting approach is often considered since parameters are obtained from the data. Regression models such as using a neural-network model, is commonly used to extract continuous upper-limb arm motion using EMG signals [43], however, movements were quite restricted to single-joint, isometric motions. Only Artemiadis and Kyriakopoulos have considered synergistic relationship between arm kinematics and muscle activation by attempting to use a framework based on low-dimensional embeddings to control a robotic arm end-effector position in 3D space using a 2D representation of EMG signals [44]. Even though the study in [44] have proposed using low-dimensional embeddings, the number of controllable DOFs have not exceeded 4 DOFs and coordinated multi-finger joint movements have not been considered.

More closely related to the topic of this thesis, some studies considered modeling the human hand along with simulating different hand motions and gestures. The human hand consists of a remarkably complex musculotendon structure designed to maximize power and dexterity while minimizing mass and bulk of the hand [45]. A total of 39 extrinsic and intrinsic muscle units control the movements of about 27 bones in each hand [45], which about 25 DOFs are available to generate sophisticated finger and wrist movements.

Anatomically realistic biomechanical models for the index finger and thumb have been studied. Valero-Cuevas et al. modeled the finger as a series of kinematic chain and whose intrinsic and extrinsic extensor muscles interconnection is viewed as a tendinous network [46, 47]. Among some of their models include a 4-DOF and 7-muscle model

for the index finger [48–50] and a 5-DOF and 8-muscle model for the thumb [51]. To show how these seemingly simple model can be quite complex, it can take about 50 or more anatomical muscle parameters to generate a biomechanically realistic thumb movement. These studies have made tremendous and critical advances towards understanding force transmission and coordination in the finger. However, due to the high dexterity of the finger, a limited number of tasks have been assessed. This has led to gaps in the ability to provide accurate predictions or estimations for the wide range of manual tasks can be performed with the hands.

In using such biomechanical models for myoelectric control, however, the forward dynamics which are driven by the activation levels of each muscle, which computes a muscle's net force (e.g. using a Hill-based muscle model [52]) often requires knowledge on anatomical properties. These properties which can be drawn from literature but may not match well with a corresponding finger kinematic model [46] Optimization over a large number of musculoskeletal parameters is also often done to find a good fit of the model based on experimental measurements [51,53]. Not to mention, that many of these finger musculoskeletal models do not consider muscle co-contractions or synergistic relationships. Because of the complexity of using biomechanical models of the fingers, a data-fitting approach using machine learning is often preferred for real-time myoelectric control and estimation of kinematics or dynamics. Using machine learning techniques can do such good performance without knowing a large number of physiological parameters.

Decoding finger movement from sEMG signals usually involves dealing with high-dimensional signals in both the input and output domains [40] and the kinematics involved are highly nonlinear [14]. In Chapter 2.3, we present some of the recent studies more closely related on decoding finger kinematics from EMG signals.

2.1.3 Characteristics of an ideal myoelectric control system

Ideally, a system for upper limb myoelectric control should fulfill all the criteria shown in Figure 2.5. Farina et al. recommended these criteria for robot prostheses as a guide for improving design and control of such devices [1]. They enumerate that an ideal upper limb myoelectric prosthesis or support should be intuitive, capable of multi-DOF control, robust, adaptive to the user, easy to set-up, fast calibration, provide feedback, limited computation complexity and reliably accurate. None of the current myoelectric



Figure 2.5: Criteria of an ideal myoelectric controller as described by Farina et al. [1].

devices in the commercial and academic community possess all of these traits. In this study, we have focused on satisfying some of these criteria. In particular, this study attempts to explicitly satisfy some of the mentioned requirements or at least implicitly discuss some of these issues in the later chapters.

To realize a more intuitive and easy-to-calibrate myoelectric control scheme, strategies based on proportional and simultaneous control are preferred over other conventional control scheme. Going into this direction, this thesis aims to estimate simultaneous and multiple finger kinematics from surface EMG signals, which is covered in the next chapter. In the succeeding chapters, we put a special attention on estimating, mapping and recovering information to as many DOFs available in the hand. This gives emphasis to the criteria of being natural, which has the potential to fully maximize the functionality of many current myoelectric-based hand controller applications.

Recently, one myoelectric control strategy that has been quite popular is the so-called *synergistic control*. We explain the notion of *synergy* in the next section and present one more myoelectric control strategy as a subsection in the next part. In the later chapters of this we present a new framework for myoelectric control using a new nonlinear and shared synergistic representation of hand and finger movement approach. It is shown in this thesis that using a shared synergistic approach can handle not only the nonlinearities of human hand motion but also handle correlations that exist in the hand and finger's high DOF.

2.2. Synergies

Muscle synergies are studied extensively in neurophysiology as a potential basis for neural control. Multiple studies support the hypothesis that the human motor system directly initiates movement through flexible combinations of muscle synergies [11–13, 54–57]. The muscle synergy hypothesis claims that the human motor system directly initiates movement through flexible combinations of control modules recruited by the central nervous system to simplify control. Similarly, the concept of synergies have also been widely used in the field of robotics, where robot control laws are expressed in low-dimensional space to drive forces applied on the higher dimensional robot space. In motion planning for example, synergies can often reduce complexity, where searching for an adequate kinematic configuration can increase exponentially with the dimensionality of the structure [14]. For hand grasping, it has also been consistently shown that functional human hand postures operate in a configuration space of much smaller dimensions, often referred to as postural synergies, than what the kinematic structure would suggest [15]. Thus, synergies can provide a natural modeling paradigm where muscle activation inputs and high-dimensional joint kinematics can be represented in low-dimensional space, where common latent features are shared. Estimating finger kinematics from EMG input signals usually involves highly correlated patterns and high dimensionality in both the input and output domains. Nevertheless, few studies have given attention in considering such correlations in doing simultaneous and proportional control of the high dimensional finger kinematics from EMG signals.

This thesis is inspired by studies in the motor control community that claims that synergistic patterns can be observed in the muscle coordination and posture space. Grinyagin et al. [58] presented different types of synergies. First, static postural synergies, that refer to correlated models between single kinematic poses. Second, kinematic synergies, that consider time dependent correlation during a motor action task [59]. Lastly, muscle synergies that uses recruited muscle coordination patterns from electromyographic (EMG) activity to address low level representations of motor control [12, 13, 60]. While only the third type of synergy have been largely used in the motor control community, the first two types have inspired a lot of work in robotics [14].

2.2.1 Synergies in robot grasping

As the number of DOFs of robotic hands starts to approach the capabilities of the human hand, effective autonomous algorithms that can handle high-dimensional configuration spaces are required in order to take advantage of the new robot hand designs. It has been pointed out in the field of robotics that if human-like grasping is intended to be reproduced in robot hands, then it would seem natural to draw inspiration not only from the hardware of the human hand but also from the software; that is, the way the hand is controlled by the brain.

Attempts to formalize human tendency to simplify the space of possible grasps can be traced back as early studies involving grasp taxonomy work in robotics [61]. While the configuration space of dexterous hands is high-dimensional and very difficult to search directly, these studies show that most useful grasps can be found in the vicinity of a small number of discrete points. These points can be thought of as pre-grasp shapes, or starting positions for finding a good grasp for a new object.

Ciocarlie et al. proposed the use of low-dimensional posture subspace for the automated grasp synthesis in complex robotic hands [62]. They presented an intuitive approach by replacing the discrete set of pre-grasp shapes with a continuous subspace derived from analysis of human hand motion during grasping. In their work, they describe that any hand posture is fully specified by its joint values, and can therefore be thought of as a point in a high-dimensional joint space. If d is the number of DOF of the hand, then a posture \mathbf{p} can be defined as:

$$\mathbf{p} = [\theta_1 \ \theta_2 \ \dots \ \theta_d] \in \mathbb{R}^d \quad (2.1)$$

where θ_i is the value of the i -th DOF.

As what has been suggested in previous studies, most grasping postures derive from a relatively small set of discrete pregrasp shapes. This would imply that the range of postures used in everyday grasping tasks will exhibit significant clustering in the d -dimensional DOF space. Santello et al. [59] verified this hypotheses by collecting a large set of data containing grasping poses from subjects that were asked to shape their hands as if they were grasping a familiar object. Principal component analysis (PCA) of their data revealed that the first two principal components account for more than 80% variance, suggesting that a very good characterization of the recorded data can be obtained using a much lower dimensionality approximation of the joint space.

In Ciocarlie et al.'s work [62], they referred to the Principal Components of these postures as *eigengrasps*. Each synergies or eigengrasp \mathbf{e}_i is a d -dimensional vector which can be thought of as direction of motion in the joint space. Motion along one eigengrasp direction will usually imply motion along all DOFs of the hand.

$$\mathbf{e}_i = [e_{i,1} \ e_{i,2} \ \cdots \ e_{i,d}] \quad (2.2)$$

By choosing a basis comprising b eigengrasps, a hand posture placed in the subspace defined by this basis can be expressed as a function of the amplitudes a_i along each eigengrasp direction:

$$\mathbf{p} = \sum_{i=1}^b a_i \mathbf{e}_i \quad (2.3)$$

which is completely defined by the amplitude vector $\mathbf{a} = [a_1 \ \cdots \ a_b] \in \mathbb{R}^b$.

Synergies have also been used as a representation that transcends differences in embodiments, which is also called the correspondence problem. This problem, also referred to as *Mapping* in Figure 2.6, deals with transferring postures or movements from one agent to another. This can be viewed as mapping human postural space \mathbf{Y}^h to robot space \mathbf{Y}^r . This can also be viewed as the eigengrasp to robot correspondences $\mathbf{X} \rightarrow \mathbf{Y}^r$. This type of synergistic representation are often used to address inherent problems related to high-dimensional representation.

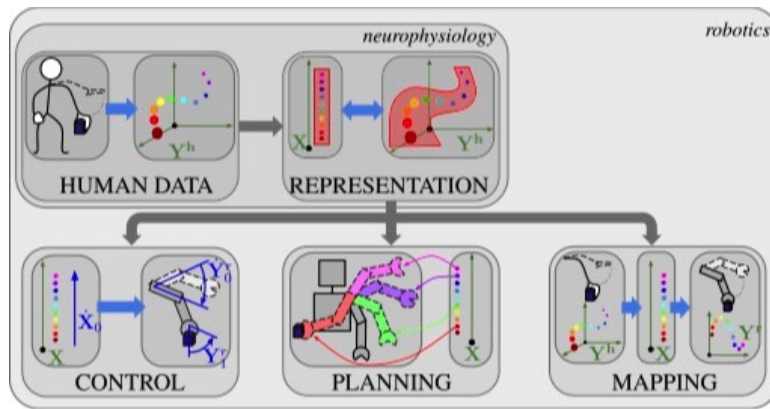


Figure 2.6: Low-dimensional representation of human posture data has been used for control of dynamic movement in robots (*Control*), search for suitable poses (*Planning*), and transferring kinematic actions (*Mapping*) [14].

2.2.2 Synergies in myoelectric control

Control schemes associating synergies with control outputs can generally be grouped into two approaches: *pattern recognition* and *motor learning*. In pattern recognition-based control, estimation models are trained via pattern recognition techniques to mimic intent based on existing synergies. While in motor learning-based control, the motor system is trained to develop and refine synergies associated with system dynamics of a specific mapping function relating EMG inputs with control outputs. The user learns the system dynamics via feedback while interacting with the control interface (see Figure 2.7).

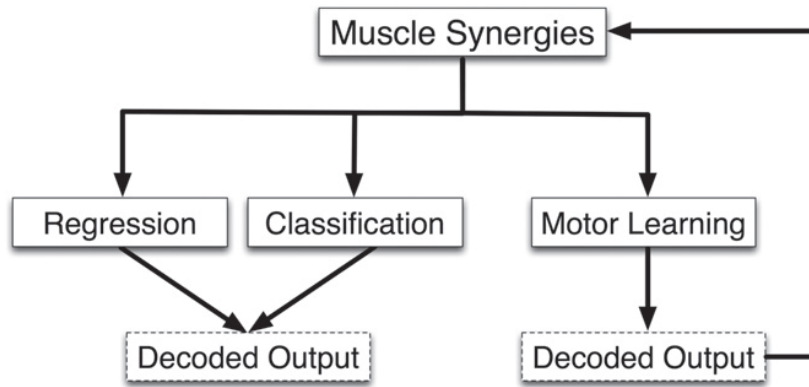


Figure 2.7: Myoelectric control schemes based on synergy representations [27]. Regression and classification schemes decode outputs based on existing synergies, disregarding any adaptations due to feedback. On the other hand, motor learning schemes incorporate feedback into the development of new muscle synergies to generate robust controls.

There is an ongoing debate between the two theories [63], and perceived muscle synergies cannot currently be proven or disproven to have a neural origin [64]. Regardless of neurological origin, muscle synergies are influential in myoelectric control schemes due to EMG inputs directly encoding muscle activation timing, shape and intensity. Synergy features extract information from multiple EMG channels simultaneously to depict time-invariant synergies representing the underlying muscle coordination behind various motor tasks. By identifying relative activations between synergistic muscles, synergy features have been shown to be inherently robust to single channel electrode shift and amplitude cancellation [39, 65].

Although time-variant synergies have been widely used and discussed to model complex movements, in this section we only discuss about time-invariant synergies. Further discussion about time-variant synergies is given in [66]. Two common types of time-invariant synergy extraction methods are based on linear decomposition methods such as using the *Non-negative matrix factorization* and *Principal component analysis*.

1. Non-negative matrix factorization (NMF) - is the most common method for extracting time-invariant synergies. NMF prescribes a synergy subspace restricting expressible data points to combinations of each non-orthogonal component [27]. Synergy components are constrained to be non-negative, which physiological represents neural and muscle output, since neurons are either firing action potentials (positive) or else in a resting state (zero).
2. Principal component analysis (PCA) - describes the major orthonormal activation patterns without imposing constraints within the space defined by the components. A similar explanation is given in Chapter 2.2.1, but instead of getting eigengrasps, here muscle synergies based on linear combinations of EMG channels are obtained.

Although NMF and PCA are similar in their underlying concept and mathematical representations, NMF has a much stricter nonnegative constraint imposed on it. Both methods, however, are linear decomposition techniques that assume that the set of measured EMG data is composed of linear combinations of a smaller number of underlying elements called synergies. This linear representation can be modeled as:

$$\mathbf{m} = \sum_{i=1}^N \mathbf{c}_i \mathbf{w}_i \quad (2.4)$$

where \mathbf{m} is a vector that represents multiple EMG channels, \mathbf{w} contains the synergies or basis functions and \mathbf{c} represents each activation of each component to the measured muscle activation patterns. See Figure 2.8 to visualize this relationship.

An example of simultaneous control of multiple DOFs was shown by Jiang et al. using muscle synergy strategies extracted from a modified NMF algorithm to estimate the torque [28] and kinematics [26, 67] of multiple DOFs produced at the wrists.

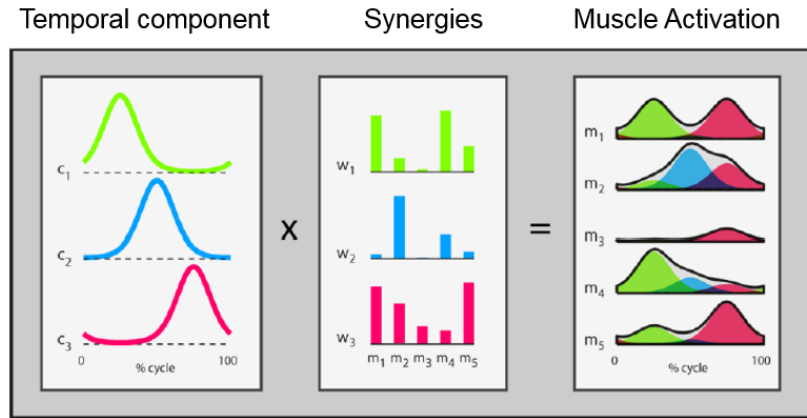


Figure 2.8: Time-invariant synergies capture spatial regularities in the motor output.

Nazarpour et al. [68] analyzed motor learning in the context of muscle synergies using cursor position control tasks. They defined a task space that requires simultaneous control of a pair of muscles to achieve a task, and test subjects on different combinations of biomechanically independent and antagonistic muscles. By examining user reactions to virtual perturbations in cursor position, they demonstrated the ability of humans to learn flexible control through the formation of dynamic, task-specific muscle synergies. They quantified these synergies in terms of inferred muscle correlation structure from variance in cursor position.

Ison and Artemiadis [65] analyzed synergy development during long term control of cursor velocities via two biomechanically independent pairs of antagonistic muscles. The synergy development was evaluated by analyzing changes in PCA across trials. Unlike in [68], redundant velocity control did not force specific synergy development in order to accomplish a task. Therefore, the resulting population-wide convergence to a common synergy space indicated the natural evolution of synergies while interacting with a particular mapping function. The synergies proved to be robust to potential electrode shifts and time off during the multi-day evaluation, and correlated with enhanced control efficiencies during interaction with the myoelectric interface.

In relation to synergistic representation in finger movements, in Ingram et al.'s [69] study on natural hand movement, they found that a substantial part of variation in daily hand activities (60% variance) could be explained by a 2D manifold using PCA on the finger joint angular velocity data.

2.3. Mapping finger kinematics from EMG

Many studies have shown that regression-based myoelectric control methods can be used to estimate simultaneous and proportional finger kinematics from EMG. Afshar and Matsuoka were able to estimate the index finger joint angles from fine-wire EMG embedded inside seven muscles that control the index finger [70]. Similarly, Shrirao et al. were able to decode one index finger joint angle from surface EMG signals. The finger motions involved in their study were periodic flexion-extension movements at three different velocities. They evaluated different groups of artificial neural network but failed to get a consistent robust optimal configuration. Furthermore, Smith et al. [23] were able to asynchronously decode individual metacarpophalangeal (MCP) joint angles of all five fingers using an artificial neural network (ANN). Their study extracted time-domain features from 16 general muscle locations in the forearm from healthy subjects.

In more recent developments, Hioki et al. [24] estimated five proximal interphalangeal (PIP) joint angles using only 4 EMG channels while also considered some dynamical relationship between EMG and the finger actuation by adopting time delay factors and feedback stream into an ANN. Their method, however, has complex parameter configuration that drastically varies across different EMG and subject settings. In other recent EMG-based estimation of finger movements, Krasoulis et al. [40] evaluated different regression methods to find superior performance in decoding multiple DOF finger movement from EMG.

In the previous studies mentioned [22–24], a time delay between the onset of the EMG signal and exerted movement was present and observed. This time delay is called hysteresis or electromechanical delay (EMD). In doing regression to map the muscle activation to the corresponding joint actuation, introducing EMG-tapped delay lines, which makes use of all the immediate and past values of the EMG can consider for this delay. However, doing so greatly increases the dimension of the inputs and thus exponentially increases the number of parameters of the regressor used. The EMD can vary depending on many different factors such as muscle shortening velocity, type of muscle fiber, and fatigue [25].

In the next chapter, we present our method and results where our study aims to overcome the above limitations by introducing EMD as a parameter, by using a so-called EMG-to-muscle activation model [25,71], which is determined along other system pa-

rameters through optimization. Very few studies have continuously estimated more than five finger positions. Here, we present a method for the continuous extraction of control information during finger movements which involves simultaneous activation of 15 DOFs provided by all five finger joints. We concurrently recorded kinematics of all five fingers in one hand and the surface EMG signals from muscles in the forearm while the subjects performed both individual and simultaneous finger flexion and extension tasks. Simultaneous estimation of the finger kinematics is done and evaluated using both a fast feedforward artificial neural network and a nonparametric Gaussian Process regression [72], with the latter having the potential to give better estimation performance.

In Chapter 4 we present a proposed framework based on synergistic representation to overcome the limitations of simultaneously estimating only a few DOFs. As previously mentioned, the use of synergies in myoelectric control is not new and have been used to estimate wrist torque [28] and kinematics [26, 73] and shown to be inherently robust to single channel electrode shift and amplitude cancellation [27, 39]. However, in all the previous studies, the number of estimated hand DOFs were limited, selection of dimensionality were heuristic and linear models still failed to represent motion correlation even in simple reaching and grasping movements [14]. No method has yet to give straightforward way of fully recreating the continuous movement of a high-dimensional full 23-joint hand model from EMG inputs, knowing that many of the dimensions are redundant and highly correlated.

To handle the nonlinear, high-dimensional and dynamic nature of finger kinematic posture and EMG, we resort to using a nonlinear dimensional reduction method, which is the Bayesian Gaussian Process Latent Variable Model (Bayesian GPLVM). In earlier studies, the use of a standard shared GPLVM framework has been successful in mapping between human silhouette and 3D poses [74], speech to facial motion data [75], and non-humanoid animation from human motion data [76]. In our earlier work [77], we modeled dynamic finger movement from surface EMG using a standard shared latent space representation method, however, the selection of dimensionality was heuristic. In Chapter 4, we describe a new strategy for handling the nonlinear, high-dimensional and automatic selection of dimensionality involved in the mapping of EMG inputs to hand pose kinematics.

Chapter 3

Continuous and simultaneous estimation of finger kinematics

Surface electromyography (EMG) signals are often used in many robot and rehabilitation applications because these reflect motor intentions of users very well. Despite the success of pattern recognition-based control of the hand, natural hand movement is continuous, coordinated and offers an infinite number of fine movement variations. Studies for proportional myocontrol of finger movements has been comparatively few. Though the use of time-domain EMG features have been tremendously successful in classifying hand gestures, these may not give optimal estimation performance in the case of proportional estimation because of inherent problems such as electromechanical delays (EMD). In this chapter, we present the use of an EMG-to-Muscle Activation model that parameterizes EMD for estimating simultaneous and multiple finger kinematics from multi-channel surface EMG signals.

Simultaneous and multiple finger joint positions, namely the metacarpophalangeal (MCP), proximal interphalangeal (PIP) and the distal interphalangeal (DIP) joints of all 5 fingers in a hand are mapped from EMG signals using a data driven approach using machine learning regression techniques. In this chapter, we have compared both the performance of using a fast feed-forward artificial neural network (ANN) and a nonparametric Gaussian Process (GP) regressor to estimate complex finger joint kinematics from muscle activation inputs. The results presented in this chapter demonstrates a potential myoelectric control strategy that can be applied for simultaneous and continuous control of multiple finger DOF(s) in robotic devices.

3.1. Inherent problems of electromechanical delay

For any intended motor action, it is known that there occurs a time delay, which is known as the *electromechanical delay* (EMD), between the onset of the EMG signals and the exerted mechanical output such as force and tension produced in the movement. EMD is also termed motor time or motor execution time in researches related to fractionated reaction time [78].

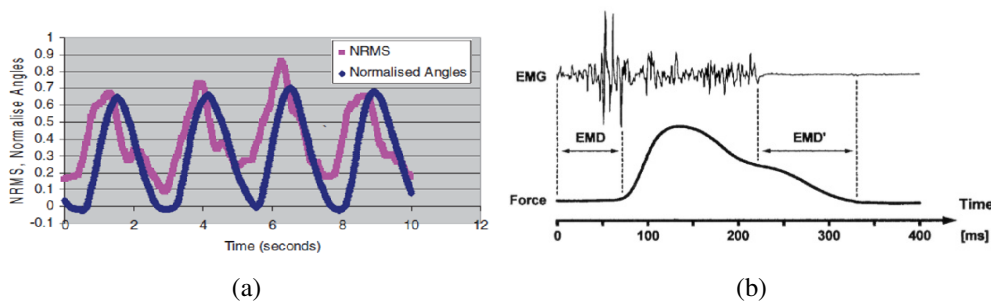


Figure 3.1: Examples of the electromechanical delays are shown as the time difference between EMG and the onset of force or actuation. (a) Time delay between the root-mean-square windowed EMG and the normalized recorded finger joint angle. (b) The EMG and force are measured from the soleus and achilles tendon of a cat, respectively. A delay of about 70 ms was found between the two measurements.

The EMD was originally found in locomotion studies in animals that used EMG measurements. Figure 3.1b shows the EMG signal from the soleus of a cat during gait. The force was measured directly from the achilles tendon. Notice that the EMG starts about 70 ms prior to force and that the EMG ends about 70 ms before the force ends. EMD has also been presented and observed by previous studies in EMG related studies involving human leg and arm motions [22, 25]. A sample is shown in Figure 3.1a. The normalized filtered EMG signal (pink) leads the recorded joint angle (blue), as EMG occurs first before force production of the task. EMD has been reported to range from 10 ms to about 150 ms, but varies differently depending on the muscle fiber type, muscle length, fatigue, training, and speed of the intended task [79].

EMD presents a challenging problem that must be resolved if valid and meaningful relationships between EMG and force, moment, or movement patterns are to be established [79]. Studies have shown that EMD varies differently and changes with certain

pathology. Relatively short EMD has been observed in patients with cerebral palsy, while prolonged EMD were seen in *anterior cruciate ligaments* or more commonly known as ACL reconstructions [78]. However for cases under normal conditions, or in studies with healthy subjects, constant EMD values has often been used to temporally align EMG and force or movement related time profiles during recorded activities.

Vint et. al. concluded in their study that EMD approached a relatively constant value regardless of initial tension levels and rate of force requirements [79]. They suggested that the temporal alignment of the EMG and force or kinetic data is mainly influenced by the state of pretension and the rate of force development. They suggests that incorporating a constant temporal offset to align EMG and kinetic data may be reasonable if the actions of interest are performed from nonresting conditions or if the rate of force development is relatively fast. The value of the assumed EMD should be determined in a manner that seeks to replicate the conditions under which the kinetic data will be collected.

Thus, EMD cannot be ignored in EMG studies involving motor actions, and must be considered accordingly.

3.2. EMG-to-muscle activation model

To learn a suitable filtered signal that automatically considers EMD, we introduce the use of a so called EMG-to-Muscle Activation model. EMG is a measure of electrical activity that spreads across muscles, which causes the muscles to activate. This results to the production of force, to which the model used transforms the EMG signals to a suitable force representation. A raw EMG signal is a voltage that is both positive and negative, whereas muscle activation is expressed as a number between 0 and 1, which is smoothed or filtered to account for the way EMG is related to force [25].

Zajac modeled this muscle activation dynamics using a first-order recursive filter [80]. Although a first-order differential equation does a fine job of characterizing activation, Buchanan et. al. created a second-order model filter that works efficiently to model the relationship between EMG and muscle activation [25]. Because the muscle fiber is activated by a single action potential, the muscles generate a twitch response and this type of response is well represented by a critically damped linear second-order

differential system to determine neural activation $u(t)$:

$$u(t) = M \frac{de^2(t)}{dt^2} + B \frac{de(t)}{dt} + Ke(t) \quad (3.1)$$

where M , B , and K are constants that define the dynamics of the second-order system. Because in the lab setting, the data are sampled at discrete time intervals, we make use of their filter in its approximate discrete version given by:

$$u_j(t) = \alpha e_j(t-d) - \beta_1 u_j(t-1) - \beta_2 u_j(t-2) \quad (3.2)$$

where $u_j(t)$ is the so-called neural activation, and $e_j(t)$ is the normalized, rectified and filtered EMG of muscle j at time t . In this model, α , β_1 , β_2 are recursive coefficients of the filter and d is the EMD. Filter stability is guaranteed by putting constraint conditions on α , β_1 , and β_2 .

$$\beta_1 = \gamma_1 + \gamma_2 \quad (3.3)$$

$$\beta_2 = \gamma_1 \cdot \gamma_2 \quad (3.4)$$

$$|\gamma_1| < 1, |\gamma_2| < 1 \quad (3.5)$$

$$\alpha - \beta_1 - \beta_2 = 1 \quad (3.6)$$

In the filter model, neural activation depends not just on the current level of EMG, but also on its recent history, or the last values of $u_j(t)$. Here, the value for the neural activation is constrained from 0 to 1.

Also because studies have also shown that while some muscles have linear isometric EMG-to-force relationship, the relationship for other muscles is nonlinear. To model this nonlinearity between neural activation and muscle activation, the transformation to the muscle activation v_j is then given by:

$$v_j = \frac{e^{A_j u_j(t)} - 1}{e^{A_j} - 1} \quad (3.7)$$

where A_j is a parameter that introduces the nonlinearity between EMG and muscle activation, and is constrained between -3 and 0 , with -3 being highly exponential and 0 being linear. The effect that the parameter A_j has on the muscle activation in terms of the neural activation is described by Figure 3.2.

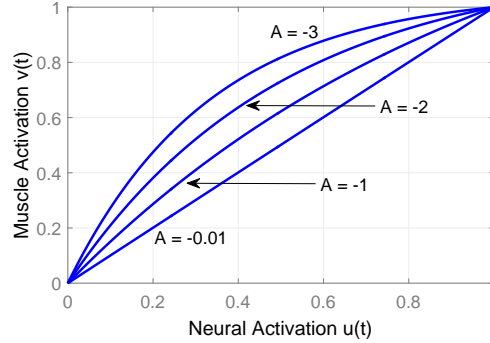


Figure 3.2: The parameter A introduces nonlinearity between the neural activation and muscle activation.

Using the model discussed, the pre-processed EMG is transformed to its muscle activation dynamics, the converted signal is now suitable and can be used as a continuous input to a regressor. The transformation from the raw EMG to its pre-processed filtered form then to its muscle activation is seen in Figure 3.3.

The EMG-to-Muscle Activation model not only solves the EMD of the muscle, but also requires only a few parameters. The parameters of this filter, γ_1 , γ_2 , d , and A are obtained by using constrained nonlinear programming in Matlab's Optimization Toolbox to minimize a mean-square error cost function:

$$\frac{1}{N} \sum_t (\theta_{est} - \theta_{target})^2 \quad (3.8)$$

where N is the total number of samples, and θ_{est} and θ_{target} are the estimated and measured finger joint angles, respectively. Aside from the constraints given in equations 3.3 to 3.6, the time delay parameter d is also constrained within its physiological limits, which is between 10 and 150 ms.

If we only want to map the EMG signals to a single finger's joint angles and if the training time needs to be really fast, then a linear estimation of the joint angles to obtain θ_{est} would suffice. However, EMG features were found to be nonlinearly related to kinematics. In Hahne et. al's work they showed that a polynomial fitting is needed to model the variance of EMG and the radial trajectories of a wrist movement [8]. They confirmed that using nonlinear regression methods or using nonlinear transformations of well established EMG features gave a superior wrist angle estimation performance

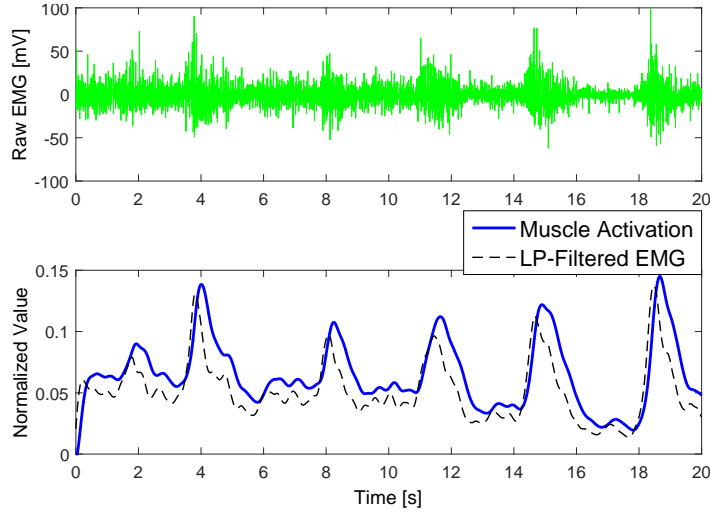


Figure 3.3: A sample raw EMG recording is low-pass filtered and converted to its muscle activation form.

compared to linear methods. Building on from their work and because there is no model that can clearly define the relationship between muscle activation and finger joint kinematics, in this study, we use a data fitting approach based on machine learning regression models. Namely, we resort to using an artificial neural network and a Gaussian Process as the nonlinear estimator.

3.3. Regression models

3.3.1 Artificial neural network

In general, artificial neural networks (*ANN* or *NN*, used interchangeably in this study) are considered to be attractive for nonlinear modelling because of their ability to approximate any arbitrary functions [81]. Because of this, we estimated all 15 joint angles of the fingers simultaneously and continuously using an ANN:

$$\theta_{est}(t) = \text{NN}(\mathbf{v}(t), \mathbf{w}) \quad (3.9)$$

where $\theta_{est}(t) \in \mathbf{R}^{15 \times 1}$ is the estimated finger joint angle, $\mathbf{v}(t) \in \mathbf{R}^{8 \times 1}$ is the muscle activation input, and \mathbf{w} are the weight parameters which represent the links between the nodes or neurons.

In our study, a multilayer feed forward network was used. The network is made up of an input layer, a hidden layer(s), and a single linear output layer (see Figure 3.4). Generally, the use of this type of ANN belongs to a class in machine learning called *supervised learning*. It is called in such a way because the training phase of the learning is carried out in a way that the ANN regressor has to learn how to associate each training input vector sample to an associated label called a *target output*.

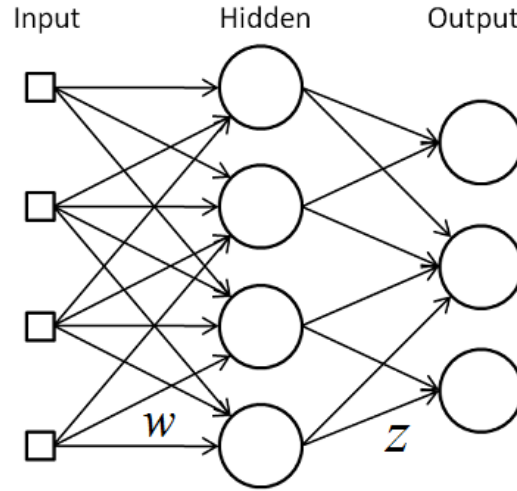


Figure 3.4: The architecture of a multilayer feedforward artificial neural network.

An ANN consists of a topological graph of neurons, with each neuron computing the activation function of the inputs and sends the result in the output layer. Suppose a set of input features is denoted by \mathbf{x} , then the first step to feedforward neural network is to transform the inputs corresponding to the weights and shift by a bias factor specific to each neuron given by a_j :

$$a_j = \sum_{i=1}^D w_{ji}^{(1)} x_i + w_{j0}^{(1)} \quad (3.10)$$

where the w_{ji} are the given weights of each neuron. Here we assume that we have a dataset D of n observations, denoted by $D = \{(x_i, y_i) \mid i = 1, \dots, n\}$. Then a_j is transformed using a select activation function such as *sigmoid* or *tan-sigmoid* activation function. In this thesis, a tan-sigmoid activation function given by z_j was used.

$$z_j = h(a_j) = \frac{e^{a_j} - e^{-a_j}}{e^{a_j} + e^{-a_j}} \quad (3.11)$$

Then the elements of the output (or target) vector \mathbf{y} is computed as:

$$a_k = \sum_{i=1}^M w_{kj}^{(2)} z_j + w_{k0}^{(2)} \quad (3.12)$$

$$y_k = a_k \quad (3.13)$$

It has been shown that for certain neural network topologies, with the right set of weights and biases, any continuous function can be accurately approximated [81].

The use of an ANN has two phases; a training phase and a test phase. During the training phase, the ANN is trained to return a specific output given a specific input. Training is done by presenting the ANN a set of training data and adjusting the parameters between each layer. The learning problem consists of finding the optimal combination of weights w_{ji} so that the network output approximates a given target output as closely as possible. To achieve this, the training algorithm tries to minimize a mean-square error between the target t and estimated output y values given by:

$$E = \frac{1}{N} \sum_i (y_i - t_i)^2 \quad (3.14)$$

In the test phase, the ANN returns the output based on the propagation of the input through all the layers.

In the scope of the thesis, the input layer had 8 nodes coming from the muscle activation of the each muscle, while the output has 15 nodes consisting of the finger joint angles. To train the network, we input a set of training data to the neural network and minimize a mean square error function. The most common way to minimize the error is through the use of a *backpropagation* algorithm. But since another method, such as the Levenberg Marquardt (LM) algorithm, appears to be the fastest method for training moderate-sized feedforward neural networks. In this thesis, we used the LM algorithm in Matlab's Neural Network Toolbox to train the model.

We evaluated the network's performance with various number of neurons in the hidden layer, ranging from 5 to 250. Using a fixed training set, we chose the specific number of neurons in the hidden layer based on which solution gave the smallest average error on an unseen test set. To avoid overfitting, total data set was divided into a training and a validation set and apply an early stopping method during training iterations [82].

3.3.2 Gaussian process for regression

In this study, we also evaluated the finger joint angle estimator performance when another general nonlinear estimator was used. We used a nonparametric Gaussian Process (GP) regressor shown in equation below:

$$\mathbf{y} = \text{GP}(m(\mathbf{x}), k(\mathbf{x}, \mathbf{x}')) \quad (3.15)$$

where \mathbf{x} is the input, \mathbf{y} is the estimated output coming from the dataset denoted by $D = \{(x_i, y_i) \mid i = 1, \dots, n\}$ and the GP is determined by a mean function $m(\mathbf{x})$ and covariance function $k(\mathbf{x}, \mathbf{x}')$. Relating this to the goal of estimating finger joint angles from EMG signal, we can substitute \mathbf{x} with \mathbf{v} which is the muscle activation input, with target \mathbf{y} with joint angle estimate θ_{est} .

The main reason why we introduced the use of another regressor, in the form of a more popular nonparametric Bayesian approach using Gaussian Process, is that we wanted to see if estimation of the small finger joint angles, namely the PIP and DIP finger joint angles, can be improved.

Gaussian processes regression is fundamentally different from feedforward networks. Rather than capturing regularities in the training data via updating neuron weights, it applies a Bayesian inference to explicitly compute a posterior distribution over possible output values y given all the data and the new input x [72, 83].

Formally, a GP generates data located throughout some domain such that any finite subset of the range follows a multivariate Gaussian distribution [84]. From an n observations in an arbitrary dataset, $\mathbf{y} = y_1, \dots, y_n$, can always be imagined as a single point sampled from some multivariate Gaussian distribution. Hence, such a data can be partnered with a GP.

Very often, it is assumed that the mean of this partner GP is zero everywhere:

$$m(\mathbf{x}) = 0 \quad (3.16)$$

What relates one observation to another in such cases is just the covariance function $k(\mathbf{x}, \mathbf{x}')$. A popular choice is a *Gaussian* or a *squared exponential* covariance function given by:

$$k(\mathbf{x}, \mathbf{x}') = \sigma_f^2 \exp \left[\frac{-(\mathbf{x} - \mathbf{x}')^2}{2l^2} \right] \quad (3.17)$$

where the maximum allowable covariance is defined as σ_f^2 . Here, σ_f and l are called *hyperparameters*. If $\mathbf{x} \approx \mathbf{x}'$, then $k(\mathbf{x}, \mathbf{x}')$ approaches the maximum covariance value, meaning the underlying function $f(\mathbf{x})$ is nearly perfectly correlated with $f(\mathbf{x}')$. Now if \mathbf{x} is distant from \mathbf{x}' , then $k(\mathbf{x}, \mathbf{x}') \approx 0$. So, for example, during interpolation at new x values, distant observations will have negligible effect. The hyperparameter l controls the effect of the separation between $f(\mathbf{x})$ and $f(\mathbf{x}')$.

Data are often treated with the consideration of noise. So each observation y can be thought of as related to an underlying function $f(x)$ through a Gaussian noise model:

$$y = f(\mathbf{x}) + \mathcal{N}(0, \sigma_n^2) \quad (3.18)$$

Generally, the problem defined for a regression is the search for the underlying function $f(x)$ that can best model the data D . To consider the noise into the covariance function, we can rewrite $k(\mathbf{x}, \mathbf{x}')$ as:

$$k(\mathbf{x}, \mathbf{x}') = \sigma_f^2 \exp\left[\frac{-(\mathbf{x} - \mathbf{x}')^2}{2l^2}\right] + \sigma_n^2 \delta(\mathbf{x}, \mathbf{x}') \quad (3.19)$$

where $\delta(\mathbf{x}, \mathbf{x}')$ is the *Kronecker Delta Function*. So given n observations of y , the objective is to estimate y_* and not the actual f_* , whose expected values are identical but with different variance due to the observational noise. To prepare the GP regression, the covariance function among all the possible points are calculated which we denote as the following:

$$K = \begin{bmatrix} k(x_1, x_1) & k(x_1, x_2) & \cdots & k(x_1, x_n) \\ k(x_2, x_1) & k(x_2, x_2) & \cdots & k(x_2, x_n) \\ \vdots & \vdots & \ddots & \vdots \\ k(x_n, x_1) & k(x_n, x_2) & \cdots & k(x_n, x_n) \end{bmatrix} \quad (3.20)$$

$$K_* = \begin{bmatrix} k(x_*, x_1) & k(x_*, x_2) & \cdots & k(x_*, x_n) \end{bmatrix} \quad (3.21)$$

$$K_{**} = k(x_*, x_*) \quad (3.22)$$

In GP modelling, the key assumption is that the data can be represented as a sample from a multivariate Gaussian distribution,

$$\begin{bmatrix} \mathbf{y} \\ y_* \end{bmatrix} \sim \mathcal{N}\left(0, \begin{bmatrix} K & K_*^\top \\ K_* & K_{**} \end{bmatrix}\right) \quad (3.23)$$

To estimate y_* , we are interested in the conditional probability $p(y_*|\mathbf{y})$, which means that given the training data \mathbf{y} , how likely is a certain estimation for y_* is. As explained more in [72, 84], the probability follows a Gaussian distribution:

$$y_*|\mathbf{y} \sim \mathcal{N}(K_*K^{-1}\mathbf{y}, K_{**} - K_*K^{-1}K_*^\top) \quad (3.24)$$

The predictive value for y_* is the mean of the probability distribution:

$$\bar{y}_* = K_*K^{-1}\mathbf{y} \quad (3.25)$$

and the uncertainty in the estimate is capture by its variance:

$$\text{var}(y_*) = K_{**} - K_*K^{-1}K_*^\top \quad (3.26)$$

The reliability of the GP regression is highly dependent on the chosen covariance function. A maximum posterior estimate of the hyperparameters \mathbf{w} (e.g. $\mathbf{w} = \{\sigma_f, \sigma_n, l\}$) occurs when the posterior probability $p(\mathbf{w}|\mathbf{x}, \mathbf{y})$ is at its greatest. Baye's theorem tells us that, assuming there is little prior knowledge about what \mathbf{w} should be, this corresponds to minimizing the negative log likelihood given by:

$$\ln p(\mathbf{y}|\mathbf{x}, \mathbf{w}) = -\frac{1}{2}\mathbf{y}^\top K^{-1}\mathbf{y} - \frac{1}{2}\ln|K| - \frac{n}{2}\ln 2\pi \quad (3.27)$$

Running a multivariate optimization algorithm (e.g. conjugate gradients), good choices for \mathbf{w} can be obtained [72].

In this thesis, GP regression was implemented using the Gaussian Process Regression and Classification Toolbox [85]. The EMG data was re-normalized and standardized to have the mean value of each feature equal to 0 and the standard deviation equal to 1. The input feature that we used was the 8-dimensional muscle activation feature vector as discussed previously in Section 3.2. The GP configuration used an assumed mean function of 0. The likelihood function was assumed to be Gaussian (with one hyperparameter σ_n), and the covariance function to be a squared exponential function, which takes two additional hyperparameters (a characteristic length-scale, l and unit signal standard deviation, σ_f) [72]. An exact inference method was used, and we optimize over the hyperparameters by minimizing the negative log marginal likelihood w.r.t. to the hyperparameters.

Unlike in the use of the ANN where one network produced all 15 joint angle outputs simultaneously, a dedicated GP regressor was created for each DOF. In the training

stage, 15 GP regressors were individually trained and then used to estimate simultaneous movements of all 15 DOFs. Also, because the learning from the log-likelihood involves the computation of the inverse of K , which is the covariance matrix whose complexity grows as the size of the input or output matrix increases. We used a fixed interval sampling to reduce the number of training samples which significantly reduces the hyperparameter learning and training time needed.

3.4. Methods

3.4.1 Experimental setup

The system is mainly composed of a wireless multi-channel surface electromyograph and a 3D optical motion capture device. Surface EMG signals, as well as the kinematics of unrestrained and continuous hand and finger movements, were simultaneously recorded.

Participants

Similar to contemporary studies that proposed new EMG-based control strategies for hand control [22–24, 26, 39, 40], healthy, able-bodied subjects participated in the experiments, which can be an initial basis before testing with disabled or amputated subjects. Ten healthy participants (7 male, 3 female, aged 27 ± 4 years), who gave informed consent to participate in the experiment protocol, volunteered in this study. The participants had no previous experience with myoelectric control nor with any 3D motion capture experiments.

EMG recording

For all the subjects, surface EMG signals were extracted from eight extrinsic muscles of the forearm that are known to contribute to wrist and finger movements. Four flexor muscles and four extensor muscles in the forearm were targeted. These target muscles along with their corresponding function related to any hand or finger movements are listed in Table 3.1.

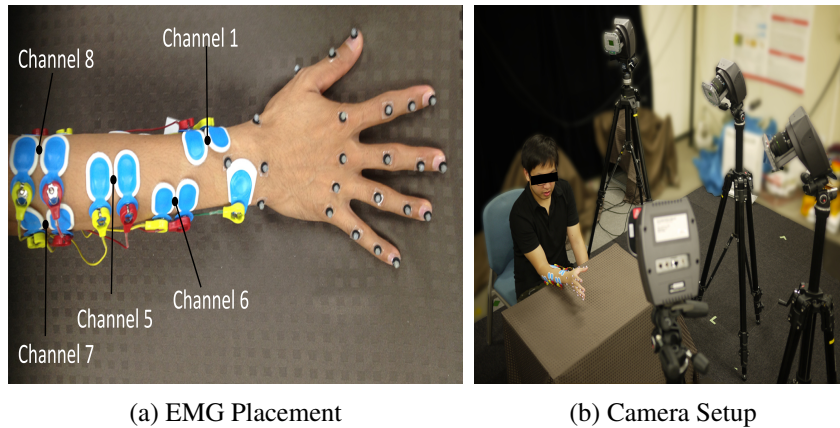


Figure 3.5: Experimental setup. (a) The surface EMG setup and the general view of EMG placement on a subject. The corresponding target muscle for each channel is shown in Table 3.1. (b) Overview of the 3D motion camera system.

Eight bipolar active-type Ag-AgCl electrodes from Ambu, with an average inter-electrode distance of 20 mm were placed on the the subjects as shown in Figure 3.5. The target muscles were mostly found by palpation, anatomical landmarks described in [86], and by visual inspection of the signal that gave the best response to describe the movements listed in Table 3.1. A single electrode was also placed on the subjects olecranon to serve as a ground and reference electrode. The surface electrodes were connected to a BA1104 pre-amplifier with a telemetry unit TU-4 (Digitex laboratory co. ltd.). The hardware provided a low-pass filter with cut-off frequency of 1 kHz during the EMG data acquisition process. The EMG signals were sampled at 2 kHz, and were digitized by an A/D converter with 12-bit precision. The EMG signals were displayed on a real-time monitor and visually inspected to ensure quality of the signal.

Finger kinematics recording

While finger movements were made, the hand and finger motion were recorded simultaneously using a MAC3D motion capture system (Motion Analysis Corp.). The camera set-up using the mounted Eagle cameras is shown in Figure 3.5b. Twenty-two passive reflective markers for motion capture were attached on the subject’s hand, with a marker located on each joint of the finger and three in the wrist area (see Figure

Table 3.1: Selected EMG channels and the target muscles

Channel	Target Muscle	Hand/Finger
1	Abductor pollicis longus	Thumb abduction
2	Flexor carpi radialis	Wrist, hand flexion and abduction
3	Flexor digitorum superficialis	2-5th finger PIP flexion
4	Flexor digitorum profundus	2-5th finger DIP flexion
5	Extensor digitorum	2-5th finger extension
6	Extensor indices	Index finger
7	Extensor carpi ulnaris	Wrist extension and abduction
8	Extensor carpi radialis	Wrist and thumb

Source: Anatomy and Kinesiology of the Hand [86].

3.5a). Small 6-mm diameter markers were used to reduce switching marker errors and to avoid getting the markers too close to each other. The optical cameras were positioned and calibrated to capture a volume ($500 \times 700 \times 500$ mm) space that would be able to effectively see and measure the small markers. The Cortex software from Motion Analysis was used to concurrently record the EMG and motion data. A sample skeleton model used in the marker data acquisition is shown in Figure 3.6b.

The marker trajectories were sampled at 200 Hz with measurement units in millimeters, having residual errors of less than 0.5 mm (as indicated during the Cortex calibration procedure). With the x , y , z positions of each marker continuously recorded, the joint positions, namely the MCP, PIP, and DIP joint angles, were calculated. Because the thumb does not have a DIP joint, the carpometacarpal (CMC) joint was considered before the MCP joint.

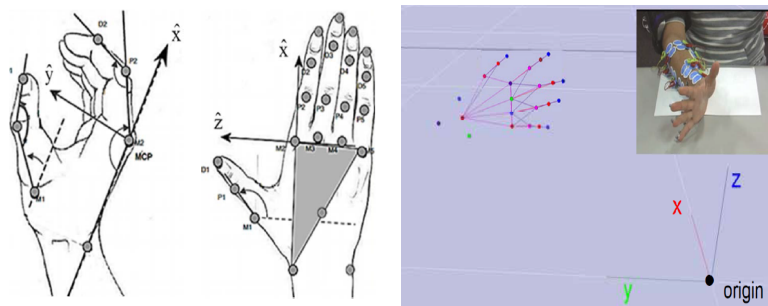


Figure 3.6: Marker placement and sample skeletal model of the hand.

3.4.2 Data collection

The participants, seated with their hand and elbow comfortably positioned on a flat surface table, were asked to do basic continuous finger movements. A demonstration of target finger movements as shown in Figure 3.7 were shown and instructed to the subjects. Because the main aim of the kinematic data is for estimation of continuous movement, all the subjects were asked to produce the movement rather than on exerting high forces. In this study, the set basic finger movements were different individual and multiple finger flexion and extension movements. These were selected from hand taxonomy and rehabilitation literature that primarily targets continuous finger movements [87–89]. Set of movements that involve static postures and object handling were not included since these motions had little kinematics and larger forces involved.

The subjects were tasked to do the following tasks shown in Figure 3.7. Task A (blue) consists of periodic flexion-extension movements from each individual finger. Task B (green) involves moving all fingers simultaneously in the flexion-extension plane. This motion resembled the opening and semi-closing of the hand. Full closing of the hand was not possible as some markers at the tip of the fingers would not be seen by the motion capture system. Task C (red) involved moving any finger/s freely in any direction. Irregular movements and random finger combinations of flexion-extension movements were encouraged from the subject. The inclusion of Task 3 was motivated to introduce non-periodicity and some degree of randomness into the dataset.


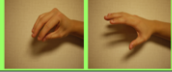

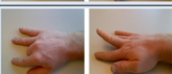

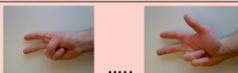

Task A			Task B		
1	Thumb flexion-extension		1	Simultaneous	
2	Index flexion-extension				
3	Middle flexion-extension		Task C		
4	Ring flexion-extension		1	Free-form	
5	Little flexion-extension				

Figure 3.7: Finger movements divided according to task.

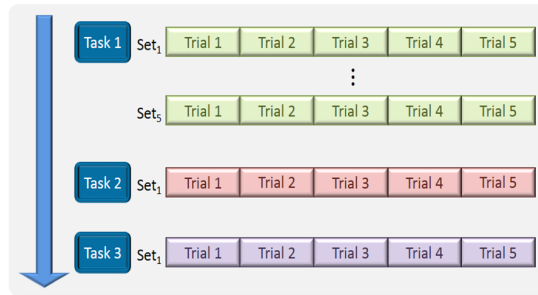


Figure 3.8: Experimental procedure in sequential order for Task A, B and C.

In the first two tasks, the subjects mainly did MCP flexion and extension, in which the PIP and DIP followed the movements of the MCP joint. The first task consisted of 5 sets of movement, one for each finger. While the remaining tasks consisted of 1 set each. Each set consisted of 5 trials with each trial lasting 20 seconds. All the trials were sequentially done and the participants were allowed to rest anytime throughout the experiment. This experimental protocol is shown in Figure 3.8. The subjects could make as many movements but were instructed to move in their own perceived normal velocity (≤ 2 cycles of movement per second) and to maintain the least amount of wrist ulnar/radial angle deviation. All the movements were limited to finger flexion and extension movements while the rest of the arm (e.g. wrist, elbow, etc.) maintained a fixed position upon instruction. Markers on the wrist joint were also recorded to ensure that the wrist maintained in a fixed position, with minimal ulnar/radial angle deviation. This dataset can be downloaded in the Dynamic Brain Platform database [90].

After collecting the EMG data along with the motion capture of the finger movements, separate trials were also done to obtain a maximum voluntary contraction (MVC) of each muscle. The subjects were asked to flex their hands and fingers in all possible planes of movement to try and induce maximum contractions for all the targeted muscles in the forearm. However, it is very hard to obtain the true maximum EMG values, so we instead obtained the maximum rectified EMG value from all the trials including the separate trials for obtaining the MVC of each muscle.

Eighty percent of all the recorded data were used for training and validation and the remaining twenty percent were used for testing. All the data in each task were concatenated together to form a larger training and test dataset. However, the data were separated and were analyzed separately for each subject.

Table 3.2: Finger joints normal range of motion.

Finger Joint	DOF	Type of Motion	Theoretical Range	Measured Range
Thumb CMC	1	Hyperextension/Flexion	−10/55 deg	9.86/50.06 deg
Thumb MCP	2	Hyperextension/Flexion	−10/55 deg	−3.05/56.51 deg
Thumb IP	3	Hyperextension/Flexion	−15/80 deg	−4.52/57.27 deg
Index MCP	4	Extension/Flexion	−45/90 deg	−39.97/62.29 deg
Index PIP	5	Extension/Flexion	0/100 deg	−14.95/72.55 deg
Index DIP	6	Extension/Flexion	0/80 deg	−16.96/45.51 deg
Middle MCP	7	Extension/Flexion	−45/90 deg	−34.07/69.39 deg
Middle PIP	8	Extension/Flexion	0/100 deg	−16.87/80.07 deg
Middle DIP	9	Extension/Flexion	0/80 deg	−15.15/57.07 deg
Ring MCP	10	Extension/Flexion	−45/90 deg	−26.35/62.51 deg
Ring PIP	11	Extension/Flexion	0/100 deg	−15.34/88.58 deg
Ring DIP	12	Extension/Flexion	0/80 deg	−14.52/58.94 deg
Little MCP	13	Extension/Flexion	−45/90 deg	−14.31/69.27 deg
Little PIP	14	Extension/Flexion	0/100 deg	−14.66/72.94 deg
Little DIP	15	Extension/Flexion	0/80 deg	−10.09/84.54 deg

Dataset: Technical Validation

The range of motion given for each of the 15 DOFs is presented in Table 3.2 taken from the average of all the subjects. These were based from the minimum and maximum value of the computed joint angle kinematics. Table 3.2 reflects the variability in range of finger motions that the subjects are capable of. Attributes such as the physical lengths and widths of the finger joints contributed to the change in range of motions.

To ensure the quality of the dataset obtained, we evaluated the effect of experimental conditions (Task Movement, Trial Repetitions and Subject) on the recorded signals. In particular, we consider the amplitude of the finger kinematics (Fig. 3.9a-c) and of the pre-processed surface EMG (Fig. 3.9d-f). The test was performed with a one-way Multivariate Analysis of Variance (MANOVA) using Matlab similar to [89].

Many factors can affect the amplitude of the kinematic signals such as acquisition setup, subject execution strategy and some degree of choice of multi-finger movements. Significant differences were found across different task movements ($P < 0.01$) and subjects ($P < 0.05$). In particular, Task 6 and 7 had larger variance compared to other tasks as these corresponded to all finger movement and random multi-finger

selection, respectively. Task 1 to 5, on the other hand, corresponded to single finger flexion-extension movement. Tasks 2 and 3 (index and middle finger) and Tasks 4 and 5 (ring and little finger) were found to be statistically similar. To check for consistencies across the data, no significant differences were across trial repetitions ($P > 0.05$).

Similar findings were found in the analysis of sEMG amplitudes across varying groups. Significant differences across different subjects ($P < 0.01$) are acceptable as they can be characterized by different anatomical features and execution strategies.

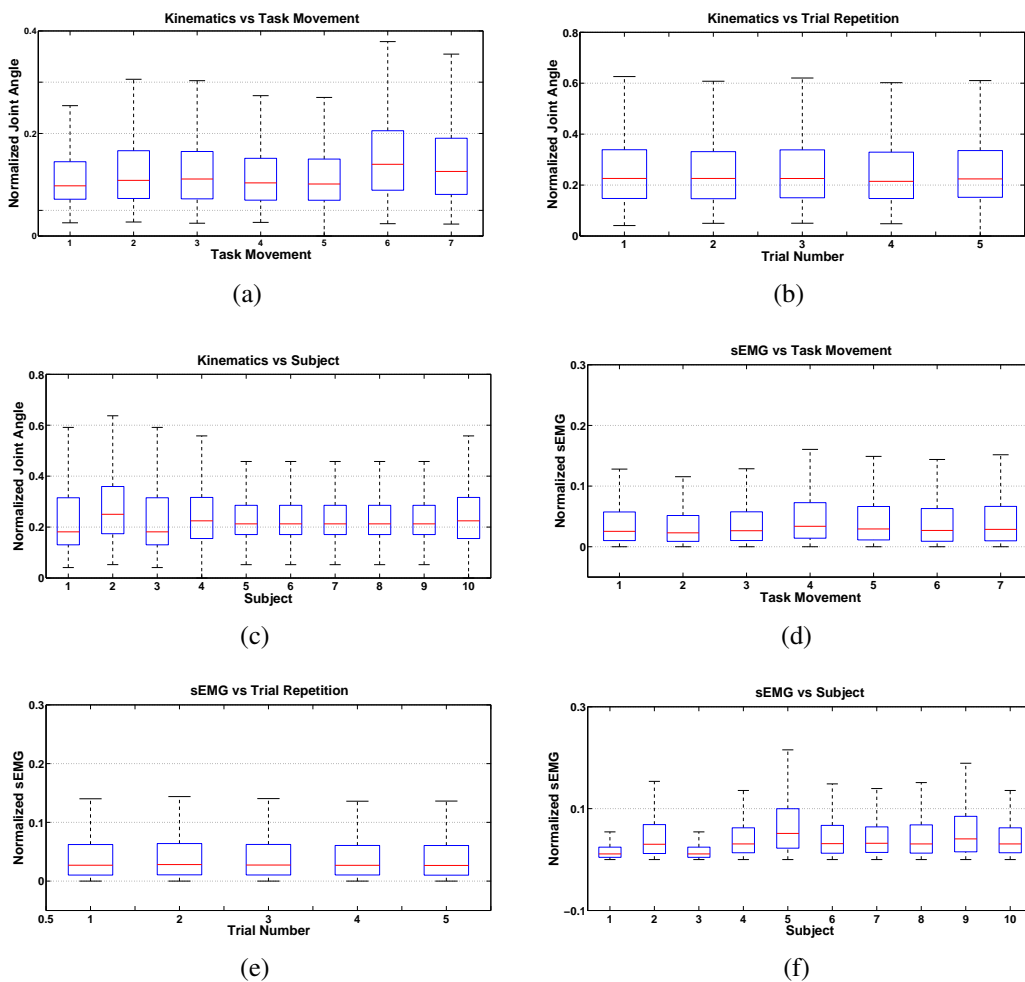


Figure 3.9: Experimental conditions' effect on the recorded data. The x-axis correspond to different conditions: task movement, trial repetitions and subject. The y-axis correspond to normalized kinematic and sEMG values.

3.4.3 Data processing

EMG signal

The raw EMG signals were first preprocessed into a form, that after further manipulation, can be used to estimate muscle activation [25]. The EMG signals were then rectified, normalized by dividing by the peak rectified EMG obtained, and low-pass filtered (4 Hz cut-off frequency, zero-phase 2nd-order Butterworth filter). This is done prior to obtaining the muscle activations, which are highly related to muscle force found in low frequencies [25]. The muscle activation parameters were then obtained through the process explained in Chapter 3.2. The obtained muscle activation features were then downsampled to 200 Hz to match that of the motion data.

For comparison, well established and commonly used time-domain EMG features were extracted and evaluated with the proposed muscle activation features. To show that the finger kinematic estimation performance was better using the proposed muscle activation model that considers electromechanical delay, we used four conventional time domain (TD) features, namely the Mean of the Absolute Value (MAV), Waveform Length (WL), Willison Amplitude (WA) and Variance (VAR) [91, 92].

- Mean of the Absolute Value (MAV):

$$MAV = \frac{1}{N} \sum_{i=1}^N |x_i| \quad (3.28)$$

- Waveform Length (WL):

$$WL = \sum_{i=1}^N |x_i - x_{i-1}| \quad (3.29)$$

- Willison Amplitude (WA):

$$WA = \sum_{i=1}^N f(|x_i - x_{i-1}|) \quad (3.30)$$

where $f(x)$ is 1 if $x >$ threshold, or 0 if otherwise.

- Variance (VAR):

$$VAR = \frac{1}{N-1} \sum_{i=1}^N (x(i)^2) \quad (3.31)$$

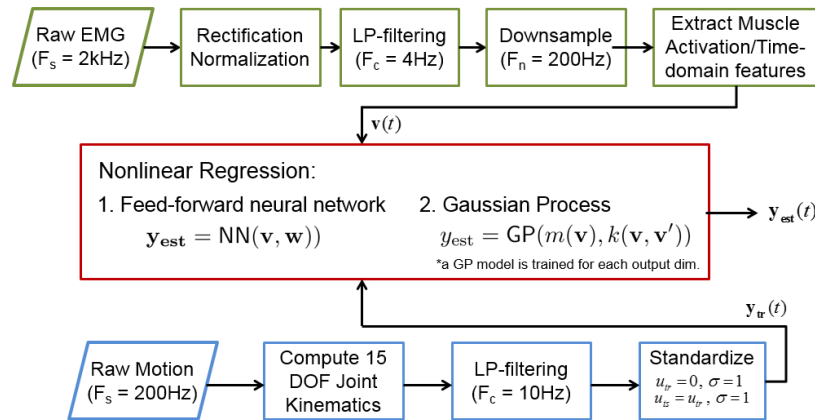


Figure 3.10: Schematic overview of the data processing and model training.

These features provide different information such as those pertaining to signal amplitude, frequency, extent of muscle contraction, and extent of the firing of motor unit action potentials. The length of the sliding window was 200 ms with a 25 ms overlap. In the preliminary investigation (not reported) of this study, other time and frequency domain features gave high correlation with the four features used and did not provide better estimation performance. These features were also used by most of the previous studies that performed finger joint kinematic and dynamic estimation from EMG [22–24, 70].

Finger kinematics

Each of the five fingers produced all three joint angles of interest. The tasks were constrained to moving the fingers only in the flexion and extension plane, thus, a total of 15 DOFs were considered. The joint angles were computed from the recorded marker trajectories. A low-pass filter with cut-off frequency of 10 Hz was also applied on the motion data, to remove any noise and jitters in the signal.

In the regression step, however, to standardize and scale all the joint angle values, we normalized each finger DOF to show a scaled value from 0 to 1. Normalization of each joint angle data was done by subtracting the minimum of the joint angle to each sample and dividing it by the difference between the maximum and minimum measured joint angle. The whole data processing and model training is shown in Figure 3.10.

3.4.4 Statistical analysis

A five-fold cross validation procedure was used to evaluate the overall statistical performance of the two different estimators and when different input features were used. Two performance indices were chosen to evaluate how accurately each finger DOF was estimated. The Pearson's correlation coefficient or the R -value index describes the total variation between the actual and estimated samples, while the normalized root-mean square error (NRMSE) describes the total residual error. These two performance indices are defined as the following:

$$R_i = \frac{\sum_{t=0}^N (\theta_{act} - \mu_{act})(\theta_{est} - \mu_{est})}{\sqrt{\sum_{t=0}^N (\theta_{act} - \mu_{act})^2} \sqrt{\sum_{t=0}^N (\theta_{est} - \mu_{est})^2}} \quad (3.32)$$

$$\text{NRMSE}_i = \sqrt{\frac{\sum_{t=0}^N (\theta_{act} - \theta_{est})^2}{N}} \quad (3.33)$$

where θ_{act} and θ_{est} are the normalized actual measured and estimated DOFs, respectively, μ represents the mean and R_i and NRMSE_i are the correlation coefficient and normalized root-mean-square error of the i th DOF, respectively.

Three different statistical analysis procedures were made in this study. A three-way analysis of variance (ANOVA) was done to compare the effects of different factors on the global estimation performance when NN regression was used. The different factors that we considered were the subject (S1-S10), the finger DOFs (15 DOF) and the type of input feature (filtered EMG, TD-based or muscle activation) used. When significant interaction was detected, focused ANOVA was conducted by fixing the levels of one of the interacting factors [73]. When no interaction was detected, a reduced ANOVA model with only the main factor was performed. Tukey-Kramers post-hoc comparison test was performed when significance was detected. The second procedure was a one-way ANOVA followed by the same post-hoc comparisons, which was used to compare any significant differences in the obtained parameters, such as the EMD between subjects. The third and final one was to investigate the effects of using different regression models or methods (such as GP versus NN) on the global estimation performance. Separate t-tests and ANOVA were used for this procedure. The significance level was set to 95% and all the procedures mentioning the global estimation performance were performed on results of the test sets.

3.5. Results

The main motivation in using an EMG-to-Muscle Activation model as input features in estimating continuous finger joint angles as discussed in Chapter 3.2 was that it considered electromechanical delay as a parameter.

Figure 3.11b and Figure 3.11c show two estimation results of a single index finger joint angle movement in a periodic flexion and extension task, one using low-pass filtered EMG, and the other using Muscle Activation inputs. Here, the estimator was an ANN trained from processed inputs shown in Figure 3.11a. Using the proposed EMG-to-Muscle Activation model is not only biologically plausible but it also determined an optimal estimate of the EMD, and requires only a few parameters for the input features. By considering EMD, we can see in Figure 3.11a that this shifts the muscle activation signal almost suitably aligning with the motion data.

With the neural network and Gaussian Process regressors trained, all 15 finger DOFs were estimated simultaneously.

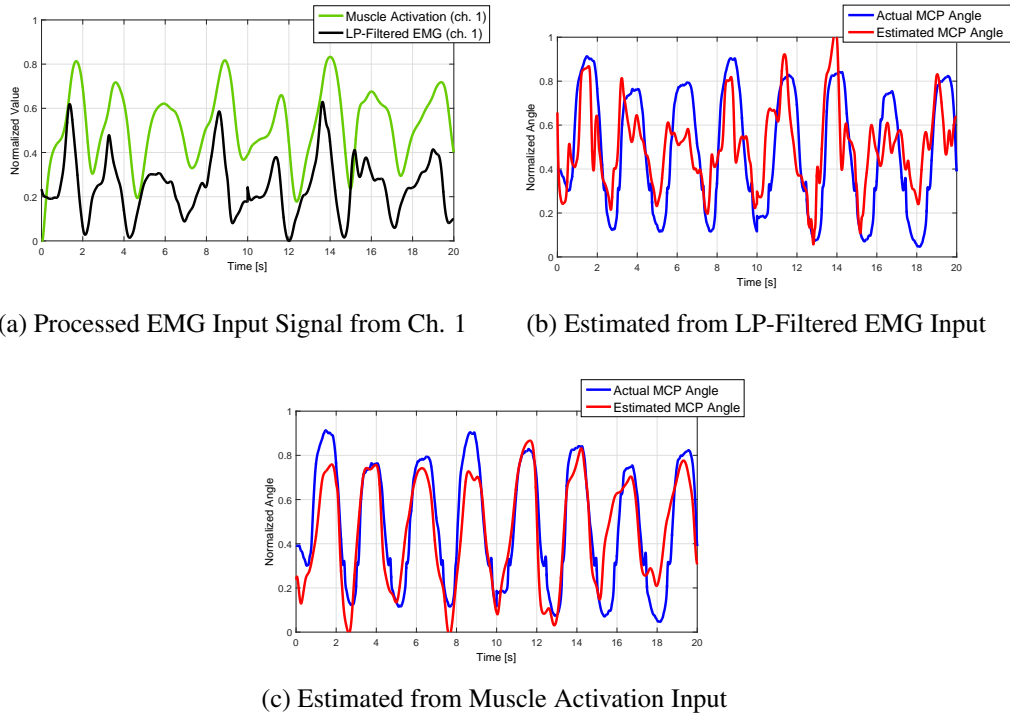


Figure 3.11: Single joint angle estimation using different EMG inputs.

Figure 3.12 shows a representative estimation result taken from 1 test trial from a subject. In this result, the subject performed simultaneous joint flexion and extension of all finger joints. Though only the MCP finger joint angles are shown in the figure, the PIP and DIP angles showed consistent results with the MCP angles since this task involved the flexion and extension of all joints simultaneously. The NN and GP regressors were trained with 4800 samples. The average correlation coefficient of the GP-estimated results were significantly higher than the NN-estimated results (R , 0.84 ± 0.0378 versus 0.71 ± 0.0981 ; $P < 0.001$). With more training samples used, correlations between the actual and estimated value for a single DOF reached as high as 0.92 for the MCP joint angle estimation. While the DOFs for the smaller finger PIP and DIP joints reached as high as about 0.85 and 0.79 in correlation, respectively.

The results in Figure 3.13 and 3.14 show that using muscle activation input features not only parameterizes and considers EMD, but also gives better overall estimation result. The global estimation performance between three types of input: filtered EMG without EMD considerations, TD-based features and the proposed muscle activation inputs are shown. The figure shows the overall mean correlation coefficients and mean normalized root-mean-square error (NRMSE) of the actual and estimated joint kinematics of all the test data. In figure 3.13, the proposed model using the muscle activation inputs, shown in red, performed better than other features shown in blue and green (averaging $7.38\% \pm 1.64\%$ better than TD features and $13.13\% \pm 2.04\%$ better than filtered EMG features). Significant differences were found when the correlation value using the muscle activation inputs was compared to the TD-based features ($P < 0.006$) and to the filtered EMG inputs ($P < 0.001$).

In figure 3.14, the estimated finger kinematics using the muscle activation inputs across all DOFs had an average root-mean-square error of $11.53\% \pm 1.76\%$. Significant differences were also found when NRMSE using the muscle activation inputs was compared to the TD-based features ($P(R3, L2, L3) < 0.05$; $P(others) < 0.03$) and to the filtered EMG inputs ($P(L3) < 0.05$; $P(others) < 0.01$).

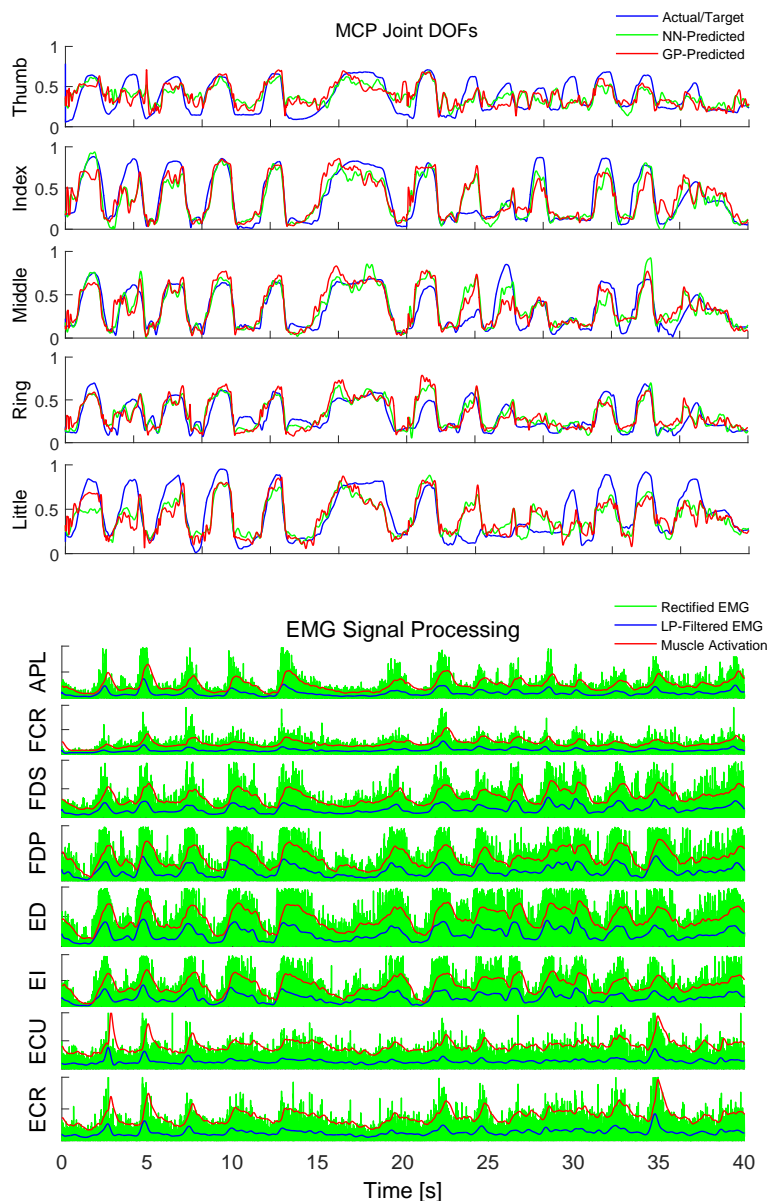


Figure 3.12: One representative estimation result. 5 out of the 15 normalized finger joint angles are shown in blue solid lines, while the NN and GP estimated results are shown in green and red, respectively. Below are the 8-channel processed EMG which includes the following: rectified EMG (green), low-pass filtered EMG (blue) and the transformed muscle activations (red). In this test data, the parameters obtained for the muscle activation model were: $A = -3$, $d = 0.045$, $\gamma_1 = \gamma_2 = -0.9539$. The labels on the y-axis of the plots correspond to the target EMG channels (in Table 3.1).

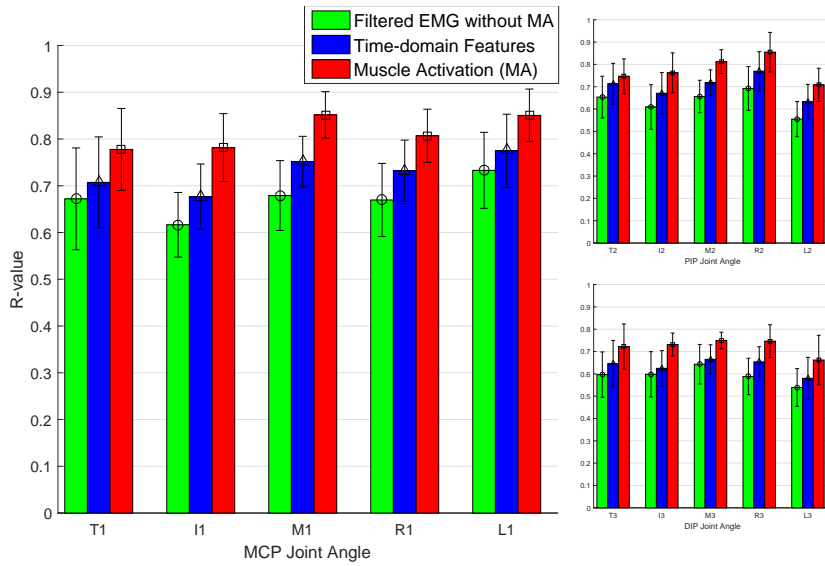


Figure 3.13: The mean correlation coefficient between the measured and estimated finger joint angle. The left figure shows the result for the MCP joints, and the right figure shows the PIP and DIP joints. The x-axis letter labels represent the thumb, index, middle, ring, and little finger.

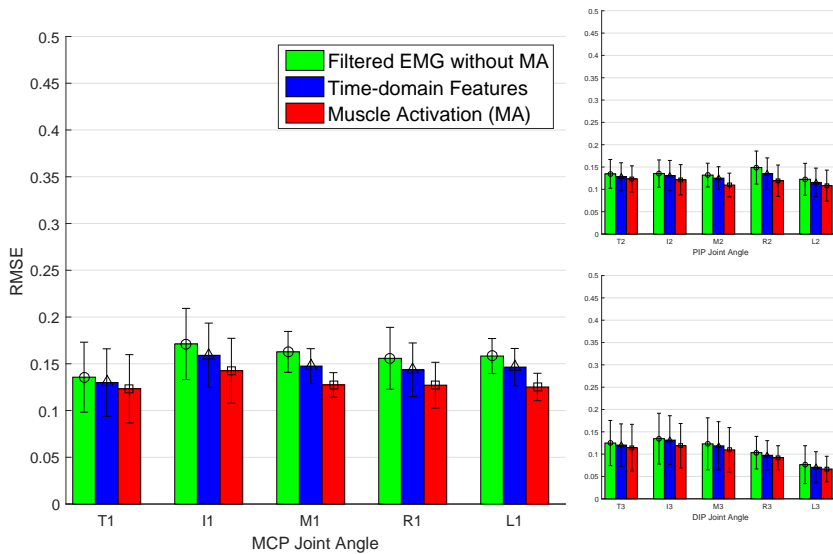


Figure 3.14: The normalized root-mean-square between the measured and estimated finger joint angle. Labels have the same finger assignment as that of Figure 3.13.

A three-way ANOVA testing the effects of different factors such as across different input features, across subjects and across finger DOFs showed significant differences in the correlations of the resulting estimation performance between the factor groups. Across the different input features used, the use of the proposed muscle activation features had significant differences, performing consistently better than other types of features used. Significant differences were also found between the different mean correlation coefficients across subjects and the finger DOF groups ($P < 0.001$). Significant interactions were found for the Subject-Finger DOF and Subject-InputFeature pairs ($P < 0.001$), while no significant interaction was found in the Finger DOF-Input Feature interaction ($P = 0.110$). Tukey-Kramers comparison test found that the estimation performance among the three different input features used were different (correlation coefficient: muscle activation $>$ TD-based $>$ filtered EMG and NRMSE: muscle activation $<$ TD-based $<$ filtered EMG).

In Figure 3.15, the obtained EMD parameter across the 10 subjects in different experiment trials are plotted. The optimized EMD value ranged from 39.6 ms to 75 ms. No significant difference was found among the mean of the EMD values obtained across the 10 subjects ($P = 0.24$). This supports our assumption that the obtained EMD across the subjects did not drastically change as the subjects tried to do the target tasks at constant velocity or at their normal and consistent pace across the trials. Obtaining an optimal value for the EMD using the optimization method described in the paper is important and can significantly improve the estimation performance compared to when no EMD is considered.

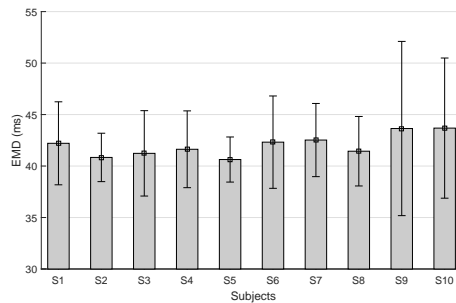
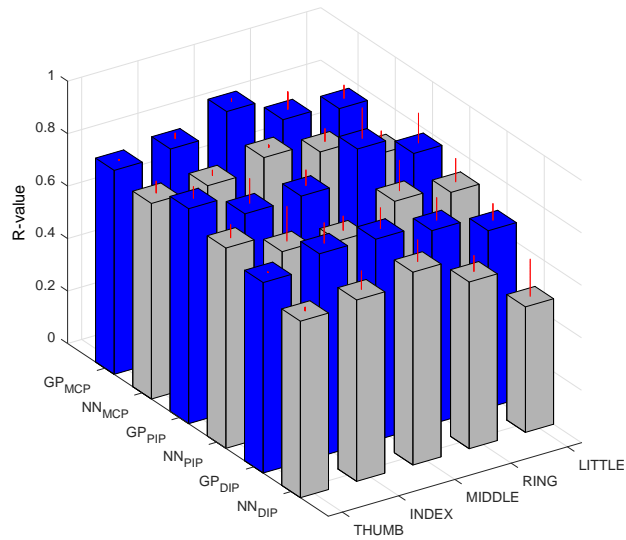
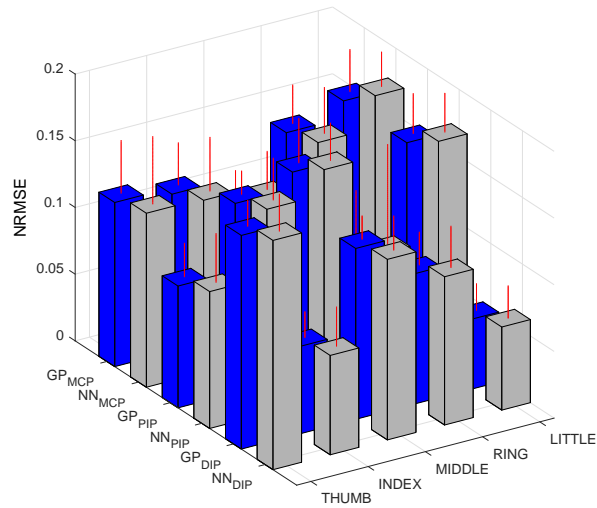


Figure 3.15: The EMD parameters obtained across all the subject participants. The electromechanical delay parameter obtained through optimization across different trials ranges from 39.6 ms to 75 ms, with a mean of 42 ms.



(a)



(b)

Figure 3.16: The correlation coefficient (R) and the normalized root-mean-square error (NRMSE) of the measured and estimated finger DOFs are shown when the NN and GP regressors were used.

In Figure 3.16, the estimation performance is shown between the two regression methods used, namely using the NN and GP regressors. The estimation performance comparing the results in NN and GP regression averaged over 10 subjects are shown

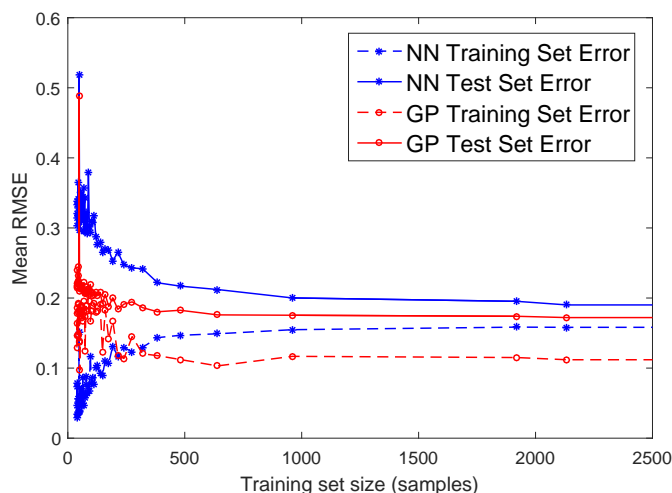


Figure 3.17: Learning curves of the neural network and Gaussian Process Regressor. The y-axis shows the mean NRMSE while the number of training samples was varied. The number of test data samples remained fixed across all the subjects.

in this figure. For these results, the GP performed consistently better in all the subjects than the NN specially when training samples were sufficient. GP showed an average of 7.18% higher correlation performances than NN regression between the actual and estimated finger kinematics and when trained with 4800 samples. There was also significant differences in the obtained correlation coefficients between GP and NN regression ($P < 0.001$). Overall, estimation of the MCP joint angles performed consistently better than the PIP and DIP estimation.

As the size of the training sample increases, NN performs better or much closer to GP with no significant increase in computation time, while GP computation suffers with the increase. Figure 3.17 shows the global performance of the estimators that we used, plotting the average RMSE of all the joint angles when the number of training samples was varied. As few as 250 samples for GP can give almost equal or even better performance as when more than 1800 samples are used to train a neural network. With more and more training samples available that captures more variability in the EMG and kinematics data, the neural network performs better reaching to the point where estimation performance is very close to GP as shown in Figure 3.12, where the estimation results showed the NN and GP performance over 4800 training samples.

3.6. Discussion

In this chapter, we presented a feasibility of estimating all finger joint kinematics using surface EMG that even considers electro-mechanical delay present in EMG-to-motion estimation applications and analysis. Compared to the use of pattern classification techniques used previously by many studies, we have presented results in doing simultaneous and proportional control of multiple finger DOFs comparing two different regression methods using EMG.

This chapter presented results taken from the smaller finger PIP and DIP joint angles, which have been rarely reported in any previous studies. Overall, our proposed method, which used the EMG-to-Muscle activation model, showed comparable, and in some instances, a more superior performance compared to that of the previous studies.

From the results of the ANOVA tests, we have shown that there are significant differences in mean estimation performance across difference factor groups such as across different types of input features used, across different subjects and across the finger DOFs. As mentioned previously, the use of the proposed muscle activation inputs gave a consistently better estimation performance compared to when other types of features were used. For the subject group used in this study, the 7 subjects' estimation performances, both correlation coefficients and RMSE between the estimated and measured DOFs, were slightly, significantly better than the other 3 remaining subjects. It is not clear why some of the subjects performed poorly than the others, although the choice of random finger movements in the free movement task set across the subjects were different. Some of the subjects chose to do periodic flexion and extension movements in the free moving task while others chose to do more random, nonperiodic and more varying simultaneous and multiple finger movements. As for the differences across the finger DOF group, this can be attributed to the better performance achieved in estimating the MCP joint DOFs than in the PIP and DIP joint DOFs. The MCP DOFs have more independent movements than the PIP and DIP, which are more closely coupled and have dependent movements.

3.6.1 On using the EMG-to-Muscle activation model features

Processing the raw EMG signals into its muscle activation dynamics was straightforward. Training was fast and requires only a few parameters which is suitable for prac-

tical applications. For most trials, the EMD obtained ranged from 45 to 65 ms, suitably aligning the EMG onset to the motion data. We hypothesize that this model works very well for motion with constant velocities, as EMD has been known to change with the velocity and frequency of the task movement [78]. In the paper [93], the authors presented the time constants of the filters used in analyzing surface EMG, which ranged from 10 to 150 ms. It was also mentioned that the time constant should be changed adaptively to the data. In our method, the appropriate filter parameters, including the EMD in the muscle activation model were obtained through an iterative optimization procedure that minimized reconstruction error.

In our previous study, for periodic motion, the PIP and DIP angles followed movements similar to the MCP angles, but for random motions, it may totally differ. The input feature sets that we used do not give an explicit feature that relates the angles to one another [94]. However, compared to feature sets used by previous studies, the proposed set of muscle activation features performed better.

Furthermore, compared to reported EMD values in the other studies, the range obtained is comparatively smaller compared to those taken from the lower limb during cycling tasks [78] or from the upper limb during object-carrying tasks [71]. This can be attributed to observations such as the tasks involved in this experiment are faster, have smaller deviation in movement trajectories, and that the targeted muscles in the forearm are physically smaller. However, it is hypothesized that as the frequency or velocity of the finger movement tasks increases, then the EMD values may also significantly change.

3.6.2 Neural network versus gaussian process regression

Currently, there is no existing model that can best describe the relationship between EMG and finger joint kinematics. This is the main reason why we chose an artificial neural network and a Gaussian Process regressor, as these give a model-free approach in mapping the EMG signals to the corresponding finger kinematics.

Using artificial neural networks has been the primary choice in mapping the EMG to kinematics application, however, in this study we present the use of a nonparametric Bayesian approach through the use of a GP regressor. GP can give better estimation of the joint angles using fewer training samples as shown in Figure 3.16 and 3.17. This advantage is particularly important in not only reducing the amount of training time

but in potentially reducing the amount of experiment protocol needed to capture large variations in the training data. In many myoelectric control strategies that are based on supervised learning, subjects have to retrain day after day as EMG signals are highly variable. With GP regressors, higher estimation accuracy compared to using neural networks can be achieved using fewer training data. Although not shown, using GP outperformed any neural network configuration, such as single output or multi-output network configurations [95], in the case of only few training samples available.

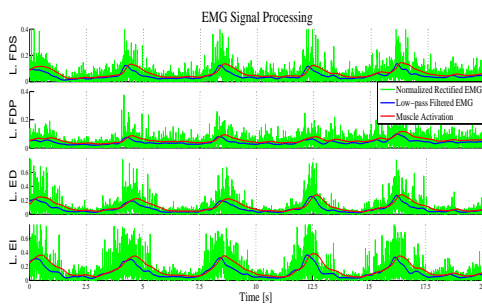
However we should point out that, though GP can handle missing data more readily than neural networks, the computation time becomes significantly higher in the former as the size of the training data increases. It took about 10 times longer to train the GP than the ANN. But with increasing computing capabilities of CPUs and computers, it will be but a matter of time before Bayesian regressors can be fully realized in practical applications. Also, in this study, the choice of covariance function was a standard Gaussian function. Other suitable choices for the covariance and mean functions may exist that can better improve the estimation performance, however, these have not been explored in this study. For this work, using GP regressors gave promising results in terms of getting better estimation using fewer training samples.

Also, in this study, we are estimating 15 finger joint kinematics simultaneously from eight muscle activation inputs. However, a dimensionality analysis on the hand kinematic data suggests that the effective dimension is less than the total DOFs available anatomically on the hand. By applying a Principal Component Analysis (PCA) on the finger kinematics data, the analysis showed that only the first 4 to 6 principal components explained the vast majority of the variance in hand posture. PCA was performed not only on the joint angular position data, but also on the joint angular velocities data because these are said to be more closely related to the motor command's driving moment [15]. This is consistent with earlier studies, where it was shown that despite the hand having more than 20 DOFs, the effective dimensionality is much lower [69]. This can be attributed to factors such as mechanical constraints in the structure of the hand, high correlations of movements between joints and possibly the existence of synergies [66, 69]. However, the extent to which each of these DOFs is independently controlled during movement is still not completely understood.

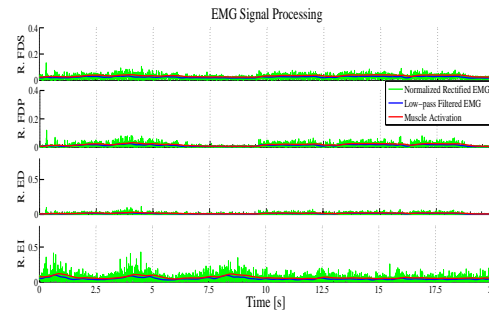
3.6.3 Application: control of a finger exoskeleton

Most of the analysis has been done offline, in this section, we show that the proposed method is also suitable in real-time applications. In using the proposed muscle activation model, training and optimization is fast as there are only a few parameters needed in the transformation of the input features. Simultaneous and proportional estimation of multi-finger DOFs with the neural network regressor can be done real-time with delays of less than 100 ms. A practical real-time application using the proposed method in controlling a custom-built one-finger exoskeleton is presented in our previous study [96].

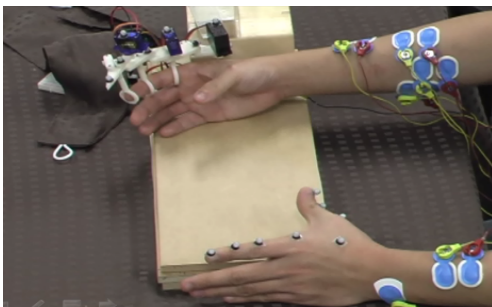
The design construction of an optimal 3-DOF index finger exoskeleton using a four-bar linkage design is presented in [96]. This customized finger exoskeleton shown in Figure 3.18c was designed to be portable and low-powered, easily adjusted for both



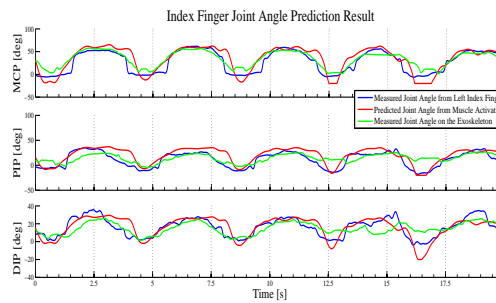
(a) Muscle activation from the left arm



(b) Muscle activation from the right arm



(c) Screenshot of the finger exoskeleton



(d) Measured and estimated index joint angles.

Figure 3.18: An application showing an EMG-based control of an index finger exoskeleton. The recorded EMG on both left and right hand are shown and the robot was controlled with input commands coming from the estimated joint angles.

Table 3.3: Performance of the nonlinear estimator and the actuation of finger exoskeleton across the three DOFs.

Joint Angle	Estimator		Exoskeleton	
	R-value	RMSE	R-value	RMSE
MCP	0.93	3.44	0.88	4.10
PIP	0.85	8.16	0.76	9.69
DIP	0.80	9.10	0.71	10.44

clinical or personal use. The linkages were customized to the users according to their own motion data and were then synthesized using rapid prototyping. To actuate and control the finger exoskeleton, an inexpensive Arduino Mega micro-controller was used to send the processed EMG motor commands to the exoskeleton. To actuate the MCP, PIP and DIP joints using the current prototype, a GWS Micro-MG and two MiniS RB90 mini RC servo with rated torques of 5.4 kg-cm and 1.6 kg-cm, respectively, was used due to its high power-to-weight ratio. To help support the exoskeleton, which weighed about 50 grams, an external support was added.

In the previous work [96], training was done using a mirror training scheme where the EMG data were obtained from a contra-lateral hand and were used to actuate the finger exoskeleton on the opposite hand. A subject was asked to move his left index finger in the flexion and extension plane while the right index finger was actuated by the exoskeleton using EMG inputs from the left side (Figure 3.18a). No exerted EMG effort came from the right finger to show that it was indeed assisted by the exoskeleton (Figure 3.18b).

The joint angle test prediction result is shown in Figure 3.18d, when the EMG was transformed into its muscle activation and used as input to predict the index finger joint angle. The blue plot shows the measured joint angle obtained from the left index finger, while the red plot shows the predicted joint angle from the regressor. The green plot shows the actuated motion of the finger exoskeleton on the right index finger. The performance of the estimator and as well as the actuation of the exoskeleton is shown in Table 3.3. Correlation as high as 0.9 and root-mean-square percentage error of less than 5 degrees were obtained between the predicted and estimated index finger MCP joint angles. Prediction of the PIP and DIP joint angles also gave reasonable results

with correlations of above 0.75 and 0.7, respectively. One way to increase estimation performance for the PIP and DIP joint angles is to explicitly consider correlations between these joints.

Overall, the predicted finger joint angles were enough to actuate the exoskeleton and to continuously assist finger flexion and extension movement. The subject felt that enough support was given to his right index finger and that the actuation of the exoskeleton was almost about the same time as the movement execution of the left index finger.

3.6.4 Implementation and limitations

The current subjects have been limited to healthy, able-bodied subjects to test the feasibility of our approach. This can be used as a benchmark for future implementation and validation for training amputees or subjects with hand impairments. The estimation of finger joint kinematics has also been confined to a static wrist and arm position. Changing the wrist's position may influence finger joint estimation from EMG similar to those observed by Jiang et al. [97]. One possible solution is to increase the amount of training data by adding finger joint information at different positions of the arm and wrist. However, getting this amount of data may be impractical to apply in the real application setting. So there is a need to check if the GP can handle variations in the arm and wrist position. If dynamic arm and wrist position are to be considered, some form of hierarchical model may be considered. Currently, only the neural network has been fully tested on a real-time application. Other works are currently ongoing, which includes implementing other regression models in real-time.

Chapter 4

Using nonlinear synergistic model for proportional myoelectric control of high-DOF finger postures

Proportional myoelectric control of multiple degrees-of-freedom (DOF) in active finger joints is important in replicating dexterous hand motion in robotic prosthesis. This is still difficult to achieve as current myoelectric control strategies often require the separate control of each joint and do not consider the high-DOF and strong correlations that exist between these joints. To address this problem, in this chapter, we propose using a shared low-dimensional representation based on nonlinear synergies to represent both the high-DOF finger joint kinematics and the coordination of muscle activities taken from electromyographic (EMG) signals in the forearm. A Bayesian Gaussian Process Latent Variable Model is used to learn a shared latent structure model that not only allows the automatic selection of the dimensionality of the shared information variance observed in EMG and hand kinematic data.

We demonstrate that dexterous finger movements can be represented in a small dimensional space using nonlinear synergistic representations and that the proposed method outperforms commonly used simultaneous regression and linear dimensionality reduction methods such as principal component analysis. Finally, we show that the proposed method is able to reconstruct the full-joint continuous finger kinematics, where data is generated from an inferred latent manifold.

This chapter presents a novel myoelectric strategy for overcoming the limitations of simultaneously estimating only a few DOFs available in the hand using muscle activation inputs. A generative model coupled with a nonlinear dimension reduction method is presented, to reconstruct the kinematics of a full 23-joint skeletal hand model. Where studies have shown individual synergy models for muscle activation and finger kinematics, we present the use of a shared model between these two different but highly correlated data. An overview of this framework is shown in Figure 4.1. We show that by using of a Bayesian Gaussian Process Latent Variable Model (GPLVM) with automatic relevance determination (ARD), a shared latent space can be learned. We also analyze how a synergistic model can be useful and interpreted in the context of myoelectric estimation of high-DOF finger kinematics. Building from our previous work [98], the combined use of an EMG-to-Muscle Activation model coupled with a Bayesian inference method can be used for estimating high-DOF finger kinematics from EMG.

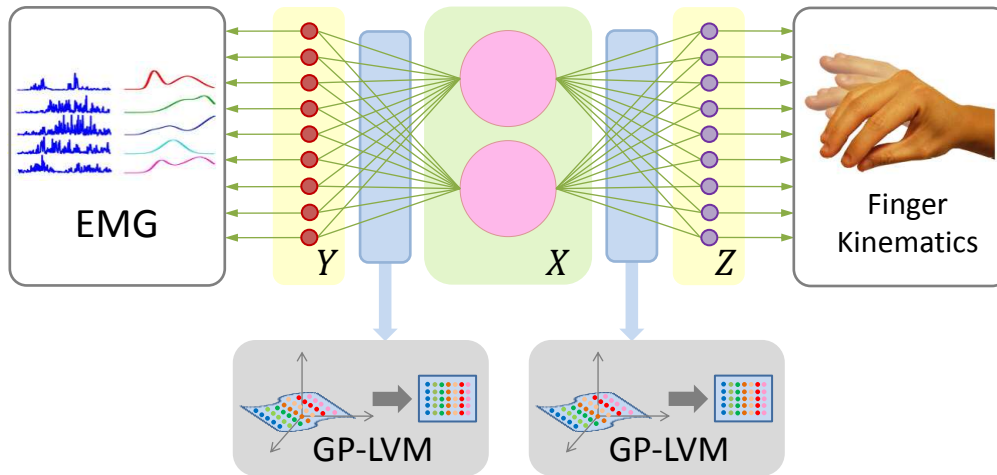


Figure 4.1: Schematic overview of the proposed shared latent representation method.

4.1. Bayesian GPLVM for multi-observation

Gaussian processes (GPs) are powerful models that can be used for classification or regression that incorporates numerous classes of function approximators [72]. In a previous study, Lawrence proposed the Gaussian Process latent variable model (GPLVM) as a new technique for nonlinear dimensionality reduction that uses GPs to find a nonlinear manifold to preserve the variance of the data in a latent space representation [99].

Several studies have been proposed to handle multiview learning. For example, Shon et al. proposed a generalization of the GPLVM that represents multiple observation spaces that are linked via a single shared latent variable model [100]. Ek et al. presented a factorized latent variable model where the shared and individual variances of two correlated observation data were represented in separate subspaces [74]. In these previous methods, however, the dimensionality of the latent spaces was heuristically set, and inference for new test data points had to rely on maximum a posteriori (MAP) search in the latent space. To overcome these limitations, Damianou et al. [101] proposed a full Bayesian factorized latent variable model based on GPLVM that allows for the automatic estimation of dimensionality of the latent space (also called Manifold Relevance Determination or MRD), and provides an approximation to the full posterior of the latent points given the data. In this study, we follow the same approach.

A latent model representation is learned from a multi-observation data coming from EMG signals in the forearm and finger posture kinematics. Applying a dimensional reduction method on each data individually, gives us some similar notion of extracting a form of muscle synergy or postural synergy, respectively. In fact, a study has shown that muscle synergy is linked to the kinematic synergy during a hand reaching, grasping and pulling task [60]. This motivates us to use a latent variable model that assumes that a portion of the data variance is shared between these two different synergy models, while remaining variance correspond to private information contained in each data.

The problem is formulated as follows: Given that we have two observation data $Y \in \mathbb{R}^{N \times D_Y}$ and $Z \in \mathbb{R}^{N \times D_Z}$, the goal of the model is to find a factorized latent variable parameterization in a space $X \in \mathbb{R}^{N \times Q}$ that relates corresponding pairs of observations from different spaces Y and Z . It is assumed that the two datasets are generated from a low dimensional manifold mapped from smooth functions $\{f_d^Y\}_{d=1}^{D_Y} : X \rightarrow Y$ and

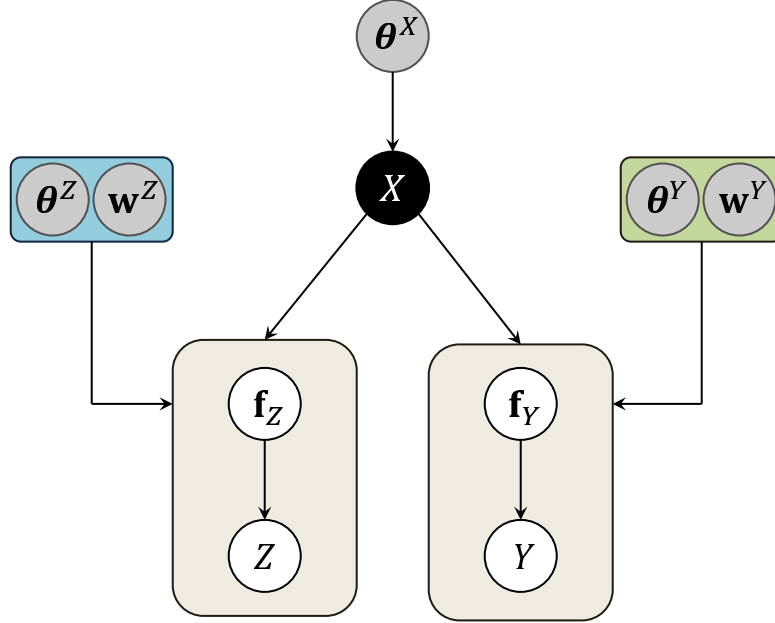


Figure 4.2: Graphical model of the Bayesian GPLVM. A distribution for latent space X is learned and the hyperparameters $\mathbf{w}^{Y,Z}$ and $\theta^{Y,Z}$ are the ARD weights that determine the dimensionality and the function model parameters, respectively.

$\{f_d^Z\}_{d=1}^{D_Z} : X \rightarrow Z$ ($Q < D$), corrupted by noise:

$$y_{id} = f_d^Y(\mathbf{x}_i) + \varepsilon_{id}^Y \quad (4.1)$$

$$z_{id} = f_d^Z(\mathbf{x}_i) + \varepsilon_{id}^Z, \quad (4.2)$$

where $\{y, z\}_{id}$ represents dimension d of sample point i and $\varepsilon_{id}^Y, \varepsilon_{id}^Z$ are sampled from a zero mean Gaussian distribution. This leads to the likelihood under the model, $P(Y, Z | X, \theta)$, where $\theta = \{\theta^Y, \theta^Z\}$ contains the parameters of the mapping functions and noise variances. Finding the latent representation X and mapping functions f^Y and f^Z is an ill-constrained problem. Lawrence provided a solution by placing GP priors over the mapping and the resulting model is the Gaussian Process Latent Variable Model (GPLVM) framework [99]. In this framework, each generative mapping is modeled as a product of independent GP's parametrized by the kernel or covariance

function $K = \{K^Y, K^Z\}$ evaluated over the latent variable X , so that

$$P(F^Y|X, \theta^Y) = \prod_{d=1}^{D_Y} \mathcal{N}(f_d^Y | \mathbf{0}, K^Y), \quad (4.3)$$

where $F^Y = \{f_d^Y\}_{d=1}^{D_Y}$ with $f_{id}^Y = f_d^Y(\mathbf{x}_i)$, and similarly for F^Z . This allows the general nonlinear mapping function F to be marginalized out leading to a likelihood function in the form of a product of Gaussian densities:

$$P(Y, Z|X, \theta) = \prod_{\mathcal{K}=\{Y,Z\}} \int p(\mathcal{K}|F^{\mathcal{K}}) p(F^{\mathcal{K}}|X, \theta^{\mathcal{K}}) dF^{\mathcal{K}} \quad (4.4)$$

Integration over (4) is then done by variationally marginalizing out X by using variational approximation techniques used for standard GPLVMs. A non-standard but analytical solution through variational learning techniques and using induced variables is described in [101–103]. Another goal of the model is also to recover the factorized latent structure composed of three subspaces, representing the shared and private variance for each observation data, $X = \{X^Y, X^S, X^Z\}$. Bayesian training automatically allocates the dimension of this factorized latent space using automatic relevance determination (ARD) priors [101]. In the automatic allocation of the dimensionality, the dimensions D_Y and D_Z of the latent functions f^Y and f^Z , respectively, are selected to be independent draws of a zero-mean GP with an ARD kernel or covariance function with the following form:

$$k^{\{Y,Z\}}(\mathbf{x}_i, \mathbf{x}_j) = (\sigma_{ard}^{\{Y,Z\}})^2 e^{-\frac{1}{2} \sum_{q=1}^Q w_q^{\{Y,Z\}} (x_{i,q} - x_{j,q})^2}. \quad (4.5)$$

where $w_q^{\{Y,Z\}} = \alpha (l_q^{\{Y,Z\}})^{-2}$, with α a constant positive scale value and length scales l . Although a common distribution for X is learned, two sets of ARD weights $W = \{\mathbf{w}^Y, \mathbf{w}^Z\}$ are obtained to automatically infer the relevance of each latent dimension for generating points in the Y and Z spaces respectively. The latent shared subspace $X^S \in \mathbb{R}^{N \times Q_S}$ is then defined by the set of dimensions $q \in [1, \dots, Q]$ for which $w_q^Y, w_q^Z > \delta$, with δ close to zero and $Q_S \leq Q$. As for the two private spaces, X^Y and X^Z , these are also inferred automatically along with their corresponding dimensionalities, Q_Y and Q_Z , respectively. More specifically:

$$X^Y = \{\mathbf{x}_q\}_{q=1}^{Q_Y} : \mathbf{x}_q \in X, w_q^Y > \delta, w_q^Z < \delta. \quad (4.6)$$

and analogously for X^Z . This model is summarized in the graphical model shown in Figure 4.2.

Model training

The training procedure of the Bayesian GPLVM model requires the maximization of the joint marginal likelihood,

$$P(Y, Z | \theta) = \int P(Y, Z | X, \theta) P(X) dX \quad (4.7)$$

where an assumed prior distribution is placed on X , typically a standard Gaussian distribution. Damianou et al. [101] provides a non-standard but analytical solution by maximizing instead a variational lower bound $F_v(q, \theta)$ on the true marginal likelihood, by relying on a variational distribution on which factorizes as $q(\Theta)q(X)$, where $q(\Theta) = q(\Theta^Y)(\Theta^Z)$ and $q(X) \sim \mathcal{N}(\mu, S)$. This lower variational bound¹ is described as the following:

$$F_v(q, \theta) \leq \log P(Y, Z) \quad (4.8)$$

$$\begin{aligned} F_v(q, \theta) &= \int q(\Theta)q(X) \log \left(\frac{P(Y|X)P(Z|X)P(X)}{q(\Theta)q(X)} \right) dX \\ &= \mathcal{L}_Y + \mathcal{L}_Z - \text{KL}[q(X)||P(X)] \end{aligned} \quad (4.9)$$

where $\mathcal{L}_{\{Y,Z\}} = \int q(\Theta^{\{Y,Z\}})q(X) \log \frac{P(Y|X)P(Z|X)}{q(\Theta^{\{Y,Z\}})} dX$. More details of this type of variational learning of inducing variables for further tractability is described in [101–103]. This objective function is then jointly maximized with respect to the latent space parameters $W = \{\mathbf{w}^Y, \mathbf{w}^Z\}$, and the variational parameters. This optimization procedure gives an approximation of $P(X|Y, Z)$, which is the posterior distribution over the latent space. Instead of relying on a fixed point MAP estimate of X , here, the Bayesian GPLVM gives the approximate posterior distribution which adds extra robustness to the model [101]. The Bayesian GPLVM Matlab library [104] was modified and used to implement the model training and dimensionality relevance determination in this study.

¹A mean field method and Jensen’s inequality is used to derive this variational lower bound, the derivation is given in [101]

4.2. Methods

4.2.1 Data collection

The same data collection process is used as that explained from Chapter 3.4.1 to 3.4.3. Surface EMG signals were extracted from eight extrinsic muscles of the hand that are known to contribute to wrist and finger movements. These are the Abductor Pollicis Longus (APL), Flexor Carpi Radialis (FCR), Flexor Digitorum Superficialis (FDS), Flexor Digitorum Profundus (FDP), Extensor Digitorum (ED), Extensor Indices (EI), Extensor Carpi Ulnaris (ECU), and Extensor Carpi Radialis (ECR) shown in Table 3.1.

A portion of total dataset used in this chapter included those of 4 healthy and intact participants (3 Male, 1 Female, aged 26-31 years old). All subjects were seated with their dominant hand and elbow comfortably positioned on a flat surface table as shown in Figure 3.5 and tasked to do the same finger movements shown in Figure 3.7 and 3.8. This dataset can be downloaded in the Dynamic Brain Platform database [90].

4.2.2 Data processing

EMG-to-Muscle activation model

The raw EMG signals were first preprocessed into a form, that after further manipulation, can be used to estimate muscle activation [25, 80]. An EMG-to-Muscle Activation model as explained in Chapter 3.2 is again used as the input EMG features for this chapter. It has been shown in previous studies, that using this feature works very well in estimating muscle force [71] and kinematics [98].

Finger kinematics

The motion data, on the other hand, were also low-pass filtered (4 Hz cut-off frequency) to remove any jitters. In this study, a shared latent representation X is extracted from the 8-channel muscle activation input $Y \in \mathbb{R}^{N \times 8}$ and from the 23-marker finger posture $Z \in \mathbb{R}^{N \times 69}$. We considered all the 3D information on each marker which summed up to a total of 69 dimensions in the hand kinematic space. Separately, we also reconstructed and estimated finger kinematics based on the joint angle space, $Z_{\text{ANGLE}} \in \mathbb{R}^{N \times 15}$, considering 15 joint angles in the flexion and extension plane.

4.2.3 Inference and estimation

In this study, we also demonstrate the model’s reconstruction of the new finger pose kinematic Z^* from X^* which is obtained using shared information involving new muscle activation inputs Y^* . Given the trained shared latent model which jointly represent Y and Z with a factorized latent space X , we infer a new set of outputs Z^* given some new unseen test points Y^* . Estimation is done by first predicting a set of latent points X^* most likely to have generated Y^* using the approximation of the posterior $p(X^*|Y^*, Y)$. This posterior has the same form as for the standard Bayesian GPLVM model [102] and is given by a variational distribution $q(X, X^*)$, which is found by optimizing on the marginal likelihood $P(Y, Y^*)$. This step involves a computationally expensive operation as it requires optimization over a ratio of marginal likelihoods that has the same form in (4.9). The next step involves finding training latent points X_{NN} which are closest to X^* in the shared latent space by using Nearest Neighbors. In the final step, we find the outputs Z from the likelihood $P(Z|X_{NN})$. This returns the set of training points Z which best match the observed test points Y^* .

The procedure relies on intensively exploring a solution in the shared latent space. To evaluate a lower bound test performance, we also use a 2nd decoding scheme (labeled as Test-constrained in Figure 4.7) where we constrain the search in the latent space. This is done by assuming that we know the test Z^* for the first few frames. Because these first few frames are assumed to be good solutions, then we can constrained the search for the solutions of the succeeding frames by nearest neighbors of the previous solutions. This can be a good initialization for finding the new X^* .

4.2.4 Cross-validation

The data were separately analyzed and latent models were separately trained for each subject. Four trials from each set of tasks (giving a total of 28 trial data) were concatenated together and used for training. The training data was further downsampled by a factor of 20 to make the training of the model feasible. This was done because training a GPLVM model is computationally expensive for large samples, but handles data with large dimensions very well. The remaining trials were used for testing purposes (7 trial data). A five-fold cross validation procedure was used to evaluate the overall finger kinematic reconstruction performance across subjects.

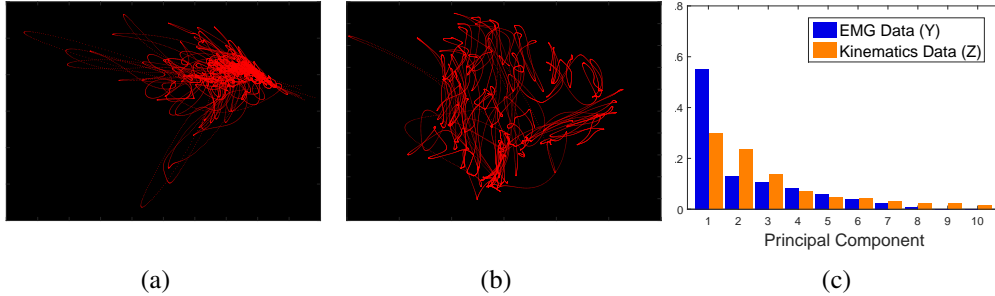


Figure 4.3: PCA projection and dimensional analysis on the observation data. (a) 2D projection on the muscle activation data. (b) 2D projection on the kinematics data. (c) Accumulated data variance comparison at each principal dimension.

The quality of finger kinematic reconstruction and estimation performance was evaluated using the root-mean-square error (RMSE):

$$\text{RMSE}_i = \sqrt{\frac{\sum_{t=0}^N (Z_{\text{TARGET}} - Z_{\text{EST}})^2}{N}} \quad (4.10)$$

where Z_{TARGET} and Z_{EST} are the target and estimated DOFs, respectively. The RMSE performance index gives the square root of the mean of the square of all of the error. Compared to other similar error metrics, RMSE amplifies and severely punishes large errors.

4.3. Results

4.3.1 Synergistic representation

In this section, we discuss how the high-dimensional finger posture observation is qualitatively distributed in the low-dimensional space. We briefly discuss the kind of synergies extracted from commonly used dimensional reduction technique such as Principal Component Analysis (PCA), synergies from a GPLVM and shared synergies from the proposed method using the Bayesian GPLVM with ARD model. The dataset obtained from subject 1 (S1) is used to for visualization of the projected data points using different synergistic models.

Principal component analysis

Principal Component Analysis (PCA) is a linear decomposition technique that assumes that the set of measured data is composed of linear combinations of a smaller number of underlying elements [105]. It finds a low-dimensional hyperplane which maximizes the variance of the data projected onto this hyperplane. PCA applies well to data whose underlying intrinsic elements are correlated in a linear subspace. To view the synergies extracted from PCA, we obtain a 2D manifold in Figure 4.3, where the data points are plotted as red dots, for easy visualization. Figure 4.3a shows the space created from the muscle activation Y , while Figure 4.3b shows the space created from the finger kinematics X .

The number of reduced dimensions or principal components is selected based on 90% total accumulated data variance. Based from this criteria, five and nine principal components were needed to explain most of the data variance in the EMG and finger kinematics data, respectively. Figure 4.3c shows the variance contribution of each principal component for each data observation. Projecting the hand kinematic data onto the two largest PC contributors, would give linear effects, such as, scaling the size and translating positions of the hand model. Using a linear model, may represent most hand kinematics data variance, for example using 9 components, but may still fail to generate nonlinear multi-finger movements.

Gaussian process latent variable model

Each point in latent space is mapped to a corresponding point in high-dimensional space via a GP. A predictive mean and variance is obtained from this functional GP-mapping. While the predictive mean corresponds to the reconstruction in the high-dimensional space, the variance gives the confidence of the model in generating the reconstructed point. How fast the variance increases while moving away from data points gives a hint on the belief of the model to generalize to previously unseen points. Figure 5 shows the data points projected onto the GPLVM latent space 2D manifold. The red dots correspond to the posterior estimate data points, while the gradient of the background correspond to the posterior variance (white for low variance and black for high variance).

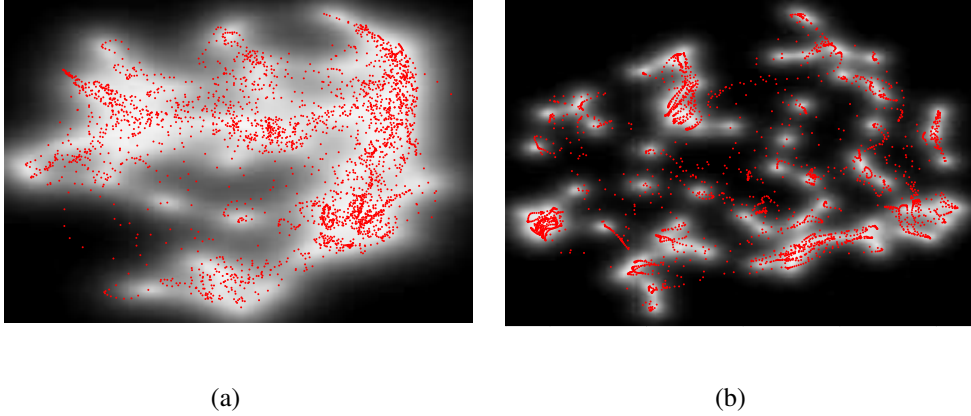


Figure 4.4: The GPLVM 2D-projections on the (a) EMG data and (b) kinematic data.

The points in the GPLVM space as shown both in Figure 4.4a and Figure 4.4b are more spread out and form different clusters. By exploring the projected points in the different clusters, different modes of finger kinematics can be reconstructed. Even in this 2D projection, a large variation of finger postures is captured in this space, such as those seen in the training data. Similarly, Romero et al. [14] showed that 2 to 3 GPLVM dimensions were enough to reconstruct 31 different grasping movements. The nonlinear character of GPLVM allows it to spread the finger kinematics, as shown in Figure 4.4b, to have better and finer differentiation between different modes. For estimating a new point using the standard GPLVM model, current methods have to rely on a single point MAP estimate for which the posterior over the latent points can be multi-modal [99].

In the proposed shared latent space model using the Bayesian GPLVM with ARD, the number of relevant dimensions is automatically obtained. Figure 4.5a shows the optimized weights for each dimensions, where the latent space is segmented according to the shared and private components for each observation data. In this figure, the shared dimensions $\{7, 8, 9\}$ contain the muscle activation synergistic features coupled with the finger movement information. Figure 4.5b shows a 2D projection onto the shared space given by dimensions $\{7, 8\}$. While, Figure 4.5c and Figure 4.5d show the projection onto the private spaces for muscle activation and finger kinematics, given by dimensions $\{1, 2\}$ and $\{11, 12\}$, respectively.

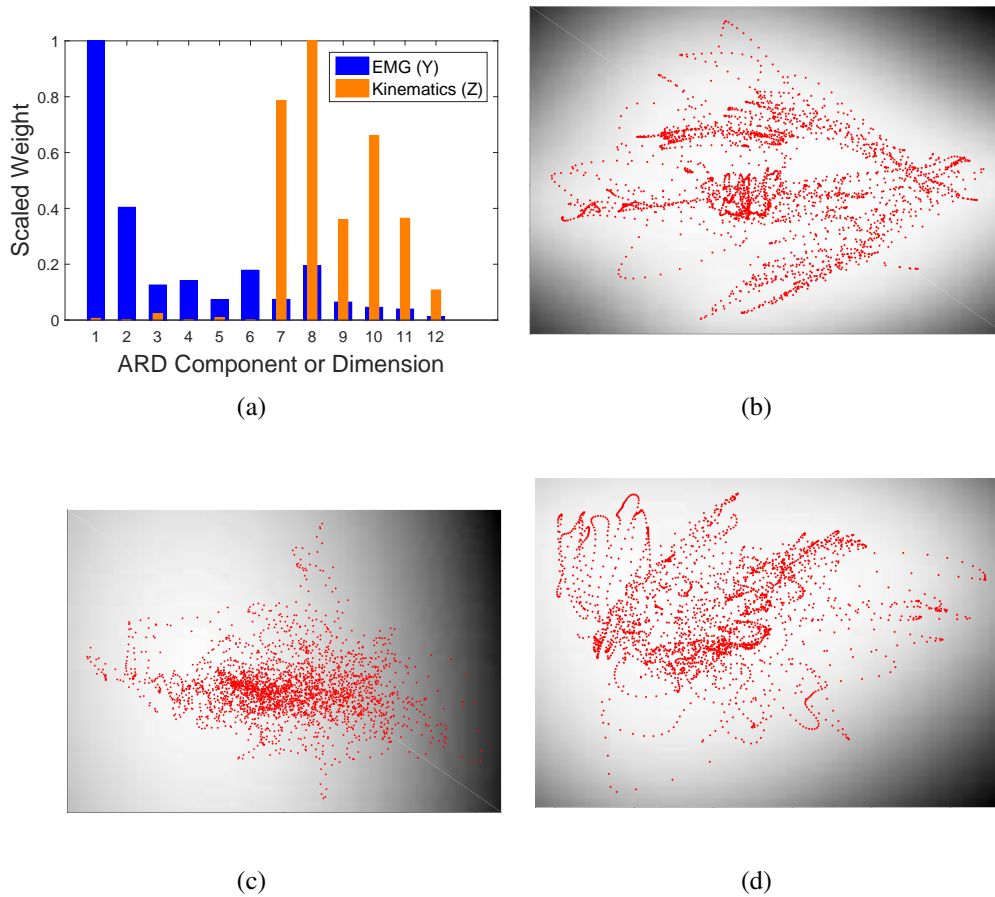


Figure 4.5: Discovered latent spaces with the Bayesian GPLVM with ARD components. (a) The optimized weights associated with each dimension. Sample 2D projection of (b) the shared space in $\dim\{7,8\}$, (c) private space to the muscle activation in $\dim\{1,2\}$, and (d) private to the kinematics in $\{11,12\}$.

The relevance weight parameters $\{w^Y, w^Z\}$ determine the contribution of each dimension associated with observation data and is responsible for the automatic selection of dimensions and pruning of the model. A higher value of the weight implies more relevance or contribution from the dimension. While, a zero or close to zero weight value implies no relevance by that dimension and can be disregarded.

As can be seen in Figure 4.5a, dimensions $\{7, 8, 9\}$ have high shared relevance between muscle activation and finger kinematic spaces. Dimensions $\{7, 8, 9\}$ in Figure

4.5a correspond to multi-finger flexion and extension movements, coupled finger (Little/Ring and Ring/Middle) movements and thumb movement, respectively. It can be seen that these shared spaces contain information about specific fingers that are either coupled or largely independent (see also Figure 4.8a). Incidentally, the blue bars in Figure 4.5a may show some synergies in the muscle activation space. For dimensions $\{7,8,9\}$, these would correspond to synergies found to contribute to specific finger movements mentioned earlier. For weakly shared dimensions $\{10,11\}$, these synergies were found to correspond to movements associated with the ring and index finger. Almost all variations of finger kinematics poses presented in the training data were found to be embedded onto the shared spaces.

The background on Figure 4.5a-4.5d also show the posterior variance and the red dots correspond to the posterior mean of each training data point projected onto a 2D space. As we explore points further away from the projected training points, novel finger kinematic postures unseen from the training dataset are also generated.

4.3.2 Estimation and reconstruction

With the Bayesian GPLVM with ARD components model trained, all finger DOFs in terms of joint marker positions and joint angles were estimated. Figure 4.6 shows the estimation and reconstruction of a representative trajectory from one trial involving a multi-finger flexion-extension movement. The projected path in Figure 4.6a shows the trajectory plotted onto a 2D shared space (dimension $\{7,8\}$). The blue square dot shows three sample data points obtained in the estimated trajectory. Figure 4.6b and Figure 4.6c show the ground truth obtained from the motion capture data and the estimated finger postures, respectively. The corresponding mean errors are 0.52, 0.63 and 0.83 mm, respectively for each frame in Figure 4.6c. This shows very high resemblance between the estimated and the original given finger kinematic posture.

In this study, we evaluate how well the proposed method is able to reconstruct the full 23-joint finger movement across four different subjects. In Figure 4.7, the overall test estimation performance across different subjects are shown. The figure shows the root-mean-square error (RMSE) of the estimated and measure finger kinematics at the training and test datasets. We evaluate on two different output spaces, one in the joint marker space and the other in the joint angle space, shown in Figure 4.7a and Figure 4.7b, respectively. The overall estimation performance across subjects showed an aver-

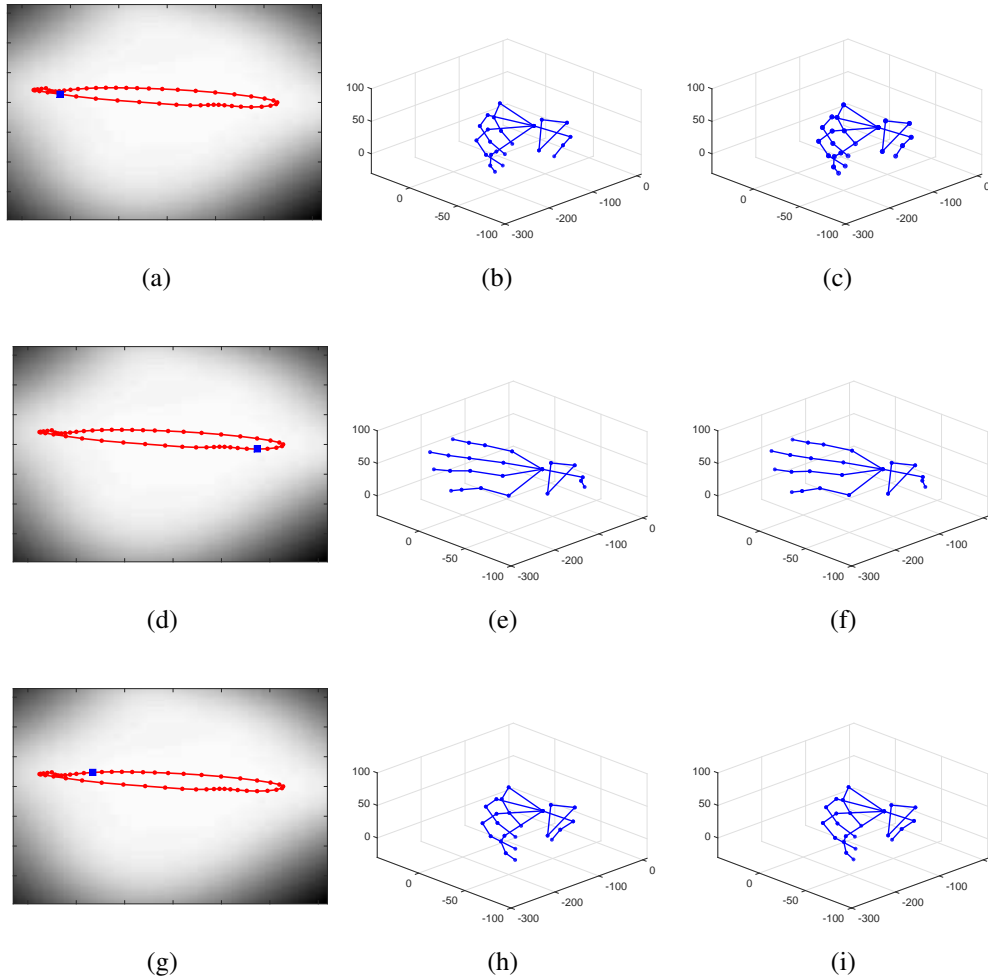


Figure 4.6: Sample finger kinematics inference of a simultaneous multi-finger flexion and extension movement. (a) The red line indicates the trajectory plotted on a 2-dimensional shared latent space. (b) Ground truth. (c) Estimated finger kinematics.

age RMSE of 9.18 ± 0.87 mm and 10.80 ± 1.55 degrees, for the joint marker position and angle, respectively. This result was from using only the shared information obtained from the new test muscle activation inputs. In the test-constrained result where partial information about the observed kinematics was used and exhaustively searching in the shared and private kinematic space, a best case average RMSE of 3.11 ± 0.23 mm and 4.32 ± 0.47 degrees were obtained for the two different output spaces, respectively. By incorporating knowledge on the kinematics, this leads to better estimation.

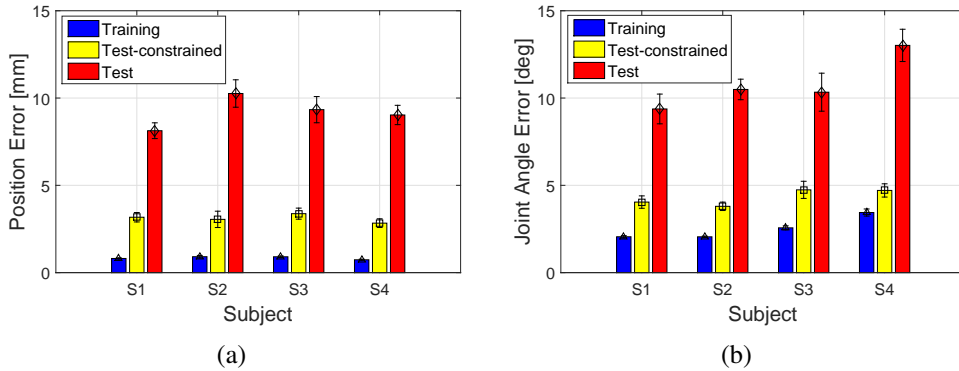


Figure 4.7: Overall estimation performance across subjects. (a) Mean square error of the positional joint marker estimation. (b) Mean square error of the joint angular estimation.

4.3.3 Synergistic representations

In Figure 4.8, the obtained optimized relevance weights of each trained model across subjects (S1-S4) are shown. The same number of shared space dimension and similar distribution are obtained even across different subjects. Below each of the bar graph are synergy model interpretations about what kinematic posture contribution does each dimensions contain. These are analyzed through visual inspection of each dimensions. About 4 to 5 shared synergies were found from each subject that corresponded to specific finger movements. Synergies that explained the most independent finger movement, such as those from the thumb, were found in dimensions $\{9, 11, 11\}$ in subjects (S1,S2,S4), respectively. Synergies that corresponded to coupled finger movements $\{8, 8, 10, 8\}$, individual index finger $\{11, 10, 12, 11\}$, and middle/ring finger $\{10, 12, 9, 12\}$ flexion-extension movements were also found in subjects (S1-S4), respectively. Interestingly, a synergy in dimension $\{1\}$ was found with more relevance in the muscle activation space. In this dimension, subjects S1 and S2 maintained a gripping movement exerting more force but with less kinematics (isometric force contraction). This dimension could have corresponded to a synergy that modulates force contraction which reflects the muscle activation space rather well. It should be noted that these synergy distributions can vary depending on the movements found in the training data.

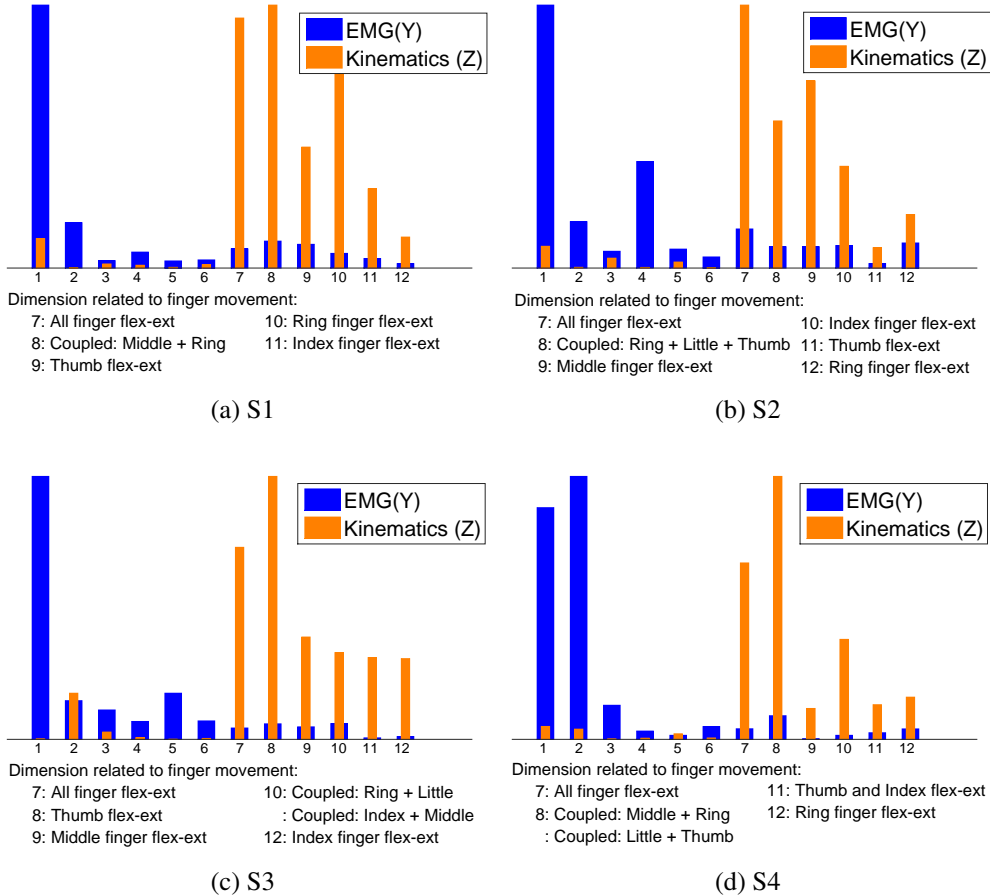


Figure 4.8: Discovered shared and private latent space dimensions with the optimized ARD components discovered across subjects. Below each plot are descriptions of some of the shared dimensions that hold finger kinematic information.

Finally, aside from looking at the reconstruction error of the finger kinematics and analysis of the extracted synergies, we show some results where we compare the proposed method with some regression methods commonly used to estimate multiple DOFs from EMG signals in the literature. We compare with regression methods such as standard linear regression on the full output dimension and on the PCA-reduced dimensions. We also compared against the performance of feedforward neural networks presented in [98] on the full and reduced output dimensions, respectively. In the reduced output dimension setting, the estimated points are then projected back

Table 4.1: The mean RMSE of the joint marker and joint angle space between the estimated and original finger kinematics.

	Pos. Err	Ang. Err
Mean Training Pose	11.72	10.74
LR on Full Dimension	10.36	9.12
LR on PCA Dimension	10.67	8.76
NN on Full Dimension	10.18	8.26
NN on PCA Dimension	10.13	8.40
Proposed Method	8.82	7.84
Proposed Method (Test-constrained)	4.03	3.30

into the original output space. The benchmark regression methods were selected since these were the commonly used methods for estimating hand kinematics from EMG [8, 22, 23, 26, 28, 39, 40, 73, 98]. The mean RMS errors are shown in Table 4.1. The proposed use of a Bayesian GPLVM model performs better than the other methods in terms of estimating continuous finger kinematics from EMG.

4.4. Discussion

This paper is the first to demonstrate the feasibility of estimating and recreating a full 23-joint high-DOF finger kinematics from surface EMG inputs using a generative model. We showed how a Bayesian GPLVM model can be used to obtain shared latent synergistic features that exists between EMG and kinematics data and provide a principled probabilistic framework for generating proportional and simultaneous high-DOF finger kinematics.

4.4.1 Shared synergistic features

Previous studies have often used different types of features or transformation of the surface EMG signal to capture both the muscular and kinematic/dynamic activity involved in particular tasks. Ideal feature extraction, such as extracting time, frequency and time-frequency domain based features, converts a set of incoming EMG signals

into distinguishable and repeatable descriptors [27]. Here in this study, we present the extraction of new shared synergistic features that contain both correlation information that exist in both EMG and the kinematic tasks. As discussed in [27], the use of the synergy-based features have advantages in being robust to single channel electrode shift and amplitude cancellation. Linear combinations of synergy features can also form complex outputs capable of reconstructing even nonlinear models and outputs [12]. Here in this study, the use of the shared synergistic features not only also offer these advantages but handle nonlinearity and high dimensionality very well. Using Bayesian techniques allowed the automatic determination of the dimensionality of the latent space. The model automatically allocates the corresponding shared spaces where synergies in the muscle activation and finger kinematic space are found.

The results reported in this paper also re-confirmed that the intrinsic dimensionality of both EMG and full hand/finger kinematics are actually lower than the full original data dimensionality [15, 40]. Four to six shared synergy modules that correspond to specific finger movement tasks were found in Figure 4.8a-4.8d. Through the experimental results, we also found that by using the information given by the shared space, we are able to infer a good estimate and reconstruct the full finger kinematics with good accuracy (Figure 4.5 and Figure 4.6).

Many muscle synergy models are presented in the EMG literature. Most of these studies use synergy extraction methods based on linear decomposition methods, such as extracting time-variant and time-invariant synergies that provide a biological plausible model and interpretation of the neural control behind the muscle coordination involved in motor tasks [11, 12]. Linear extraction methods, such as PCA or NMF, which extracts synergy modules based on the weighted contribution of each EMG channel can give a descriptive physiological interpretation. In the context of muscle activation patterns, neurons are either firing action potential (positive signal or weights) or are in resting state (zero signal) [105]. In this study, the use of a nonlinear synergy model may be more difficult to give a physiological interpretation. Intuively, however, we can inspect each dimension to correspond to specific finger kinematic movements such as what we have shown in Figure 4.8. One advantage of using the proposed shared synergistic model is its ability to consider nonlinear mappings using GPs with an ARD covariance function shown in equation (4.5). This gives a data-driven approach to address the compact representation of both the EMG and high-DOF finger kinematics.

The overall performance of the extracted nonlinear synergies by the GPLVM model show good results in terms of hand kinematic posture reconstruction error from EMG inputs. As previously mentioned, human hand is generally nonlinear, therefore an algorithm that can cope with nonlinearities is better suited for this problem. From the best of our knowledge, this is also the first study where a shared latent model was used to extract shared synergies from both muscle activation and finger kinematics simultaneously.

4.4.2 Reconstruction and estimation for control

The experimental results in the previous section show that Bayesian GP-LVM with automatic dimensionality determination of the latent spaces is a good model for learning the correlation that exists between EMG and finger kinematics. Although the dimensions were highly redundant in the joint kinematic space, we showed that we were able to retrieve back as large as 69 dimensions on the hand skeleton model. The choice of operating in the output joint marker space was to induce high dimensionality in the output space. One other advantage of the proposed method is that it can learn corresponding latent space manifolds from any data representation or output spaces, such as control commands in the joint angle (see Figure 4.7b), joint velocity or joint torque and stiffness [106] space. Operating in these spaces is particularly useful since these can be explicitly used as direct control signals for robotic devices.

A continuous finger movement trajectory can be reconstructed using information from the shared space as seen in Figure 4.6. Smooth trajectories of other finger motions (e.g. individual finger flexion-extension) can also be plotted. Different high-DOF finger movements can be found in exploring different shared dimensions. Particular finger movement should reside near corresponding cluster data points (modes) that closely resemble that specific movement found in the training dataset. It was also seen in Figure 4.7, that by using some kinematic knowledge led to better results. Searching in the latent spaces can give multimodal solutions, thus, constraining the search space, for example, considering information about the dynamics or intent may improve the estimation performance.

Although not explicitly shown, the errors across the each finger joint angles were consistent (3.71 ± 0.69 deg). Across varying tasks, however, estimation for Task (3), where fingers freely and randomly, showed larger errors (6.23 ± 0.44 deg) compared to

the other tasks (3.28 ± 0.84 deg). This was possibly due to new movement variations found in the test data that did not resemble any similar movements in the training data. This limitation can be improved by increasing the amount of training data to include more variations of finger movement or to constrain the tasks further, for example, by including only functional hand kinematic poses useful in activities of daily living (ADL) such as those prescribed in [107, 108].

4.4.3 Implementation and limitations

This study is limited to offline analysis with data from healthy and able-bodied subjects to test the feasibility of our approach. Though this can be used as an initial benchmark for future implementations, further verification and validation has to be done for training different models using data from amputees or subjects with hand impairments. A good candidate for this is to use large EMG and motion datasets obtained from both healthy and impaired subjects such as those provided by the Ninapro database [89]. With our study evaluated on four able-bodied subjects, our results suggest that there is large variability in how the subjects execute different finger movement tasks. Although we found motion-specific synergies (see Figure 4.8) across subjects, we should also investigate motion-invariant synergies that may exist across different subjects. Moreover, the main findings of our study is not limited to proposing the use of a new shared synergistic representation of EMG and motor task, but is to also transfer joint control commands in robots to produce dynamic finger movements.

The movement tasks used in this study was limited to basic (flexion-extension) of individual and multi-finger movements. Some degree of randomness in the movement was included where subjects could freely choose random finger movements of their choice. Because the focus of this study was on simultaneous and proportional myoelectric control, then kinematic data of continuous finger movement were of more importance than other hand configurations such as static postures or grasping objects (where large forces are important than large movements). However, some insights can be gained on how the proposed method of using a shared latent model may be adjusted to consider different grasping and objects. When grasping postures of different objects or profiles of finger forces are introduced in the training of the model, then additional relevant latent dimensions may be obtained. These dimensions could correspond to synergies representing different finger force profiles or different object information.

This notion is quite similar to the results presented in Chapter 4.3.3 where latent dimensions describing different finger movements were obtained.

Also, similar to Santello et al.'s study [59], a study on a large dataset of 51 static grasping poses showed that a large grasp data variance is contained in only 2 principal components, while other dimensions contained object information. This type of multi-view representation of information in grasp and object properties were also consistent in [14, 62]. In the long term, to give robotic hands true dexterity from myoelectric control, considering basic finger movements, different grasping configuration and object manipulation should be considered.

Complexity

In practice, it is desirable for the controller to use as little calibration data as possible and should generalize to movements for which exhaustive training data is not available [8]. The complexity of the proposed method comes in two different parts: the training and the testing. Most of the computational time (98%) is due to the training of the shared Bayesian GPLVM model. The typical computational complexity of a sparse implementation of a GPLVM is $O(Nm^2)$, where N is the number of data sample used, and m is the number of inducing points. Testing with the Bayesian GPLVM is linear in the number of data points $O(N)$.

In all the experiments, the number of inducing points was set to 100. A runtime evaluation conducted on a desktop machine with an Intel i7 2.8 GHz processor to compare the computational time needed to train and test each model. This can give us some indication of possible delays in the real-time estimation. An unoptimized Matlab implementation of the proposed shared Bayesian GPLVM model was evaluated and compared with other conventional methods. To standardize the comparison, a fixed 2200 samples was used for training and 1400 samples used for testing. The absolute time and normalized time (i.e., absolute time divided by the total number of samples) were used. Table 4.2 shows the comparison of computation time for both training and testing.

Inference with optimization of a new variational distribution on a single test data point took 1.3 seconds. Since an optimization step was involved in approximating for the posterior, where the ratio between two marginal likelihoods were computed. By replacing this optimization part to using nearest neighbor (NN) instead to find the

Table 4.2: Computational time for training and testing using different models. *NN*: nearest neighbor; *Optim*: optimization procedure.

	Training		Testing	
	AT (s)	NT (ms)	AT(s)	NT(ms)
LR-Full	0.08	0.03	0.003	0.002
LR-PCA	0.02	0.009	0.001	0.0007
NN-Full	12.30	5.59	0.032	0.02
NN-PCA	12.08	5.49	0.039	0.03
Proposed Method - <i>NN</i>	11,580	5263	6.01	4.3
Proposed Method - <i>Optim</i>			1902	1358

closest neighbors in the training data, inference time improved to 0.004 seconds. This makes real-time inference quite realizable.

The training time, however, can be quite prohibitive in many EMG applications where re-calibration is often done to adapt to the time-varying nature of EMG. So in the future work, we propose a slightly different approach in creating a new type of myoelectric interface, where the latent space map is pre-trained and includes co-adaptation from the users to intuitively learn the internal control dynamics to seamlessly control a robot hand.

Chapter 5

Conclusion

This study shows how proportional and simultaneous myoelectric control of multiple degree-of-freedom (DOFs) available in the hand can be achieved. In Chapter 3, we presented an alternative and improved method in estimating simultaneous finger kinematics from surface electromyographic (EMG) signals using a muscle activation model that parameterizes electromechanical delay, which has been observed by numerous investigators. Overall, the proposed method in this chapter captures the general trend of finger movements and is able to estimate multiple finger DOFs with usable accuracies. We have shown that using a data-driven approach such as using an artificial neural network and a nonparametric Gaussian Process for regression is suitable for this application. Though neural networks are fast and perform robustly well when the training data is sufficient, using a Gaussian Process regressor gives better performance when the training samples are small. This shows much promise in being able to reduce the amount of experiment training protocols substantially and can work better than using neural networks. Compared to the previous related studies, the dataset collected introduced more variation and some degree of randomness between basic continuous individual and multi-finger joint movement.

In Chapter 4, we presented an extension of the study presented in Chapter 3. We extend the proposed model to handle not only the nonlinearity of finger movements but also the high degrees-of-freedom and correlations that exists in the hand kinematics, in the context of myoelectric proportional control. In this part, we present a more natural view on how both the coordination of muscle activation and finger joint postures can be viewed in terms of synergies. It is known that muscle activation coordination is

highly correlated with finger kinematics, so the proposal of using a shared synergistic model between these two observation data makes sense. We showed how a Bayesian GPLVM with Automatic Relevance Determination (ARD) framework can be used to obtain shared latent synergistic features between EMG and finger posture kinematics. We showed a probabilistic approach for generating high-DOF finger kinematics, and that dexterous finger movements can be represented in a small dimensional space using a nonlinear synergistic representation with the GPLVM model. We have also shown that the proposed method outperforms commonly used linear dimensionality reduction method coupled with simultaneous regression used in the previous studies.

To this date, the resulting use of the proposed shared model is promising as very few studies has been able to recreate the continuous movements of a full 23-joint high-dimensional finger posture kinematics from EMG inputs. The proposed approach presents a viable solution for a myoelectric control strategy for handling high-DOF control in robotic hand prostheses and hand interfaces. Our method validates the feasibility of a position-based control of high-DOF finger movements from EMG.

Chapter 6

Directions for future research

For the future direction of this study, instead of mapping the full-DOF hand kinematics solely from EMG, one strategy is to create a new type of EMG-based interface where a subject needs only to learn a low-level control strategy in navigating a visual latent space in order to generate dynamic high-DOF finger movements. For example, Nazarpour et al [68] have analyzed motor learning in the context of muscle synergies using 2D-cursor position control tasks. They found that subjects were able to learn easily and robustly the flexible control of the 2D-cursor via EMG, through the formation of task-specific muscle synergies.

Building on this idea, we can create a 2D manifold where dynamic high-DOF finger movement is embedded in this space. Using myoelectric control to explore in this 2D latent space, subjects can learn to control a high-DOF robot quickly and intuitively by, with each point having a GP-mapping to the high dimensional kinematic space. Visual feedback via the presented latent space would not only close the control loop for better real-time performance but may also let users learn some internal system dynamics while interacting with the control interface. Real-time execution in this new interface is not only fast, as the latent space is trained beforehand, but may also be robust as the new process involves some degree of co-adaptive learning from the users. Such pre-training can be used to target different modes such as continuous finger movements, fixed grasping postures, and trajectories for object handling. Using the nonlinear synergistic low-dimensional representation in the latent space model, high-dimensional complex movements useful for prostheses control or rehabilitation can be trained.

Despite having to learn a completely new and unfamiliar mapping from muscle activity to movement trajectories, we hypothesize that such an interface can induce synergy development during the long-term cursor control. This could result in the development of population-wide convergence to common synergies while interacting with a particular low dimensional mapping function, similar to that described in [65]. We believe that providing a tool to enhance development of new synergies, providing visual feedback during training and developing co-adaptive learning strategies between the user and control agent are key improvements that could potentially improve the next generation myoelectric controllers in the context of human-robot interaction.

Acknowledgements

First of all I would like to express my sincerest gratitude to my supervisors, Professor Kazushi Ikeda and Professor Tomohiro Shibata who without any reservations, continuously guided and supported me. This work would not have been possible without them. Professor Ikeda welcomed and took me under his guidance. His generosity have allowed me to complete my studies in Japan. To Professor Shibata, who is more than my adviser and mentor, I will be forever grateful for his dedication to his students. His words and encouragement have always inspired and brought out the very best in us.

To Assistant Professor Tomoya Tamei and Associate Professor Takatomi Kubo, thank you very much for all your guidance and support. Because of their patience and relentless guidance, I was able to overcome many hurdles in my research. This work would not have come to fruition without their indispensable advice and mentorship.

In the completion of this work, many people have helped me along the way. I would like to thank Lorlynn Mateo for helping me proofread many of the materials and for being hugely supportive throughout the years. To my parents, brother and sister, who have continuously poured me with support and encouragements. I would also like to thank Hiroyuki Funaya, Nishanth Koganti, Chihiro Obayashi, Akihiro Nakamura, Bryan Lao and Shinta Hara for their valuable insights and contributions. I am also very fortunate to have worked with wonderful people in the Mathematical Informatics Lab in NAIST and in the Human and Social Intelligence Lab in KyuTech. Both the staff and students in the lab have made my stay truly memorable and worthwhile.

Finally, I would like to thank the Japan Government MEXT Scholarship Program and the Grant-in-Aid for Scientific Research from Japan Society for the Promotion of Science, for the support in my education and research. Without them, my dream of studying in Japan would never have come true. Thank you for the valuable opportunity.

References

- [1] D. Farina, N. Jiang, H. Rehbaum, A. Holobar, B. Graimann, H. Dietl, and O. Aszmann, “The extraction of neural information from the surface EMG for the control of upper-limb prostheses: Emerging avenues and challenges,” *IEEE Trans. on Neural Syst. and Rehabil. Eng.*, vol. 22, no. 4, pp. 797–809, 2014.
- [2] Shadow robot. [Online]. Available: <http://www.shadowrobot.com/>
- [3] Eh1 milano hand. [Online]. Available: <http://www.prensilia.com/>
- [4] O. Van Der Niet Otr, H. A. Reinders-Messelink, R. M. Bongers, H. Bouwsema, and C. K. Van Der Sluis, “The i-LIMB hand and the DMC plus hand compared: a case report,” *Prosthetics and orthotics international*, vol. 34, no. 2, pp. 216–220, 2010.
- [5] C. Medynski and B. Rattray, “Bebionic prosthetic design,” in *Proceedings of the MEC’11 conference*. Myoelectric Symposium, 2011.
- [6] J. T. Belter, J. L. Segil, A. M. Dollar, and R. F. Weir, “Mechanical design and performance specifications of anthropomorphic prosthetic hands: a review,” *J Rehabil Res Dev*, vol. 50, no. 5, pp. 599–618, 2013.
- [7] M. Grebenstein, “Analysis of the current state of robot hands,” in *Approaching Human Performance*. Springer, 2014, pp. 11–37.
- [8] J. Hahne, F. Biebmann, N. Jiang, H. Rehbaum, D. Farina, F. Meinecke, K.-R. Muller, and L. Parra, “Linear and nonlinear regression techniques for simultaneous and proportional myoelectric control,” *IEEE Trans. on Neural Syst. and Rehabil. Eng.*, vol. 22, no. 2, pp. 269–279, March 2014.
- [9] V. Kumar, Y. Tassa, T. Erez, and E. Todorov, “Real-time behaviour synthesis for dynamic hand-manipulation,” in *IEEE Int. Conf. on Robotics and Automation (ICRA)*. IEEE, 2014, pp. 6808–6815.
- [10] W. Penfield and T. Rasmussen, “The cerebral cortex of man; a clinical study of localization of function.” 1950.

- [11] A. d'Avella, P. Saltiel, and E. Bizzi, "Combinations of muscle synergies in the construction of a natural motor behavior," *Nature neuroscience*, vol. 6, no. 3, pp. 300–308, 2003.
- [12] A. d'Avella, A. Portone, L. Fernandez, and F. Lacquaniti, "Control of fast-reaching movements by muscle synergy combinations," *The Journal of neuroscience*, vol. 26, no. 30, pp. 7791–7810, 2006.
- [13] L. H. Ting, "Dimensional reduction in sensorimotor systems: a framework for understanding muscle coordination of posture," *Progress in brain research*, vol. 165, pp. 299–321, 2007.
- [14] J. Romero, T. Feix, C. H. Ek, H. Kjellstrom, and D. Kragic, "Extracting postural synergies for robotic grasping," *IEEE Trans. on Robotics*, vol. 29, no. 6, pp. 1342–1352, 2013.
- [15] E. Todorov and Z. Ghahramani, "Analysis of the synergies underlying complex hand manipulation," in *Engineering in Medicine and Biology Society, 2004. IEMBS'04. 26th Annual International Conference of the IEEE*, vol. 2. IEEE, 2004, pp. 4637–4640.
- [16] H.-P. Huang and C.-y. Chen, "Development of a myoelectric discrimination system for a multi-degree prosthetic hand," in *Robotics and Automation, 1999. Proceedings. 1999 IEEE International Conference on*, vol. 3. IEEE, 1999, pp. 2392–2397.
- [17] J. Chu, I. Moon, and M. Mun, "A real-time pattern recognition for multifunction myoelectric hand control," in *International conference on control, automation and systems*. ICCAS, June 2005.
- [18] Y. Huang, K. B. Englehart, B. Hudgins, and A. D. Chan, "A gaussian mixture model based classification scheme for myoelectric control of powered upper limb prostheses," *IEEE Trans. on Biomedical Eng.*, vol. 52, no. 11, pp. 1801–1811, 2005.
- [19] A. J. Young, L. H. Smith, E. J. Rouse, and L. J. Hargrove, "Classification of simultaneous movements using surface EMG pattern recognition," *IEEE Trans. on Biomedical Eng.*, vol. 60, pp. 1250–1258, 2013.

- [20] M. Ortiz-Catalan, R. Brånemark, and B. Håkansson, “Biopatrec: A modular research platform for the control of artificial limbs based on pattern recognition algorithms.” *Source code for biology and medicine*, vol. 8, no. 11, 2013.
- [21] N. Jiang, J. Vest-Nielsen, S. Muceli, and D. Farina, “EMG-based simultaneous and proportional estimation of wrist/hand kinematics in uni-lateral trans-radial amputees,” *J. Neuroeng. & Rehab.*, vol. 9, 2012.
- [22] N. Shrirao, N. Reddy, and D. Kosuri, “Neural network committees for finger joint angle estimation from surface EMG signals,” *Biomedical Engineering Online*, vol. 8(2), pp. 1–11, 2009.
- [23] R. Smith, F. Tenore, D. Huberdeau, R. Etienne-Cummings, and N. Thakor, “Continuous decoding of finger position from surface EMG signals for the control of powered prostheses,” in *30th Annual Int. IEEE EMBS Conference*, August 2008, pp. 197–200.
- [24] M. Hioki and H. Kawasaki, “Estimation of finger joint angles from sEMG using a neural network including time delay factor and recurrent structure,” *International Scholarly Research Network (ISRN) Rehabilitation*, vol. 2012, 2012.
- [25] T. Buchanan, D. Lloyd, K. Manal, and T. Besier, “Neuromusculoskeletal modeling: Estimation of muscle forces & joint moments and movements from measurements of neural command,” *Journal of Applied Biomechanics*, vol. 20(4), pp. 367–395, November 2004.
- [26] N. Jiang, H. Rehbaum, I. Vujaklija, B. Graimann, and D. Farina, “Intuitive, online, simultaneous, and proportional myoelectric control over two degrees-of-freedom in upper limb amputees,” *IEEE Trans. on Neural Syst. and Rehabil. Eng.*, vol. 22, no. 3, pp. 501–510, 2014.
- [27] M. Ison and P. Artemiadis, “The role of muscle synergies in myoelectric control: trends and challenges for simultaneous multifunction control,” *Journal of Neural Engineering*, vol. 11, no. 5, p. 051001, 2014. [Online]. Available: <http://stacks.iop.org/1741-2552/11/i=5/a=051001>

- [28] N. Jiang, K. B. Englehart, and P. A. Parker, "Extracting simultaneous and proportional neural control information for multiple-DOF prostheses from the surface electromyographic signal," *IEEE Transactions on Biomedical Eng.*, vol. 56, no. 4, pp. 1070–1080, 2009.
- [29] A. Fougner, Ø. Stavadahl, P. J. Kyberd, Y. G. Losier, P. Parker *et al.*, "Control of upper limb prostheses: terminology and proportional myoelectric control a review," *Neural Systems and Rehabilitation Engineering, IEEE Transactions on*, vol. 20, no. 5, pp. 663–677, 2012.
- [30] N. Jiang, S. Dosen, K.-R. Müller, and D. Farina, "Myoelectric control of artificial limbs—is there a need to change focus," *IEEE Signal Process. Mag*, vol. 29, no. 5, pp. 152–150, 2012.
- [31] P. Erik Scheme MSc and P. Kevin Englehart PhD, "Electromyogram pattern recognition for control of powered upper-limb prostheses: State of the art and challenges for clinical use," *Journal of rehabilitation research and development*, vol. 48, no. 6, p. 643, 2011.
- [32] O. Fukuda, T. Tsuji, M. Kaneko, and A. Otsuka, "A human-assisting manipulator teleoperated by EMG signals and arm motions," *IEEE Trans. on Robotics and Automation*, vol. 19, no. 2, pp. 210–222, 2003.
- [33] M. Davies, "Bebionic hand product brochure: Teenager who lost three limbs to meningitis now has a bionic hand - and hopes to swim for england in the 2016 paralympics," *Daily Mail Uk*, 2014. [Online]. Available: <http://www.dailymail.co.uk/health/article-2890180/>
- [34] N. Ho, K. Tong, X. Hu, K. Fung, X. Wei, W. Rong, and E. Susanto, "An EMG-driven exoskeleton hand robotic training device on chronic stroke subjects: task training system for stroke rehabilitation," in *Rehabilitation Robotics (ICORR), 2011 IEEE International Conference on*. IEEE, 2011, pp. 1–5.
- [35] R. Steeper, "Bebionic hand product brochure," 2013. [Online]. Available: <http://www.bebionic.com/wpcontent/uploads/bebionic-Product-Brochure-Final.pdf>
- [36] J. V. Basmajian, "Muscles alive. their functions revealed by electromyography." *Academic Medicine*, vol. 37, no. 8, p. 802, 1962.

- [37] (2011) Motor unit adaptation. Accessed: 20/12/2012. [Online]. Available: <http://kin450-neurophysiology.wikispaces.com/Motor+Unit+Adaptation>
- [38] P. Konrad, “The ABC of EMG - a practical introduction to kinesiological electromyography,” Noraxon INC. USA, Scottsdale, AZ 85254, April 2005.
- [39] S. Muceli, N. Jiang, and D. Farina, “Extracting signals robust to electrode number and shift for online simultaneous and proportional myoelectric control by factorization algorithms,” *IEEE Trans. on Neural Systems and Rehab. Eng.*, vol. 22, no. 3, pp. 623–633, 2014.
- [40] A. Krasoulis, S. Vijayakumar, and K. Nazarpour, “Evaluation of regression methods for the continuous decoding of finger movement from surface EMG and accelerometry,” in *7th Int. IEEE/EMBS Conf. on Neural Eng. (NER)*. IEEE, 2015, pp. 631–634.
- [41] A. Hill, “The heat of shortening and the dynamic constants of muscle,” *Proceedings of the Royal Society of London B: Biological Sciences*, vol. 126, no. 843, pp. 136–195, 1938.
- [42] F. E. Zajac, “Muscle and tendon: properties, models, scaling, and application to biomechanics and motor control.” *Critical reviews in biomedical engineering*, vol. 17, no. 4, pp. 359–411, 1988.
- [43] Y. Koike and M. Kawato, “Estimation of dynamic joint torques and trajectory formation from surface electromyography signals using a neural network model,” *Biological cybernetics*, vol. 73, no. 4, pp. 291–300, 1995.
- [44] P. K. Artemiadis and K. J. Kyriakopoulos, “Emg-based control of a robot arm using low-dimensional embeddings,” *Robotics, IEEE Transactions on*, vol. 26, no. 2, pp. 393–398, 2010.
- [45] S. W. Lee and D. G. Kamper, “Transmission of musculotendon forces to the index finger,” in *The Human Hand as an Inspiration for Robot Hand Development*. Springer, 2014, pp. 77–97.

- [46] F. J. Valero-Cuevas, “An integrative approach to the biomechanical function and neuromuscular control of the fingers,” *Journal of biomechanics*, vol. 38, no. 4, pp. 673–684, 2005.
- [47] F. J. Valero-Cuevas, V. V. Anand, A. Saxena, and H. Lipson, “Beyond parameter estimation: extending biomechanical modeling by the explicit exploration of model topology,” *Biomedical Engineering, IEEE Transactions on*, vol. 54, no. 11, pp. 1951–1964, 2007.
- [48] F. J. Valero-Cuevas, F. E. Zajac, and C. G. Burgar, “Large index-fingertip forces are produced by subject-independent patterns of muscle excitation,” *Journal of biomechanics*, vol. 31, no. 8, pp. 693–703, 1998.
- [49] F. Valero-Cuevas, “Muscle coordination of the human index finger,” Ph.D. dissertation, Doctoral Dissertation, Stanford University, Stanford, CA, 1997.
- [50] D. G. Kamper, H. C. Fischer, and E. G. Cruz, “Impact of finger posture on mapping from muscle activation to joint torque,” *Clinical Biomechanics*, vol. 21, no. 4, pp. 361–369, 2006.
- [51] F. J. Valero-Cuevas, M. E. Johanson, and J. D. Towles, “Towards a realistic biomechanical model of the thumb: the choice of kinematic description may be more critical than the solution method or the variability/uncertainty of musculoskeletal parameters,” *Journal of biomechanics*, vol. 36, no. 7, pp. 1019–1030, 2003.
- [52] E. Cavallaro, J. Rosen, J. C. Perry, S. Burns, and B. Hannaford, “Hill-based model as a myoprocessor for a neural controlled powered exoskeleton arm-parameters optimization,” in *Robotics and Automation, 2005. ICRA 2005. Proceedings of the 2005 IEEE International Conference on*. IEEE, 2005, pp. 4514–4519.
- [53] W. Yan, *Biomechanical Simulation of the Human Hand and Forearm*. Citeseer, 2012.
- [54] M. C. Tresch, P. Saltiel, and E. Bizzi, “The construction of movement by the spinal cord,” *Nature neuroscience*, vol. 2, no. 2, pp. 162–167, 1999.

- [55] G. Torres-Oviedo, J. M. Macpherson, and L. H. Ting, “Muscle synergy organization is robust across a variety of postural perturbations,” *Journal of neurophysiology*, vol. 96, no. 3, pp. 1530–1546, 2006.
- [56] G. Torres-Oviedo and L. H. Ting, “Muscle synergies characterizing human postural responses,” *Journal of neurophysiology*, vol. 98, no. 4, pp. 2144–2156, 2007.
- [57] M. Berniker, A. Jarc, E. Bizzi, and M. C. Tresch, “Simplified and effective motor control based on muscle synergies to exploit musculoskeletal dynamics,” *Proceedings of the National Academy of Sciences*, vol. 106, no. 18, pp. 7601–7606, 2009.
- [58] I. V. Grinyagin, E. V. Biryukova, and M. A. Maier, “Kinematic and dynamic synergies of human precision-grip movements,” *Journal of neurophysiology*, vol. 94, no. 4, pp. 2284–2294, 2005.
- [59] M. Santello, M. Flanders, and J. F. Soechting, “Postural hand synergies for tool use,” *The Journal of Neuroscience*, vol. 18, no. 23, pp. 10 105–10 115, 1998.
- [60] M. Tagliabue, A. Ciancio, T. Brochier, S. Eskiizmirliler, and M. Maier, “Differences between kinematic synergies and muscle synergies during two-digit grasping,” *Frontiers in human neuroscience*, vol. 9, 2015.
- [61] M. R. Cutkosky, “On grasp choice, grasp models, and the design of hands for manufacturing tasks,” *Robotics and Automation, IEEE Transactions on*, vol. 5, no. 3, pp. 269–279, 1989.
- [62] M. T. Ciocarlie and P. K. Allen, “Hand posture subspaces for dexterous robotic grasping,” *The International Journal of Robotics Research*, vol. 28, no. 7, pp. 851–867, 2009.
- [63] M. C. Tresch and A. Jarc, “The case for and against muscle synergies,” *Current opinion in neurobiology*, vol. 19, no. 6, pp. 601–607, 2009.
- [64] J. J. Kutch and F. J. Valero-Cuevas, “Challenges and new approaches to proving the existence of muscle synergies of neural origin,” *PLoS Comput. Biol.*, vol. 8, no. 5, 2012.

- [65] M. Ison and P. Artemiadis, “Proportional myoelectric control of robots: muscle synergy development drives performance enhancement, retainment, and generalization,” *IEEE Trans. on Robotics*, vol. 31, no. 2, pp. 259–268, 2015.
- [66] A. d’Avella, P. Saltiel, and E. Bizzi, “Combination of muscle synergies in the construction of a natural motor behavior,” *Nature Neuroscience*, vol. 6, pp. 300–308, 2003.
- [67] N. Jiang, I. Vujaklija, H. Rehbaum, B. Graimann, and D. Farina, “Is accurate mapping of EMG signals on kinematics needed for precise online myoelectric control?” *IEEE Trans. on Neural Syst. and Rehabil. Eng.*, vol. 22, no. 3, pp. 549–558, May 2014.
- [68] K. Nazarpour, A. Barnard, and A. Jackson, “Flexible cortical control of task-specific muscle synergies,” *The Journal of Neuroscience*, vol. 32, no. 36, pp. 12 349–12 360, 2012.
- [69] J. N. Ingram, K. P. Körding, I. S. Howard, and D. M. Wolpert, “The statistics of natural hand movements,” *Experimental brain research*, vol. 188, no. 2, pp. 223–236, 2008.
- [70] P. Afshar and Y. Matsuoka, “Neural-based control of a robotic hand: evidence for distinct muscle strategies,” in *IEEE Int. Conf. on Robotics and Automation*, vol. 5, 2004, pp. 4633–4638.
- [71] T. Tamei and T. Shibata, “Fast reinforcement learning for three-dimensional kinetic human–robot cooperation with an EMG-to-activation model,” *Advanced Robotics*, vol. 25, no. 5, pp. 563–580, 2011.
- [72] C. Rasmussen and C. Williams, *Gaussian processes for machine learning*. MIT Press, Cambridge, MA, USA, 2006.
- [73] N. Jiang, I. Vujaklija, H. Rehbaum, B. Graimann, and D. Farina, “Is accurate mapping of EMG signals on kinematics needed for precise online myoelectric control?” *IEEE Trans. on Neural Syst. and Rehabil. Eng.*, vol. 22, no. 3, pp. 549–558, May 2014.

- [74] C. H. Ek, J. Rihan, P. H. Torr, G. Rogez, and N. D. Lawrence, “Ambiguity modeling in latent spaces,” in *Machine Learning for Multimodal Interaction*. Springer, 2008, pp. 62–73.
- [75] S. Deena and A. Galata, “Speech-driven facial animation using a shared gaussian process latent variable model,” in *Advances in Visual Computing*. Springer, 2009, pp. 89–100.
- [76] K. Yamane, Y. Ariki, and J. Hodgins, “Animating non-humanoid characters with human motion data,” in *Proceedings of the 2010 ACM SIGGRAPH/Eurographics Symposium on Computer Animation*. Eurographics Association, 2010, pp. 169–178.
- [77] J. Ngeo, T. Tamei, K. Ikeda, and T. Shibata, “Modeling dynamic high-DOF finger postures from surface EMG using nonlinear synergies in latent space representation,” in *37th IEEE EMBS Conf.*, 2015, pp. 2095–2098.
- [78] L. Li and B. S. Baum, “Electromechanical delay estimated by using electromyography during cycling at different pedaling frequencies,” *Journal of Electromyography and Kinesiology*, vol. 14, no. 6, pp. 647–652, 2004.
- [79] P. F. Vint, S. P. McLean, and G. M. Harron, “Electromechanical delay in isometric actions initiated from nonresting levels.” *Medicine and science in sports and exercise*, vol. 33, no. 6, pp. 978–983, 2001.
- [80] K. Manal, R. Gonzalez, D. Lloyd, and T. Buchanan, “A real-time EMG-driven virtual arm,” *Computers in Biology and Medicine*, vol. 32(1), pp. 25–36, 2002.
- [81] B. C. Csáji, “Approximation with artificial neural networks,” *Faculty of Sciences, Eötvös Loránd University, Hungary*, vol. 24, 2001.
- [82] C. Bishop, *Pattern recognition and machine learning*. Springer New York, 2006, vol. 4.
- [83] M. Frean, M. Lilley, and P. Boyle, “Implementing gaussian process inference with neural networks,” *International Journal of Neural Systems*, vol. 16, pp. 321–327, 2006.

- [84] M. Ebden. (2008) Gaussian processes for regression: A quick introduction. [Online]. Available: <http://www.robots.ox.ac.uk/~mebden/reports/GPtutorial.pdf>
- [85] C. Rasmussen and H. Nickisch. (2010) Gaussian processes regression and classification toolbox version 3.1. [Online]. Available: <http://gaussianprocess.org/gpml/code>
- [86] N. Pratt, “Anatomy and kinesiology of the hand,” *Rehabilitation of the Hand and Upper Extremity*, pp. 3–17, 2011.
- [87] T. Feix, R. Pawlik, H.-B. Schmiebmayer, J. Romero, and D. Kragic, “A comprehensive grasp taxonomy,” in *Robotics, Science and Systems: Workshop on Understanding the Human Hand for Advancing Robotic Manipulation*, 2009, pp. 2–3.
- [88] S. J. Edwards, D. J. Buckland, and J. McCoy-Powlen, *Developmental & functional hand grasps*. Slack Thorofare, 2002.
- [89] M. Atzori, A. Gijsberts, C. Castellini, B. Caputo, A.-G. M. Hager, S. Elsig, G. Giatsidis, F. Bassetto, and H. Müller, “Electromyography data for non-invasive naturally-controlled robotic hand prostheses,” *Scientific data*, vol. 1, 2014.
- [90] J. Ngeo, T. Tamei, and T. Shibata. Dataset for surface electromyographic signals and kinematics of the hand for simultaneous and proportional finger movements. [Online]. Available: <https://dynamicbrain.neuroinf.jp/modules/xoonips/detail.php?id=EMG101>
- [91] M. Zecca, S. Micera, M. Carrozza, and P. Dario, “Control of multifunctional prosthetic hands by processing the electromyographic signal,” *Critical Reviews in Biomedical Engineering*, vol. 30, pp. 459–485, 2002.
- [92] M. A. Oskoei and H. Hu, “Myoelectric control systems: A survey,” *Biomedical Signal Processing and Control*, vol. 2, no. 4, pp. 275–294, 2007.

- [93] T. D'Alessio and S. Conforto, "Extraction of the envelope from surface EMG signals," *Engineering in Medicine and Biology Magazine, IEEE*, vol. 20, no. 6, pp. 55–61, 2001.
- [94] J. Ngeo, T. Tamei, and T. Shibata, "Continuous estimation of finger joint angles using muscle activation inputs from surface EMG signals," in *Engineering in Medicine and Biology Society (EMBC), 2012 Annual International Conference of the IEEE*. IEEE, 2012, pp. 2756–2759.
- [95] —, "Estimation of continuous multi-dof finger joint kinematics from surface EMG using a multi-output gaussian process," in *Engineering in Medicine and Biology Society (EMBC), 2014 36th Annual International Conference of the IEEE*. IEEE, 2014, pp. 3537–3540.
- [96] —, "Control of an optimal finger exoskeleton based on continuous joint angle estimation from EMG signals," in *Engineering in Medicine and Biology Society (EMBC), 2013 Annual International Conference of the IEEE*. IEEE, 2013, pp. 338–341.
- [97] N. Jiang, S. Muceli, B. Graimann, and D. Farina, "Effect of arm position on the prediction of kinematics from EMG in amputees," *Medical & biological engineering & computing*, vol. 51, no. 1-2, pp. 143–151, 2013.
- [98] J. G. Ngeo, T. Tamei, and T. Shibata, "Continuous and simultaneous estimation of finger kinematics using inputs from an EMG-to-muscle activation model," *J Neuroeng Rehabil*, vol. 11, no. 122, pp. 3–11, 2014.
- [99] N. Lawrence, "Probabilistic non-linear principal component analysis with gaussian process latent variable models," *The Journal of Machine Learning Research*, vol. 6, pp. 1783–1816, 2005.
- [100] A. Shon, K. Grochow, A. Hertzmann, and R. P. Rao, "Learning shared latent structure for image synthesis and robotic imitation," in *Advances in Neural Information Processing Systems*, 2005, pp. 1233–1240.
- [101] A. Damianou, C. Ek, M. Titsias, and N. Lawrence, "Manifold relevance determination," *arXiv preprint arXiv:1206.4610*, 2012.

- [102] M. K. Titsias and N. D. Lawrence, “Bayesian gaussian process latent variable model,” in *International Conference on Artificial Intelligence and Statistics*, 2010, pp. 844–851.
- [103] A. Damianou, M. K. Titsias, and N. D. Lawrence, “Variational gaussian process dynamical systems,” in *Advances in Neural Information Processing Systems*, 2011, pp. 2510–2518.
- [104] A. Damianou, M. K. Titsias, and N. Lawrence. Vargplvm software for Matlab and R. [Online]. Available: <https://github.com/SheffieldML/vargplvm>
- [105] L. H. Ting and S. A. Chvatal, “Decomposing muscle activity in motor tasks,” *Motor Control Theories, Experiments and Applications. Oxf. Univ. Press, New York*, pp. 102v–138, 2010.
- [106] D. Shin, J. Kim, and Y. Koike, “A myokinetic arm model for estimating joint torque and stiffness from EMG signals during maintained posture,” *Journal of neurophysiology*, vol. 101, no. 1, pp. 387–401, 2009.
- [107] P. J. Kyberd, A. Murgia, M. Gasson, T. Tjerks, C. Metcalf, P. H. Chappell, K. Warwick, S. E. Lawson, and T. Barnhill, “Case studies to demonstrate the range of applications of the southampton hand assessment procedure,” *The British Journal of Occupational Therapy*, vol. 72, no. 5, pp. 212–218, 2009.
- [108] C. Metcalf. Southampton hand assessment procedure southampton. [Online]. Available: <http://www.shap.ecs.soton.ac.uk>
- [109] I. Nabney, *NETLAB: algorithms for pattern recognition, Advances in Pattern Recognition*. Springer, Berlin, 2001.
- [110] G. Gioioso, G. Salvietti, M. Malvezzi, and D. Prattichizzo, “Mapping synergies from human to robotic hands with dissimilar kinematics: an approach in the object domain,” *IEEE Trans. on Robotics*, vol. 29, no. 4, pp. 825–837, 2013.
- [111] J. Wang, A. Hertzmann, and D. M. Blei, “Gaussian process dynamical models,” in *Adv. in NeuInfo Processing Systems*, 2005, pp. 1441–1448.

- [112] G. Naik, A. Al-Timemy, and H. Nguyen, "Transradial amputee gesture classification using an optimal number of sEMG sensors: An approach using ICA clustering," *IEEE Trans. on Neural Syst. and Rehabil. Eng.*, 2015.

Publication List

Peer-reviewed Journal Papers

1. Jimson Ngeo, Tomoya Tamei, Takatomi Kubo, Kazushi Ikeda, and Tomohiro Shibata. Using Nonlinear Synergistic Model for Proportional Myoelectric Control of High-DOF Finger Postures. *IEEE Transactions of Neural Systems and Rehabilitation Engineering (TNSRE)*, 2016. [Submitted and under review].
2. Jimson Ngeo, Tomoya Tamei, and Tomohiro Shibata. Continuous and Simultaneous Estimation of Finger Kinematics using Inputs from an EMG-to-Muscle Activation Model. *Journal of Neuroengineering and Rehabilitation (JNER)*, vol. 11, no. 122, pp. 3-11. 2014.

International Conferences

1. Jimson Ngeo, Tomoya Tamei, Kazushi Ikeda and Tomohiro Shibata. Modeling Dynamic High-DOF Finger Postures from Surface EMG Using Nonlinear Synergies in Latent Space Representation. *37th IEEE-EMBC*, pp. 2095-2098, 2015.
2. Nishanth Koganti, Jimson Ngeo, Tomoya Tamei, Kazushi Ikeda and Tomohiro Shibata. Cloth Dynamics Modelling in Latent Spaces and its Application to Robotic Clothing Assistance. *IEEE-IROS*, pp 3464-3469, 2015.
3. Jimson Ngeo, Tomoya Tamei, and Tomohiro Shibata. Estimation of Continuous Multi-DOF Finger Joint Kinematics from Surface EMG Using a Multi-output Gaussian Process. *36th IEEE-EMBC*, pp. 3537-3540, 2014.
4. Jimson Ngeo, Tomoya Tamei, M. Felix Orlando, Laxmidhar Behera, Anupam Saxena, Ashish Dutta and Tomohiro Shibata. Control of an Optimal Finger Exoskeleton Based on Continuous Joint Angle Estimation from EMG Signals. *35th IEEE-EMBC*, pp. 338-341, 2013.

Domestic Conferences

1. Tomohiro Shibata and Jimson Ngeo. Continuous Estimation of Multiple Finger Postures from Surface EMG Signals. Neurocomputing (NC): Implementation of Neuro Computing, Analysis and Modeling of Human Science, etc., 2016.